Electron capture in stars

K Langanke[1,2], G Martínez-Pinedo[1,2,3] and R.G.T. Zegers[4,5,6]

[1]GSI Helmholtzzentrum für Schwerionenforschung, D-64291 Darmstadt, Germany
[2]Institut für Kernphysik (Theoriezentrum), Department of Physics, Technische Universität Darmstadt, D-64298 Darmstadt, Germany
[3]Helmholtz Forschungsakademie Hessen für FAIR, GSI Helmholtzzentrum für Schwerionenforschung, D-64291 Darmstadt, Germany
[4] National Superconducting Cyclotron Laboratory, Michigan State University, East Lansing, Michigan 48824, USA
[5] Joint Institute for Nuclear Astrophysics: Center for the Evolution of the Elements, Michigan State University, East Lansing, Michigan 48824, USA
[6] Department of Physics and Astronomy, Michigan State University, East Lansing, Michigan 48824, USA

E-mail: k.langanke@gsi.de, g.martinez@gsi.de, zegers@nscl.msu.edu

Abstract. Electron captures on nuclei play an essential role for the dynamics of several astrophysical objects, including core-collapse and thermonuclear supernovae, the crust of accreting neutron stars in binary systems and the final core evolution of intermediate mass stars. In these astrophysical objects, the capture occurs at finite temperatures and at densities at which the electrons form a degenerate relativistic electron gas.

The capture rates can be derived in perturbation theory where allowed nuclear transitions (Gamow-Teller transitions) dominate, except at the higher temperatures achieved in core-collapse supernovae where also forbidden transitions contribute significantly to the rates. There has been decisive progress in recent years in measuring Gamow-Teller (GT) strength distributions using novel experimental techniques based on charge-exchange reactions. These measurements provide not only data for the GT distributions of ground states for many relevant nuclei, but also serve as valuable constraints for nuclear models which are needed to derive the capture rates for the many nuclei, for which no data exist yet. In particular models are needed to evaluate the stellar capture rates at finite temperatures, where the capture can also occur on excited nuclear states.

There has also been significant progress in recent years in the modelling of stellar capture rates. This has been made possible by advances in nuclear many-body models as well as in computer soft- and hardware. Specifically to derive reliable capture rates for core-collapse supernovae a dedicated strategy has been developed based on a hierarchy of nuclear models specifically adapted to the abundant nuclei and astrophysically conditions present at the various collapse conditions. In particular at the challenging conditions where the electron chemical potential and the nuclear Q values are of the same order, large-scale diagonalization shell model calculations have been proven as an appropriate tool to derive stellar capture rates, often validated by experimental data. Such situations are relevant in the early stage of the core collapse of massive stars, for the nucleosynthesis of thermonuclear supernovae as well for the final evolution of the core of intermediate-mass stars, involving nuclei in the mass range $A \sim 20 - 65$.

This manuscript reviews the experimental and theoretical progress achieved recently in deriving stellar electron capture rates. It also discusses the impact these improved rates have on the various astrophysical objects.

Submitted to: *Rep. Prog. Phys.*

1. Introduction

Electron capture is one of the fundamental nuclear processes mediated by the weak interaction. In this reaction, a free proton or one bound inside a nucleus is transformed into a neutron by capture of an electron producing an electron neutrino. Electron captures on nuclei play an important role in various dense astrophysical environments and all three properties which characterize this process (change of the nuclear charge, reduction of the number of electrons and energy release by neutrinos) have important consequences in these astrophysical environments [1]. Stellar electron captures, however, differ significantly from those which can be studied in the laboratory. In the latter, the decay occurs within an atom (or ion) by capturing an electron from the atomic cloud where electrons in tightly bound orbitals are strongly preferred due to their larger probability density at the nucleus. However, in the high-density, high-temperature environments of stars the atoms are strongly (like in our Sun) or completely ionized (in advanced stellar burning stages or supernovae). Hence stellar capture rates differ from laboratory rates and are, unfortunately, yet not directly experimentally accessible and have to be modelled.

Supernovae are arguably the most important astrophysical sites in which electron captures on nuclei play a decisive role. This includes the core collapse of massive stars [2, 3, 4], the final evolution of the ONeMg cores in intermediate-mass stars [5, 6], the crust evolution of neutron stars in binaries [7, 8] as well as the nucleosynthesis occurring in thermonuclear (Type 1a) supernovae [9, 10]. In all scenarios the densities at which electron captures play a role are in excess of about 10^9 g cm^{-3} and at finite temperatures which range from 10^8 K in electron-capture supernovae to above 10^{10} K which are encountered in the advanced core collapse of massive stars. Under these conditions electrons are characterized by a relativistic Fermi gas with Fermi energies of MeV to tens of MeV. As a consequence, electron captures can occur under these conditions also on nuclei which, under laboratory conditions, are stable [2].

At the relatively low electron energies the capture is dominated by allowed Gamow-Teller (GT) transitions, with forbidden transitions contributing at the higher densities/temperatures or in exceptional cases [2, 3, 11, 12, 13]. This observation has been the basis to recognize the importance of electron captures in core-collapse supernova, but also of the decisive progress that has been achieved in recent years to derive reliable stellar capture rates. The pioneering work of Bethe, Brown, Applegate, and Lattimer [2] derived capture rates on the basis of a single GT transition transforming an $f_{7/2}$ proton into an $f_{5/2}$ neutron. This assumption was motivated by the Independent Particle Model (IPM) structure of ^{56}Fe which is quite abundant during the early collapse phase. The important insight into the collapse dynamics drawn in their pioneering work was that electron capture is a very efficient cooling mechanism and that the entropy stays low during the entire collapse. As a consequence the composition of the core is predominantly made by heavy nuclei rather than being dissociated into free nucleons. The challenge of deriving an improved set of stellar capture rates was taken up by Fuller,

Fowler and Newman who, in a series of papers, outlined the formalism to determine stellar capture rates and applied it to calculate rate tables for nuclei in the mass range $A = 21-60$ at appropriate temperature and density conditions in the core [14, 3, 15, 16]. These derivations were based again on the IPM, but considered experimental data wherever available. Fuller noticed that, within the IPM, GT transitions from pf proton orbitals are Pauli blocked for nuclei with $N \geq 40$ for which the pf shell for neutrons is completely filled [17]. Based on this observation Bruenn derived a parametric description for stellar electron capture rates which assumed vanishing capture rates for all nuclei with neutron numbers $N > 40$ [18]. Although Cooperstein and Wambach pointed out that the Pauli blocking could be overcome at high temperatures and by forbidden transitions [11], the Bruenn prescription has been the default for electron captures in supernova simulations until the early 2000s (e.g. [1]). On this basis, simulations predicted that during the advanced collapse phase for densities in excess of 10^{10} g cm^{-3} electron capture proceeds on free protons rather than on nuclei. As free protons are significantly less abundant than nuclei during the collapse, electron capture and the associated core cooling was drastically throttled once capture on nuclei was blocked.

During the last two decades the role played by electron captures for the supernova dynamics has been decisively revised. This was made possible by new theoretical insights, improved models and not the least by the development of novel experimental techniques to determine nuclear GT strength distributions. This breakthrough was made possible by the observation that strongly forward-peaked cross sections in charge-exchange reactions, mediated by the strong interaction, are dominated by the spin-isospin operator needed to derive weak-interaction GT transitions [19, 20]. The pioneering GT measurements were performed at TRIUMF using the (n, p) charge-exchange reaction [21, 22, 23]. Despite of its moderate energy resolution of about an MeV, these measurements clearly showed that the nuclear GT strength is significantly more fragmented and also reduced in total strength compared to the predictions of the IPM. These findings were subsequently confirmed by measurements performed at KVI, Groningen using the $(d, {}^2\mathrm{He})$ [24, 25, 26] and at NSCL, Michigan State University by exploiting $(t, {}^3\mathrm{He})$ charge-exchange reactions, respectively [27]. With both techniques, experimenters were successful to measure GT strength distributions for many pf shell nuclei with an energy resolution nearly an order of magnitude better than being possible in the pioneering TRIUMF experiments. These measurements became an indispensable constraint for nuclear models, which were developed in parallel to the experimental progress.

Due to the strong energy dependence of phase space electron capture rates are quite sensitive to the detailed fragmentation of the GT strength if the Fermi energies of the electron reservoir and the nuclear Q value are of the same magnitude [12, 28]. This is the case during hydrostatic silicon burning and at the onset of the collapse at core densities up to about 10^{10} g cm^{-3}. Under these conditions the core consists mainly of nuclei in the Fe-Ni mass range, while sd shell nuclei are also present during silicon burning [29]. The method of choice to describe the properties of these nuclei

is the interacting shell model [30]. Due to advances in computational capabilities and progress in software and an improved understanding of the decisive ingredients of the residual interaction, diagonalization shell model calculations became possible for the complete *sd* shell and for *pf* shell nuclei at a truncation level that guaranteed sufficiently converged results for the nuclear quantities needed to derive reliable electron capture rates. This in particular includes detailed description of the GT strength distributions which, except for a slightly shell-dependent constant factor, reproduced the total GT strength and its fragmentation quite well [31, 32]. This success was first used by Oda and collaborators to derive shell model electron capture rates for *sd* shell nuclei [33]. This was followed by the calculation of individual capture rates for nuclei in the mass range $A = 45$–65 based on GT strength distributions derived in large-scale shell model calculations [12, 34]. Due to the finite temperature of the astrophysical environment the shell model calculations also include GT transitions occurring from thermally excited nuclear states. The shell model rates became the new standards in supernova simulations for intermediate-mass nuclei. It turned out to be quite relevant that the shell model rates for *pf* shell nuclei are systematically and significantly smaller compared to the prior rates based on the IPM [12]. As a consequence, simulations with the shell-model rates showed a noticeably slower deleptonization and resulted in different Fe-core masses at the end of the presupernova phase when the collapse sets in [29, 35].

The Pauli blocking of the GT strength at the $N = 40$ shell closure exists in the IPM [17], but can be overcome by correlations which move protons or neutrons into the next major shell (the *sdg* shell) [36]. To describe such cross-shell correlations within the diagonalization shell model requires usually model spaces with dimensions which are not feasible with today's computers. However, such studies exist for ^{76}Se (the intermediate nucleus in the double-beta decay of ^{76}Ge) showing that its GT strength is small, but non-vanishing, even for the ground state [37]. This finding is in good agreement with the experimental determination of the GT strength by the $(d, ^2\mathrm{He})$ technique [38]. As a consequence the stellar electron capture rate on ^{76}Se is sizable, showing that the assumption of neglecting the capture on nuclei with $N > 40$ is not justified. To derive at the stellar capture rate for such nuclei a hybrid model had already been proposed and applied prior to the shell model studies of ^{76}Se. This model is based on two steps [36, 39]: At first, the crucial cross-shell correlations are studied using the Shell Model Monte Carlo approach [40, 41], which is a stochastical approach to the shell model allowing to calculate nuclear properties at finite temperature considering correlations in unprecedentedly large model spaces. These calculations have been applied to determine partial occupation numbers for protons and neutrons in the combined *pf*-*sdg* shells and at finite temperature. In the second step, these partial occupation numbers served as input in RPA calculations of the GT and forbidden strength distributions and subsequently the stellar capture rates. The use of the RPA for these nuclei is justified as they dominate the core abundance only at higher densities and temperatures where the Fermi energy of the electron gas is noticeable larger than the Q value of the respective nuclei requiring only a reasonable reproduction of the total strength and its centroid for

a reasonable estimate of the rate. The hybrid model has been applied to about 200 nuclei in the mass range $A = 65 - 110$ [28]. The studies clearly implied that Pauli blocking of the GT strength is overcome by cross-shell correlations at the temperature/density conditions at which these nuclei are abundant [28, 42]. The SMMC calculations also yield rather smooth trends in the partial occupation numbers at the relevant temperature of about 1 MeV. Based on observation a simple parametrization of the occupation numbers has been derived which was the basis of RPA calculations of stellar capture rates for another 2700 nuclei [13].

On the basis of the shell model calculations for *sd* and *pf* shell nuclei, of the hybrid model for cross-shell $N = 40$ nuclei and the parametric study for the heavier nuclei an electron capture rate table has been derived for core-collapse conditions [13]. The nuclear composition of the core has been assumed to be in nuclear statistical equilibrium (NSE) [43]. When incorporated into supernova simulations these rates had significant consequences for the collapse dynamics. In particular, the simulations show that capture on nuclei dominate over capture on free protons during the entire collapse. Furthermore, the dominating capture on nuclei leads to a stronger deleptonization of the core and to smaller temperatures and entropies, in comparison to the previous belief that capture on nuclei would vanish due to Pauli blocking [28, 42].

As an alternative to the hybrid model, the temperature-dependent Quasiparticle RPA model has been developed and applied to stellar electron capture for selected nuclei by Dzhioev and coworkers [44]. This approach formally improves the hybrid model as it describes correlations and strength function calculations consistently within the same framework. In contrast to the hybrid model it restricts correlations to the 2p-2h level which due to the diagonalization shell model studies is not completely sufficient to recover all cross-shell correlations. This shortcoming is relevant for ground state strength functions, but gets diminished with increasing temperatures. Satisfyingly both quite different approaches yield similar capture rates in the density/temperature regimes where nuclei with neutron gaps at $N = 40$ and $N = 50$ matter during the collapse [45].

Electron capture also plays a role for the final fate of the O-Ne-Mg cores of intermediate-mass stars [46, 47] and for the nucleosynthesis occurring behind the burning flame during a thermonuclear supernova [48, 49]. In these scenarios only *sd*- and *pf*-shell nuclei are relevant and hence the respective diagonalization shell model rates can be applied. For the dynamics of the O-Ne-Mg cores, however, also beta decays are quite decisive for selected nuclei. The relevant rates can also be calculated quite reliable within the shell model (e.g. [33, 50]. It has been pointed out that the electron capture on ^{20}Ne constitutes a very unusual case as its rate is dominated by a second-forbidden ground-state-ground-state transition in the relevant density/temperature regime [51]. As an experimental milestone this transition has very recently been experimentally determined with quite considerable consequences for the fate of intermediate-mass stars [52].

Electron captures on selected nuclei play also a role during hydrostatic stellar burning or during s-process nucleosynthesis. In these environments, ions are not completely stripped from electrons so that the capture predominantly occurs from bound

(K-shell) electrons (however, modified by screening from the surrounding plasma), but also from 'free' electrons out of the plasma. The description of these capture processes requires a different treatment as described here. We will not review these capture processes in this manuscript, but list a few relevant references for the interested readers. An important example for capture during hydrostatic burning is the one on ^{7}Be which is a source of high-energy solar neutrinos. The respective solar rate is derived in [53, 54, 55, 56, 57]. Electron capture on ^{7}Be is also important in evolved stars as it affects the abundance of ^{7}Li in red giant branch and asymptotic giant branch stars [58]. During s-process nucleosynthesis certain pairs of nuclei (like ^{187}Rh-^{187}Os, ^{205}Tl-^{205}Pb) serve as potential cosmochronometers [59]. These pairs are characterized by very small Q values against electron captures so that, in the inverse direction, β decay with an electron bound in the ionic K-shell (or higher shells) becomes possible and even dominates the decay. Such bound-state β decay strongly depends on the degree of ionization and of corrections due to plasma screening, while the competing electron capture process is often modified by contributions due to thermally excited nuclear levels. The formalism to describe the relevant electron capture, β and bound-state β-decay rates for the appropriate s-process temperature and density conditions is derived in [60]; detailed rate tables can be found in [61]. Application of these rates in s-process simulations are discussed in [62]. For reviews of s-process nucleosynthesis the reader is referred to [63, 64].

In this review we will summarize the theoretical and experimental progress achieved during the last two decades in describing stellar electron captures on nuclei. Section 2 is devoted to the experimental advances describing the various techniques to measure Gamow-Teller strength distributions. Section 3 starts with some general remarks defining the strategy how to derive the rates at the relevant conditions, followed by some brief discussions of the adopted models and the rates derived within these approaches.In Section 4 we summarize the consequences of modern electron capture rates in core-collapse supernovae, for the fate of O-Ne-Mg cores in intermediate-mass stars and for the nucleosynthesis in thermonuclear supernovae.

2. Experimental techniques and progress

To accurately estimate electron-capture rates on nuclei present in stellar environments, it is key to have accurate Gamow-Teller strength distributions from which the electron-capture rates can be derived. Direct information about the Gamow-Teller strength distribution can in principle be obtained from β-decay and electron-capture measurements, but this provides only information about transition strengths between ground states and a limited number of final states. Moreover, since in most astrophysical phenomena electron captures near the valley of stability and/or on neutron-rich isotopes are most important, the Q value for β^+/EC decay is often negative and direct information is available only on the Gamow-Teller transition strength from the ground state of the mother to the ground state of the daughter that is derived from β^- decay in the inverse direction, and only if the ground-state to ground-state decay is associated

with a Gamow-Teller transition. Therefore, an indirect method is needed to gain information about Gamow-Teller strength distributions and to benchmark and guide the development of theoretical models for Gamow-Teller strengths. Charge-exchange reactions [20, 65, 66, 67, 26] at intermediate beam energies ($E_b \gtrsim 100$ MeV) have served as that indirect method, as it is possible to extract the Gamow-Teller strength distribution up to sufficiently high excitation energies to perform detailed assessments of the validity of the theoretical models employed. The remarkable feature of this method is that detailed information about transitions mediated by the weak nuclear force can be extracted from reactions with hadronic probes mediated by the strong nuclear force. The methods and associated experimental techniques are described in this section.

It is important to note that only a limited number of charge-exchange experiments can be carried out and that these experiments only provide data on transitions from the ground state of the mother nucleus. Since in many astrophysical scenarios a relatively large number of nuclei play a significant role and, if the stellar environment is at high temperature, transitions from excited states also play a role, it is rarely possible to rely on experimental data of Gamow-Teller strength distributions only. To make accurate estimates for electron-capture rates in stars, theoretical nuclear models are necessary, which can be tested against charge-exchange data where available. Another important consideration is that electron captures in stars take place on stable and unstable nuclei. Hence, the obtain information about the latter, charge-exchange experiments with unstable nuclei are needed. As described below, such experiments are challenging and relevant techniques for performing charge-exchange experiments in inverse kinematics are still in development, although good progress have been made over the past decade.

For the purpose of extracting Gamow-Teller strength distribution of relevance for electron captures in stars, charge-exchange experiments in the β^+/EC direction or (n,p) direction are necessary and the primary focus in this section. These experiments probe proton-hole, neutron-particle excitations. However, charge-exchange data in the β^- or (p,n) direction (neutron-hole, proton-particle excitations) are important as well. Firstly, the development of the techniques to extract Gamow-Teller strengths has been primarily developed by using charge-exchange reaction in the β^- direction, starting with the pioneering work by [68]. Many detailed studies have been performed by using the (^{3}He,t) reaction. benefiting in part from the fact that for mirror nuclei the β^+ decay of the neutron-deficient nucleus and the (p,n)-type reaction on the mirror neutron-rich nucleus populate states with the same isospin. This allows for detailed comparisons of Gamow-Teller strengths through β decay and charge-exchange reactions [69].

Secondly, for certain astrophysical phenomena, detailed information about the Gamow-Teller strengths in the β^- direction are needed. Thirdly, by assuming isospin-symmetry, information about Gamow-Teller strengths in the β^+/EC direction can sometimes be derived from data in the β^- direction. Finally, the theoretical models used to calculate Gamow-Teller strength distributions in the β^+ direction usually rely on the same parameters of the nuclear interaction as those calculated in the β^- direction. Hence, by comparing the results of models against data from charge-

exchange experiments in the β^- direction, additional information about the strengths and weaknesses of those models is obtained. The summed Gamow-Teller strengths in the β^+ and β^- directions are connected through a sumrule, first developed by Ikeda, Fujii and Fujita [70]:

$$S_{\beta^-}(GT) - S_{\beta^+}(GT) = 3(N - Z) \tag{1}$$

Although experimentally, only about 50–60% of the sum-rule strength is observed in the Gamow-Teller resonance at excitation energies below ~ 20 MeV [71, 72], referred to as the "quenching" phenomenon [20], it allows one to obtain information about the strength in the β^+/EC direction from the measurement in the β^- direction. However, as the electron-capture rates that are derived from the Gamow-Teller strength strongly depends on the strength distribution and not just the magnitude of the strength, measurement of the strength in the β^- direction is of limited use for detailed evaluations of the strength distribution. This is especially true for nuclei with increasing neutron number for fixed atomic number as S_{β^-} becomes increasingly larger than S_{β^+}. On the other hand, the Ikeda sum rule is a very useful constraint for the total GT strength for the cross section calculation of charged-current (ν_e, e^-) reactions for neutron-rich nuclei [73, 74].

2.1. The extraction of Gamow-Teller strengths from charge-exchange data

The extraction of the Gamow-Teller strength distribution from charge-exchange reaction data at intermediate beam energies is based on the proportionality between the Gamow-Teller transition strength $B(\mathrm{GT})$ for small linear momentum transfer, $q \approx 0$, expressed through the following relationship [68]:

$$\left[\frac{d\sigma}{d\Omega}(q,\omega)\right]_{GT} = F(q,\omega)\hat{\sigma}B(\mathrm{GT}), \tag{2}$$

in which $\frac{d\sigma}{d\Omega}(q,\omega)$ is the measured differential cross section for a transition associated with energy transfer $\omega = Q_{gs} - E_x$ and linear momentum transfer q. Q_{gs} is the ground-state reaction Q value that is negative for a transition that requires energy. E_x is the excitation energy of the final nucleus. $B(\mathrm{GT})$ is the Gamow-Teller transition strength and represents the same matrix elements as probed in β and EC decay transitions between the same initial and final states. The condition that $q = 0$ requires that the cross section is extracted at or close to a center-of-mass scattering angle of zero degrees and that an extrapolation is required based on a calculation to correct for the finite reaction Q value. This extrapolation is represented by the factor $F(q,\omega)$. The factor $\hat{\sigma}$ is the so-called unit cross section, which depends on the reaction kinematics, the nuclei involved in the interaction and the properties of the nucleon-nucleon (NN) interaction. In the Eikonal approximation [68], these components are factorized:

$$\hat{\sigma} = KN|J^2_{\sigma\tau}|. \tag{3}$$

In this factorization, K is a calculable kinematic factor, N is a distortion factor, and $J_{\sigma\tau}$ is the volume integral of the spin-transfer, isospin-transfer $\sigma\tau$ component of the NN interaction [75]. The distortion factor accounts for the distortion of the

incoming (outgoing) particle by the mean-field of the target (residual) nucleus and can be estimated by taking the ratio of a distorted-wave impulse or Born approximation calculation to a plane-wave calculation [68]. The strength of the method to extract Gamow-Teller distributions from charge-exchange data is that the details of the components that make up the unit cross section do not need to be known since the unit cross section is conveniently calibrated by using transitions for which the B(GT) is known from β-decay experiments. Once established for one or a few transitions for given nucleus and charge-exchange reaction, the proportionality can be applied to all transitions identified as being associated with $\Delta L = 0$ and $\Delta S = 1$, except for the extrapolation to $q = 0$ through the factor $F(q, \omega)$ of Eq. 2. This extrapolation carries a relatively small uncertainty. Calibrations against known transitions from β decay are not always possible. Therefore, mass-dependent parametrizations of the unit cross sections have been successfully developed for the $(p, n)/(n, p)$ [76] and $(^3\mathrm{He}, t)/(t, ^3\mathrm{He})$ [77, 78] reactions, which provide a convenient way to extract Gamow-Teller strength distributions for such cases.

In order to use Eq. 2 and extract the Gamow-Teller strength distribution from measured differential cross sections, one must first identify the contributions to the experimental spectra that are associated with monopole ($\Delta L = 0$) and spin-transfer ($\Delta S = 1$). This is performed by investigating the differential cross sections as a function of scattering angle, since excitations that are associated with increasing units of angular momentum transfers have angular distributions that peak at larger scattering angle. Therefore, through a process called multipole decomposition analysis (MDA) [79], in which the measured differential cross sections of a particular peak or data in an excitation-energy bin is fitted by a linear combination of calculated angular distributions for different units of ΔL, the $\Delta L = 0$ contribution to the cross section is extracted. An example for the $^{46}\mathrm{Ti}(t, ^3\mathrm{He})$ reaction is shown in Fig. 1. Since the $\Delta L = 0$, $\Delta S = 0$ contribution is almost completely associated with the excitation of the isobaric analog state, it does not contribute to the $\Delta L = 0$ yield for (n, p)-type reactions for nuclei with $N \geq Z$, as the isospin of states in the final nucleus always exceed that of the target. The Fermi sum rule of $S_- - S_+ = (N - Z)$ is nearly fully exhausted by the excitation of the isobaric analog state in the β^- (p, n) direction.

For (n, p)-type reactions, at excitation energies $\gtrsim$ 10 MeV, contributions to the $\Delta L = 0$ yield arise from the excitation of the isovector giant monopole resonances (IVGMR) and isovector spin giant monopole resonance (IVSGMR) [65]. In charge-exchange reactions with beam energies of $\gtrsim$ 100 MeV, the IVSGMR dominates. Since the angular distribution of the IVSGMR is very similar to that of Gamow-Teller excitations, the two are not easily separable experimentally. Only through a comparison between (n, p) and $(t, ^3\mathrm{He})$ data it is possible to disentangle the two contributions [81]. Since the transition density for the IV(S)GMR has a node near the nuclear surface, a cancellation occurs for the (n, p) probe that penetrates relatively deeply into the nuclear interior, whereas such a cancellation does not occur for the peripheral $(t, ^3\mathrm{He})$ reaction [82, 83]. Hence, the excitation of the IV(S)GMR is enhanced for the latter

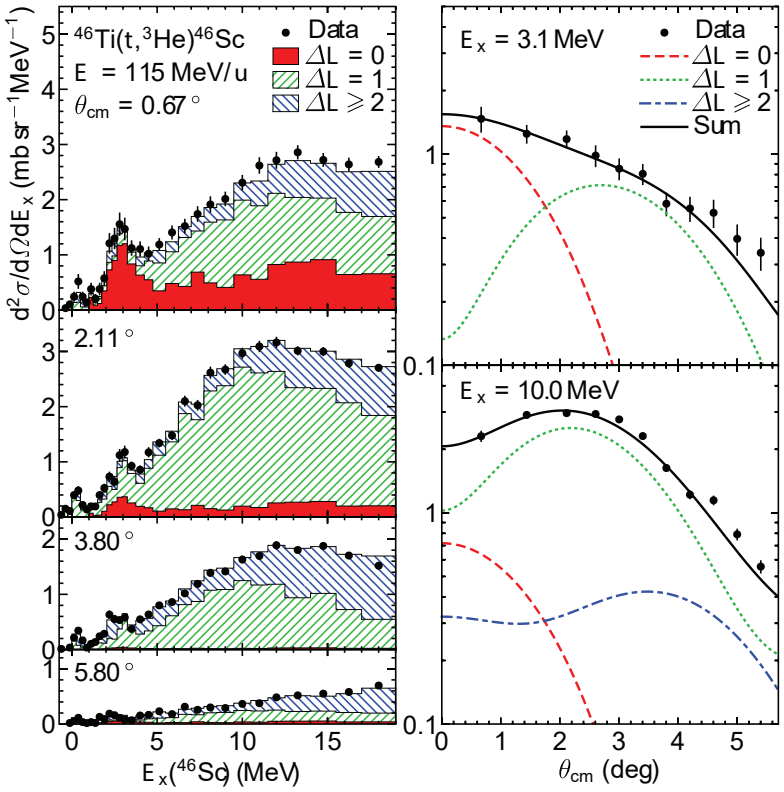

Figure 1. An example of the MDA for the ^{46}Ti$(t,{}^3$He) reaction at 115 MeV/u. On the left-hand side, differential cross sections at 4 scattering angles are shown. On the right-hand side, the MDA analyses for two excitation energy bins (at 3.1 MeV and 10 MeV) in ^{46}Sc are shown. At 3.1 MeV (10.0 MeV), the $\Delta L = 0$ ($\Delta L = 1$) contribution is strongest. The stacked colored histogram on the left-hand side indicate the contributions from the different angular momentum transfers based on the MDA. (from Ref. [80]).

probe. As this comparison between probes is generally not available, the extraction of Gamow-Teller strengths for the purpose of estimating electron-capture rates and bench marking the theory is usually limited to excitation energies up to about 10 MeV.

Since the extracted Gamow-Teller strengths from the charge-exchange data are calibrated against known weak transitions strengths, the uncertainties introduced by the need to extract absolute cross sections through careful beam intensity normalizations and target thickness measurements are absent. If phenomenological relationships between the unit cross section and mass number are utilized [77] to determine the unit cross section, usually a measurement with a target for which the unit cross section has been well established is included in an experiment, so that a relative normalization can be performed, rather than relying on an absolute cross section measurement that is usually more uncertain. This helps to reduce experimental systematic uncertainties to about 10% [77].

The main remaining uncertainties in the extraction of Gamow-Teller strengths arise

from effects that perturb the proportionality of Eq. 3. It has been shown [27, 84] that the leading cause for the perturbation of the proportionality is due to the interference between $\Delta L = 0$, $\Delta S = 1$ and $\Delta L = 2$, $\Delta S = 1$ amplitudes that both contribute to $\Delta J = 1$ transitions in which the parity does not change. This interference is mediated by the tensor-τ component of the NN force [75, 20]. The uncertainty introduced by this effect depends on the magnitude of the Gamow-Teller transition strength and was estimated [27] to be $\approx 0.03 - 0.035 \ln(B(\mathrm{GT}))$, which amounts to an uncertainty of about 20% for $B(\mathrm{GT})$=0.01. The results of this study are shown in Fig. 2. A $B(\mathrm{GT})$ of 0.01 is close to the detection limit in charge-exchange experiments. It has been shown that this uncertainty estimate is not strongly dependent on the nucleus studied [84]. It is also clear that the systematic deviation fluctuates around 0, and after integrating over many states, the uncertainty in the summed or average transitions strength is small.

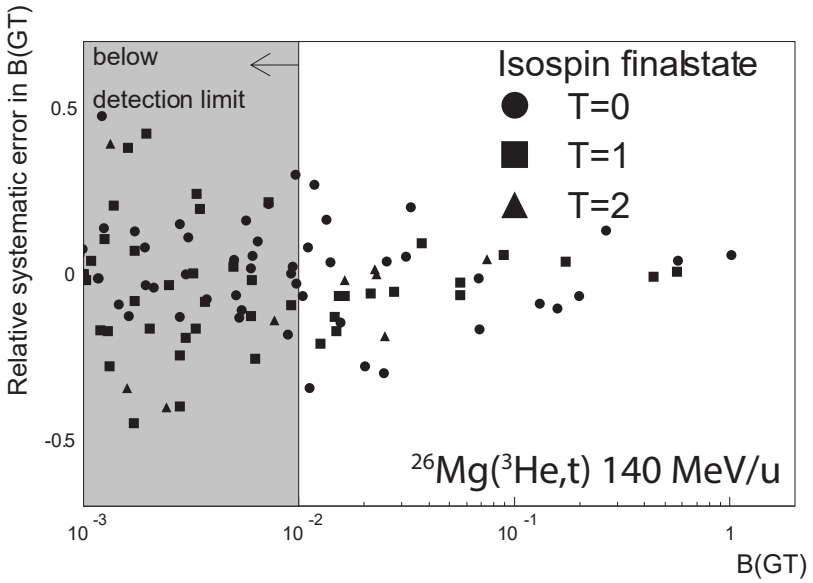

Figure 2. Results from a theoretical study to estimate the magnitude of the uncertainty in the proportionality between Gamow-Teller strength and differential cross sections for the ^{26}Mg(^{3}He, t) reaction at 140 MeV/u due to the effects of the tensor-τ component of the NN interaction. Transitions to final states in ^{26}Al with isospin $T = 0, 1$, and 2 are included. The uncertainty increases with decreasing $B(\mathrm{GT})$. The detection limit of 0.01 is indicated. (from Ref. [27]).

2.2. Probes

The extraction of Gamow-Teller strengths from charge-exchange reactions in the β^+ direction for the purpose of constraining electron-capture rates has primarily been performed with three probes: the (n, p), $(d, {}^2\mathrm{He})$, and $(t, {}^3\mathrm{He})$ reactions. In this subsection, a brief overview of these three probes and experimental methods will be provided.

2.2.1. (n,p) *reaction* Although (n,p) charge-exchange reactions have been performed at a variety of facilities, the pioneering work at TRIUMF has been particularly impactful for the purpose of testing theoretical models used to estimate electron-capture rates for astrophysical simulations. The nucleon charge-exchange facility at TRIUMF [85, 86] utilized the (p,n) reaction on a ^{7}Li target to produce neutrons of about 200 MeV associated with transitions to the ground and first excited state of ^{7}Be that were subsequently impinged on the reaction target of interest. The setup used a segmented target chamber, which allowed for the insertion of several targets simultaneously. Events induced by reactions on different targets were disentangled through the analysis of hitpatterns in multi-wire proportional chambers placed in-between the targets. Usually, one of the targets was a CH_2 target, so that the well-known ^{1}H(n,p) reaction could be utilized to perform absolute normalizations of the neutron beam intensity. Protons produced in the (n,p) reaction were momentum analyzed in the medium-resolution spectrometer (MRS). Measurements at different scattering angles were utilized to determine the differential cross sections as a function of center-of-mass angles, facilitating the multipole decomposition analysis and extraction of Gamow-Teller strength from the proportionality between strength and differential cross section discussed above. A wide variety of experiments were performed for the purpose of extracting Gamow-Teller strengths for astrophysical purposes, primarily on stable nuclei in the pf shell (see e.g. [87, 88, 89, 90, 91, 92, 93]). The excitation energy resolutions achieved varied between 750 keV and 2 MeV, depending on the experiment. In Fig. 3, three examples of the extracted $\Delta L = 0$ contributions for the ^{60,62,64}Ni(n,p) reactions are shown, displaying a concentration of Gamow-Teller strength at low excitation energies, with a long tail up to higher excitation energies.

2.2.2. $(d,{}^{2}\mathrm{He})$ *reaction* The $(d,{}^{2}\mathrm{He})$ reaction has become one of the most powerful probes to study the Gamow-Teller strengths in the β^+ direction. This probe was first developed for the purpose of extracting Gamow-Teller strengths at RIKEN by using a 260 MeV deuteron beam [94], followed by the development of this probe at Texas A&M [95] by using a 125 MeV deuteron beam. In these experiments, a resolution of 500–700 keV could be achieved, and the beam intensities were limited due to the background from deuteron break-up reactions. The method was perfected in experiments with the Big-Bite Spectrometer at KVI in combination with the EuroSuperNovae (ESN) detector [96] and using deuteron beams of $\sim$ 170 MeV. Owing to the use of data signal processing, two-proton coincidence events could be selected online, strongly reducing the background from deuteron break-up reactions and making it feasible to run at higher incident beam rates. In addition, the excitation energy resolution was improved to values of typically 150 keV. A recent overview of the $(d,{}^{2}\mathrm{He})$ program at KVI can be found in Ref. [26].

The use of the $(d,{}^{2}\mathrm{He})$ probe requires that the momentum vectors of the two protons from the unbound ^{2}He must be measured with high accuracy in order to reconstruct the momentum of the ^{2}He particle created in the $(d,{}^{2}\mathrm{He})$ reaction, as well as the

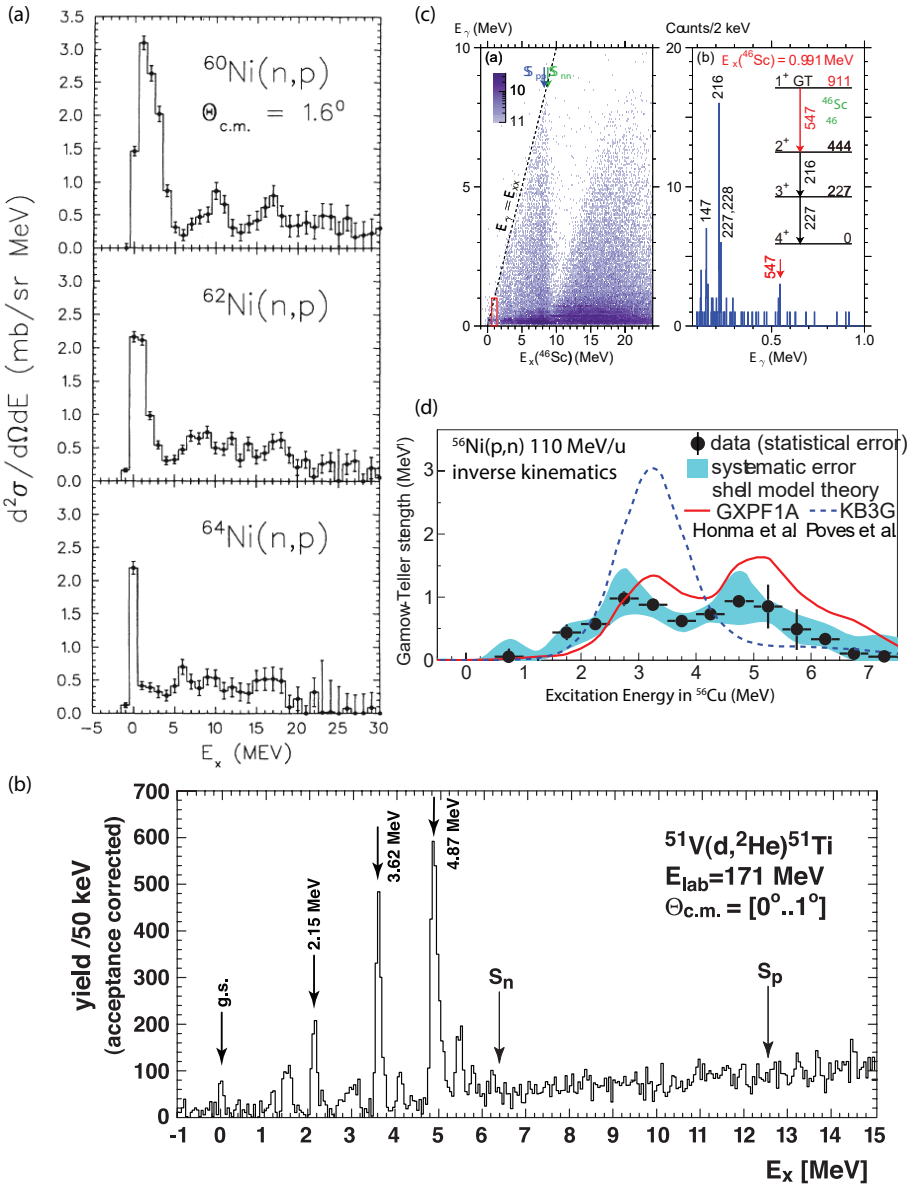

Figure 3. (a) Differential cross sections associated with $\Delta L = 0$ for the ^{60,62,64}Ni(n,p) reaction at 198 MeV (from Ref. [93]). (b) Differential cross sections at forward scattering angles for the ^{51}V$(d,^2$He) reaction at 170 MeV. Owing to the high-resolution, individual transitions are well resolved (from Ref. [97]). (c) left: γ energy versus excitation energy for the ^{46}Ti$(t,^3$He+$\gamma)$ reaction (see also Fig. 1). right: by gating on the ^{46}Sc excitation-energy range around 0.991 MeV, the decay by a very weak 1^+ state can be identified, sufficient for estimating the Gamow-Teller transition strength to this state (from Ref. [80]). (d) Extracted Gamow-Teller strength distribution from the ^{56}Ni(p,n) reaction at 110 MeV/u, performed in inverse kinematics. Two sets of shell model-calculations with different interactions are super imposed (from Ref. [98]).

relative energy ϵ between the two protons. On the other hand, the determination of the relative energy makes it possible to enhance the spin-transfer nature of the probe. As the incident deuterons are primarily in the $^3S_1$ state, a spin-transfer ΔS of 1 is ensured if the outgoing protons couple to the $^1S_0$ state, which can be accomplished by reconstructing the relative energy between the protons and selecting events that have small relative energies (typically smaller than 1 MeV). This removes transitions associated with $\Delta S = 0$ from the spectra and makes it easier to isolate the $\Delta S = 1$ Gamow-Teller transitions.

A variety of $(d, ^2\mathrm{He})$ experiments were performed at KVI with the goal to extract Gamow-Teller strengths for testing theoretical models used to estimate electron-capture rates of interest for astrophysical simulations, see e.g. Refs. [99, 97, 100, 101, 102, 103, 104]. Because of the high resolution achieved, detailed studies of the Gamow-Teller strength distribution could be performed, including for nuclei for which it was difficult to obtain the targets, such as ^{50,51}V [97, 100], as shown in Fig. 3(b). Clearly, the excellent resolution achieved makes it possible to extract very detailed information about the Gamow-Teller strength distribution.

2.2.3. $(t, ^3\mathrm{He})$ *reaction* The use of the $(t, ^3\mathrm{He})$ reaction has the disadvantage that it is complicated to generate tritium beams. Although tritium has been used to produce primary beams (see e.g. Ref. [105]), experiments performed for the purpose of extracting Gamow-Teller strength distributions for astrophysical purposes utilized secondary tritium beams. These experiments are performed at NSCL with the S800 Spectrometer [106]. A primary ^{16}O beam is impinged on a thick Beryllium production target to produce a secondary tritium beam of 345 MeV [84]. Because the momentum spread of the secondary beam is large (typically 0.5%), the dispersion-matching technique [107] is utilized to achieve excitation-energy resolutions ranging from $200-350$ keV. At present, the beam intensities are limited to about 10^7 particles per second, but with the completion of the Facility for Rare Isotope Beam (FRIB), the beam intensities will increase significantly.

In addition to the good excitation-energy resolution that can be achieved with the $(t, ^3\mathrm{He})$ reaction, it has the advantage that the inverse $(^3\mathrm{He}, t)$ reaction is studied in great detail and with excellent resolution at comparable beam energies [67, 78, 26]. This makes it possible to utilize the dependence of unit cross section on mass number determined from $(^3\mathrm{He}, t)$ data for extracting Gamow-Teller strengths from $(t, ^3\mathrm{He})$ experiments [27, 77, 78].

As for the (n, p) and $(d, ^2\mathrm{He})$ reactions, the $(t, ^3\mathrm{He})$ reaction has been used to study a variety of nuclei to test theoretical models used in the estimation of electron-capture rates in astrophysical scenario, e.g. Refs. [108, 109, 110, 111, 112, 80, 113, 114]. Since the electron-capture rate is very sensitive to the transitions to the lowest-lying final states in the daughter nucleus, especially at low stellar densities, the $(t, ^3\mathrm{He})$ probe was combined with the high-resolution detection of γ-rays in the Gamma-Ray Energy Tracking In-beam Nuclear Array (GRETINA) [115]. This has made it possible to extract

Gamow-Teller transition strengths of as low as 0.01 [80], as shown in Fig. 3c for the ^{46}Ti$(t, {}^3\mathrm{He}+\gamma)$ reaction, for which the $B(\mathrm{GT})$ for the transition to the first 1^+ state at 0.991 MeV could only be determined due to the measurement of the decay γ rays.

In recent years, the focus of the experiments has shifted from nuclei in the pf-shell to nuclei near $N = 50$ [108, 109, 110] given their relevance for electron capture rates during the collapse of massive stars (see section 4.1).

2.2.4. (p, n) reaction and isospin symmetry For nuclei with $N > Z$, the Gamow-Teller transition strength in the β^+ direction can also be extracted from (p, n) reactions under the reasonable assumption that isospin-symmetry breaking effects are small. Hence, states with isospin T_0+1 populated from a (n, p)-type reaction for a nucleus with ground-state isospin of T_0, have analogs in the (p, n)-type reaction on that same nucleus. By measuring the (p, n)-type reaction and identifying the T_0+1 states in the spectrum, the Gamow-Teller transition strengths of relevance for estimating electron-capture rates can be extracted. Unfortunately the excitation of states with higher isospin is suppressed compared to states with lower isospin [116], and the $T_0 + 1$ states sit on a strong background of states with isospin $T_0 - 1$ and T_0, which are also excited in a (p, n)-type reaction on a nucleus with isospin T_0. Still for nuclei near $N = Z$ Gamow-Teller strengths have been extracted from (p, n) data for the purpose of testing theoretical models used to estimate electron-capture rates in nuclei [117, 118].

For nuclei with $N = Z$ and assuming isospin symmetry, the Gamow-Teller strength distribution in the β^+ and β^- directions are identical and a (p, n)-type measurements can be used to directly obtain the Gamow-Teller strength distribution of relevance for the electron-capture rates. This feature was used to extract the Gamow-Teller strength distribution from ^{56}Ni. By using a novel method to perform a (p, n) experiment in inverse kinematics [98, 119], the Gamow-Teller strength distribution in ^{56}Cu was extracted (see Fig. 3(d), which is the same as the Gamow-Teller strength distribution from ^{56}Ni to ^{56}Co. In this experiment, the excitation-energy spectrum in ^{56}Cu was reconstructed by measuring the recoil neutron from the (p, n) reaction when the ^{56}Ni beam was impinged on a liquid hydrogen target. Since it is important to measure the reactions at small linear momentum transfer to main the proportionality of Eq. 2, the relevant recoil neutrons have very low energies and were detected in a neutron-detector array developed especially for that purpose [120]. With this method, it became possible to measure (p, n) reaction in inverse kinematics on any unstable nucleus and it was recently used to study ^{132}Sn [121].

2.3. (n, p)-type charge-exchange reactions on unstable isotopes

Since many of the nuclei that undergo electron captures in stellar environments are unstable, it is important to develop experimental techniques to perform (n, p)-type charge-exchange experiments in inverse kinematics. This poses a significant challenge. A neutron target is not available and all candidate reactions have a light low-energy

charged particle as the recoil, which is not (easily) detectable as it interacts with the target material. Therefore, unlike in the (p,n) reaction, the recoil particle is not readily available for the precise reconstruction of the excitation energy and scattering angle of the reaction. If the excitation-energy of the residual nucleus after the charge-exchange reaction is below the nucleon separation energy, a precise measurement of the momentum and scattering angle of the residual can be sufficient to reconstruct the event kinematics. This method was used to extract the low-lying β^+ Gamow-Teller strength distributions from unstable nuclei ^{12}B and ^{34}Si through the (^{7}Li, ^{7}Be) reaction in inverse kinematics [122, 123]. Unfortunately, this probe is very difficult to use for studying Gamow-Teller strength distributions in unstable nuclei heavier than ^{34}Si. If the excitation energy of the residual exceeds the nucleon separation energy, it is necessary to measure the decay nucleon in addition to measuring the residual and achieving the necessary energy and angular resolutions to reconstruct the event kinematics becomes challenging because of the strong forward kinematic boost of the laboratory reference frame [122].

Most recently, efforts have been initiated to utilize the $(d, ^2\mathrm{He})$ reaction in inverse kinematics to study (n,p)-type charge-exchange reactions on unstable isotopes. In such experiments, the rare-isotope beam is impinged on an active-target time projection chamber in which deuteron gas serves both as the target and the detector medium [124]. The tracks from the two protons originating from the unbound ^{2}He particle can be used to reconstruct the momentum of the ^{2}He particle, from which the excitation energy and scattering angle of the charge-exchange reaction can be determined. The unique two-proton event signature is also very helpful to separate the $(d, ^2\mathrm{He})$ reaction from other types of reactions that occur in the time projection chamber and that have much higher cross sections. If successful, the method will be equally powerful for the extraction of Gamow-Teller strengths in the β^+ direction as the (p,n) reaction in inverse kinematics is for the extraction of Gamow-Teller strengths in the β^- direction.

3. Strategy and model to calculate stellar electron capture rates

During their long lasting lives stars balance gravitational contraction thanks to the energy gained from nuclear fusion reactions in their interior. Massive stars develop a sequence of core burning stages (started by hydrogen burning via the CNO cycle, then followed by helium, carbon, neon, oxygen and the finally silicon burning). During this evolution the density ρ and temperature T in the core increases gradually and has reached values in excess of 10^9 g cm^{-3} and 10^9 K, respectively, at the end of silicon core burning. At these high temperatures nuclear reactions mediated by the strong and electromagnetic force are in equilibrium with their inverse reactions. This situation is called Nuclear Statistical Equilibrium (NSE) and determines the nuclear composition for given values of temperature, density and the proton-to-neutron ratio (usually defined by the proton-to-nucleon ratio Y_e). Once NSE is reached the star cannot generate energy from nuclear fusion reactions anymore. Hence the core looses an important source of

pressure against gravitational contraction. This situation is reached in the core produced by silicon burning. This core is usually called Fe core because it is made of nuclei in the Fe-Ni mass range which are favored under the core density and temperature conditions and for a Y_e value only slightly smaller than 0.5. However, the electrons, present in the core to balance the charges of protons, form a highly degenerate relativistic gas and can balance the gravitational contraction of a stellar mass up to the famous Chandrasekhar limit $M_{Ch} = 1.44(Y_e)^2 M_\odot$ with the solar mass denoted by $M_\odot$. Once this limiting mass is exceeded to continued silicon burning or, as we will see below, due to electron captures, the electron gas cannot stabilize the core anymore. The core collapses under its own gravity.

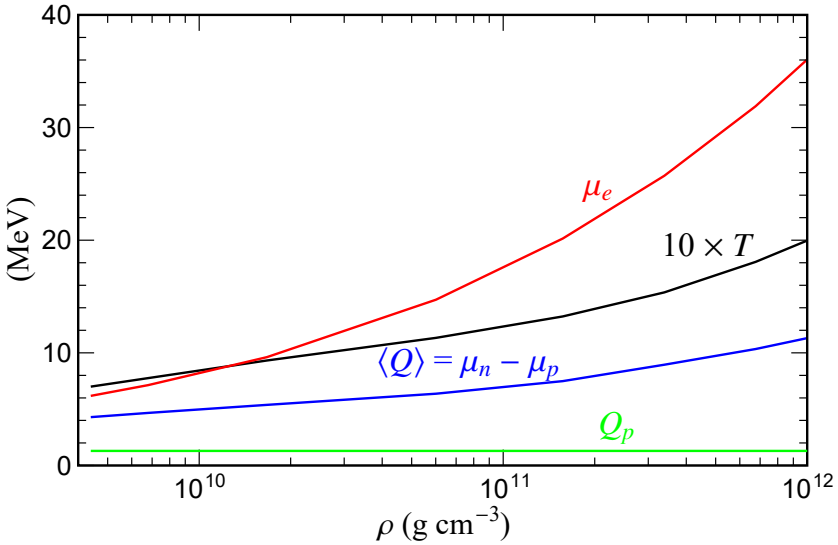

Figure 4. Various energy scales related to electron captures on nuclei and protons as function of density during the collapse. Shown are the temperature, T, the chemical potential of electrons, μ_e, the Q value for electron capture on protons (constant) and the average Q value for electron capture on nuclei approximated as the difference in chemical potential of neutrons and protons (adapted from [25]).

It is important to note that Y_e can be modified by charge-changing reactions which, however, can only be mediated by the weak interaction. Such reactions (electron capture, beta decay) are not in equilibrium under the early collapse conditions (as for example the neutrinos produced by the processes can leave the star and hence are not available to initiate inverse reactions) and can change the nuclear composition. It is also very important to note that under core-collapse supernova conditions, i.e. at sufficiently high densities, electron capture and beta decay do not balance each other. The reason for this unbalance lies in the fact that the electron Fermi energy, which scales like $\rho^{1/3}$, grows noticeably faster than the Q values of the nuclei present in the core (see Fig. 4). As a consequence, the electron capture rates are accelerated, while beta decays on the opposite are throttled due to Pauli blocking of the final electron states. Hence electron captures win over beta decays with three very important consequences. First, electron captures reduce the number of electrons and hence the degeneracy pressure which the

electron gas can stem against the gravitational collapse. Second, the neutrinos produced in the capture process can leave the star nearly unhindered during the early phase of the collapse. They carry energy away which serves as an effective cooling mechanism and keeps the core temperature and entropy low. As consequence of the low entropy heavy nuclei exist during the entire collapse phase. The situation changes when the collapse reaches densities of order 10^{12} g cm^{-3} where the diffusion time scale due to coherent scattering on nuclei becomes longer than the collapse time of the core. Neutrinos are then effectively trapped in the core which until bounce collapses as a homologous unit. Third, electron capture reduces Y_e and makes the core composition more neutron-rich. The NSE composition is driven to heavier nuclei with larger neutron excess (see Fig. 5). This effect is the reason why nuclei with valence protons and neutrons in different major shells become relevant for electron captures, introducing the Pauli unblocking as mentioned above.

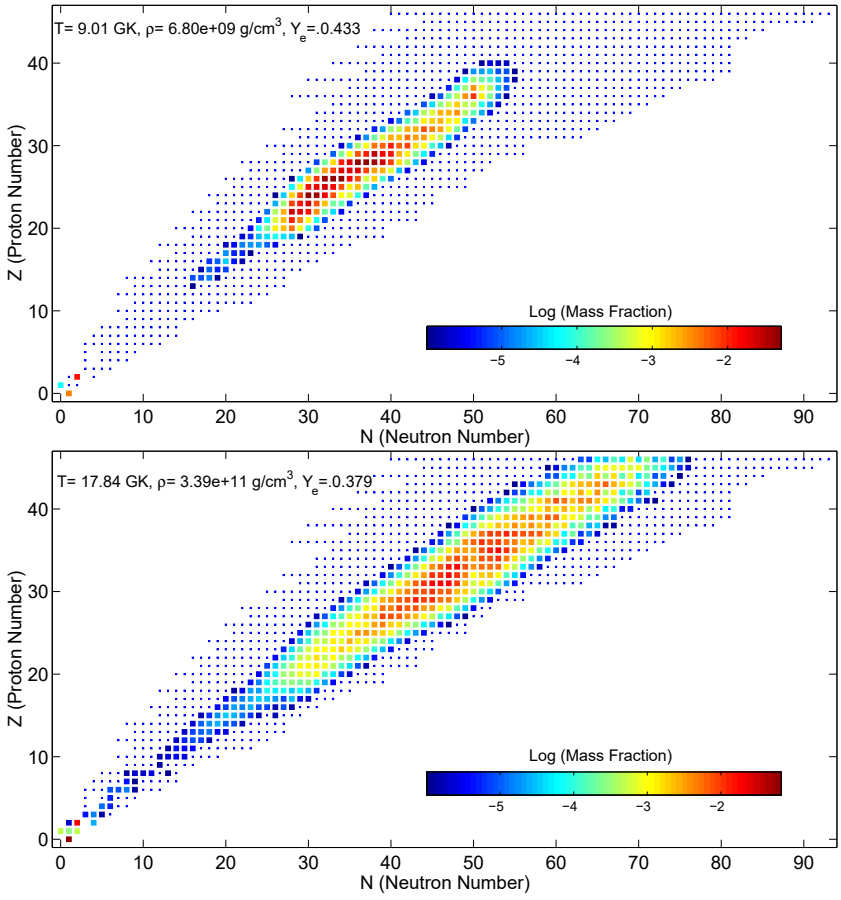

Figure 5. Mass fraction of nuclei in Nuclear Statistical Equilibrium at conditions which resemble the presupernova stage (top) and the neutrino trapping phase (bottom) of core-collapse simulations (courtesy of W.R. Hix).

Electron capture plays an important role for the dynamics of the core collapse of massive stars for core densities between 10^9 g cm^{-3} and 10^{12} g cm^{-3}. Fig. 4 shows the evolution of crucial energy scales for this density regime. The strongest growing quantity

is the electron chemical potential μ_e which increases from 6 MeV to about 40 MeV. As nuclei get increasingly more neutron rich due to continuous electron captures, the average electron capture $\langle Q \rangle$ value of the nuclear composition present at the various stages of collapse grows too, but this increase is noticeably smaller from about 4 MeV to 12 MeV. At all stages the average nuclear $\langle Q \rangle$ value is larger than for free protons (1.29 MeV). Finally the temperature in the core also grows during the collapse, from about $T = 0.8$ MeV to $T = 2.0$ MeV. The comparison of these different energy scales allows us to derive a strategy how to determine electron capture rates at the various stages of collapse.

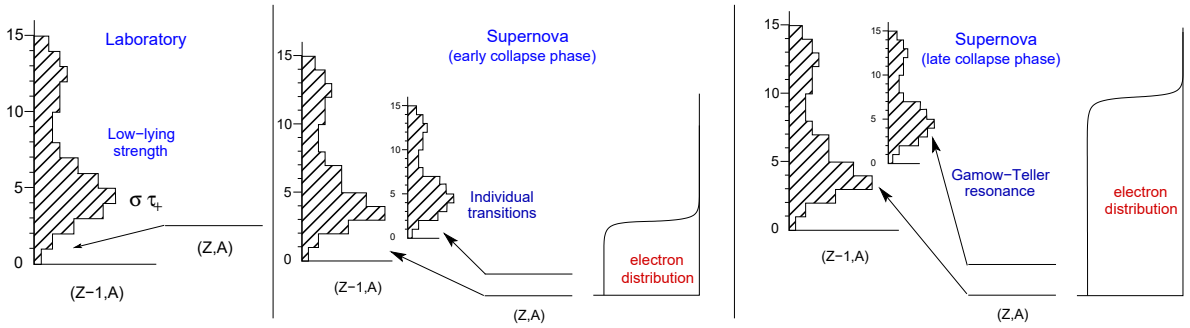

Figure 6. Sketch of electron capture conditions at different conditions: a) in the laboratory (left) where the electron is captured from an atomic orbital, b) in the early collapse phase (middle) where the electron is captured from a Fermi-Dirac (FD) distribution with an electron chemical potential of order the nuclear Q value, and c) later in the collapse at higher densities where the electron is captured from a FD distribution with a chemical potential which are noticeably larger than the nuclear Q values. It is important that, with increasing core density, the electron chemical potential grows faster than the average nuclear Q value. Electron captures in the star (middle and left) can also proceed from thermally excited states where the temperature, respectively average nuclear excitation energy, is increasing during the collapse.

Fig. 6 depicts the consequences which the different behavior of the energy scales has for the electron capture process. We schematically compare the situation in the laboratory with the one in the early stage of the collapse where $\mu_e \approx \langle Q \rangle$ and at an advanced stage with $\mu_e \gg \langle Q \rangle$. In the laboratory the daughter nucleus must be more bound than the decaying nucleus ($Q < 0$). In our schematic sketch of the GT strength distribution we indicate that the strongest GT transitions at a few MeV excitation energies are not accessible in laboratory electron captures. The situation changes completely in the stellar interior, as the capture occurs from a degenerate electron gas. In the early collapse phase (middle diagram) electron Fermi energy and nuclear Q value are similar (for example the Q value of the abundant ^{56}Fe is 4.20 MeV) which makes the calculation of the rate quite sensitive to the reproduction of the low-lying GT strength distribution. An additional complication arises from the fact that the stellar environment has a finite temperature. Hence the capture can also occur from thermally excited nuclear states which can have different GT strength distributions than the ground state. The nuclear composition at this stage of the collapse is dominated by

nuclei of the Fe-Ni range. This is a fortunate situation as diagonalization shell model calculations for pf shell nuclei are now feasible and have been proven to reproduce GT strength distributions and energy levels quite well. Thus, diagonalization shell model is the method of choice to determine the capture rates for pf shell (and sd shell) nuclei.

Due to continuous electron captures the nuclei abundant in the core composition become more neutron rich and heavier. The right panel of Fig. 5 shows the NSE distribution for the conditions reached around the onset of neutrino trapping. The most abundant nuclei correspond to nuclei with valence protons in the pf shell, while the valence neutrons occupy orbitals in the sdg shell. Hence the description of cross-shell correlations is the challenge to determine capture rates for these nuclei. We also note that at the higher densities more nuclei contribute to the NSE abundances. This is an effect of the slight increase of core entropy as neutrino-trapping sets in and of the decrease of the relative differences of nuclear binding energies as the composition moves to heavier neutron-rich nuclei. The right part of Fig. 6 describes the energy situation encountered at higher densities in the collapse (a few 10^{10} g cm^{-3} and above). At first, the electron chemical potential is now significantly larger than the average nuclear Q-value. For example, the neutron-rich nuclei ^{66}Fe (with $N = 40$) and ^{82}Ge ($N = 50$) have Q-values of 13.8 MeV and 13.0 MeV, respectively. Furthermore the temperature has grown to about $T = 1$ MeV. At such temperatures the average nuclear excitation energy, estimated in the Fermi gas model as $E^* = A\,T^2/8$ is 8.3 MeV for ^{66}Fe and 10.2 MeV for ^{82}Ge and the capture, on average, occurs from excited states, making it even easier for electron capture to overcome the Q value. Under these conditions calculations of stellar capture rates for the abundant nuclei on the basis of the diagonalization shell model are not appropriate nor possible. At first, diagonalization shell model studies of nuclear GT strength distributions for the relevant cross-shell nuclei is not feasible due to model space restrictions yet. Moreover, there are simply too many thermally excited nuclear states in the mother nucleus which can contribute to the capture process. However, the detailed reproduction of the GT strength distribution — as required at lower densities where pf shell nuclei dominate — is not needed at the advanced conditions of the collapse. At first, the fact that the electron Fermi energy and the average nuclear excitation energy are together noticeably larger than the average nuclear Q value makes the capture rate less sensitive to the detailed reproduction of the GT strength distribution. Thus it suffices if the total GT strength and its centroid are well described. This is possible within the Random Phase approximation (RPA). Second, due to the exponential increase of the level density with excitation energy, there will be many states which contribute to the capture so that some averaging is expected over the GT strength functions. However, there are two further demands which have to be considered. The Pauli unblocking of the GT strength requires the consideration of multi-particle-multi-hole correlations. These correlations are not expected to be the same at the higher excitation energies than for the ground state. A many-body method which accounts for both of these effects is the Shell Model Monte Carlo approach which allows the calculation of average nuclear properties at finite temperature considering all many-body correlations in unprecedentedly large

model spaces [41]. Hence a hybrid model has been proposed to calculate stellar electron capture rates for heavy nuclei: In the first step partial proton and neutron occupation numbers are determined within the SMMC, which, in the second step, become the input of RPA calculations of the GT and forbidden strength distributions from which finally the capture rates are evaluated [39]. An alternative method to the hybrid model is the temperature-dependent Quasiparticle RPA approach which treats the ground state and thermally excited states consistently on the level of 2p-2h correlations [44]. This approach has also been used to describe astrophysically important neutrino-nucleus reactions at finite temperatures [125, 126] (for a review on this subject see [74]).

3.1. Capture rates for nuclei with $A < 65$

The method of choice to determine electron capture and beta decay rates for medium mass nuclei is the diagonalization shell model. As the shell model allows for the description of individual states and their properties, within the chosen model space, the stellar electron capture rate can be determined on the basis of the state-by-state formalism from states in the parent nucleus at energy E_i to final states in the daughter nucleus at E_f. This formalism explicitly considers that the stellar interior has finite temperature T Thus beta decays and electron captures can occur from excited nuclear levels, where the thermal nuclear ensemble is described by a Boltzmann distribution. Beta-decay λ_β and electron capture rates λ_{ec} can be derived in perturbation theory and the respective formulas and derivations are presented in [14, 34]. Analytical approximations are provided in [51]. In the derivation of the weak-interaction rates only Gamow-Teller transitions are included (with an important exception for ^{20}Ne, as discussed below).

3.1.1. pf shell nuclei The first derivation of stellar weak interaction rates for the pf-shell nuclei relevant for core-collapse supernovae has been presented in Ref. [12]. The calculations are based on diagonalization shell model calculations considering either all correlations in the complete pf shell or at a truncation level which basically guaranteed convergence of the low-energy spectra and the GT strength distributions which are the essential quantities to calculate electron capture and beta decay rates. The GT strength functions were determined using the Lanczos method. Hence it represents the strength for individual states at low energies, while at moderate excitation energies the GT strength is not completely converged and gives the average value for a rather small energy interval. We note that the shell model gives in general a good account of nuclear properties in the pf shell if appropriate residual interactions including monopole corrections are used (see Ref. [30] and references therein). Ref. [32] presented detailed studies of the GT strength distributions and validated the method by comparison to the charge-exchange data available at that time. In fact, good agreement with data was found, if the shell model GT distributions were reduced by a constant factor $(0.74)^2$ ([127, 128]). The origin of this renormalization (often called quenching of GT strength)

is caused by the fact that shell model calculations performed within a single shell miss short-range correlations which shift GT strength to significantly higher energies [129, 130]. Modern many-body techniques which are able to account for these short-range correlations recover indeed most of the GT renormalization [131].

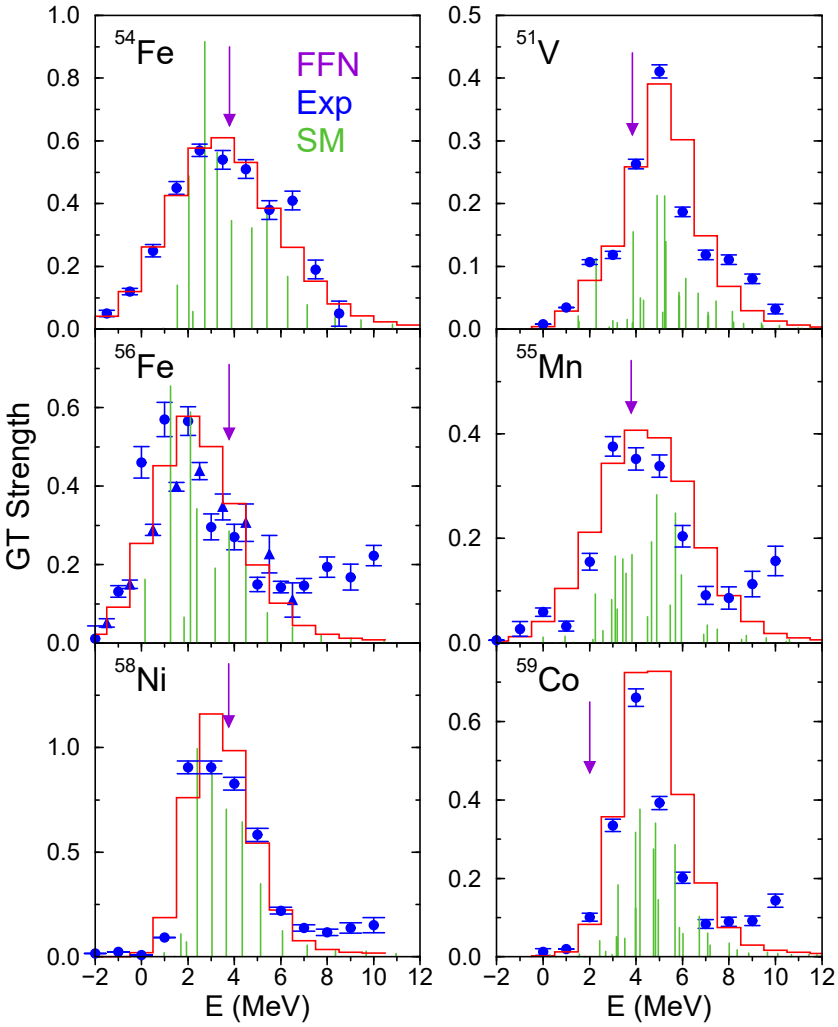

Figure 7. Comparison of experimental and shell model GT strength distributions for several pf shell nuclei. The data are derived from (n,p) charge-exchange experiments [91, 92, 89]. The shell model results are given as histograms and folded with the experimental energy resolution. The energies at which the FFN evaluation placed the GT strengths are shown as arrows.

Fig. 7 compares the shell model GT_+ strength distributions with the experimental data derived from (n,p) charge-exchange reactions and the energy position at which the FFN rates assumed the total GT_+ strength to reside. The fragmentation of the GT strength is quite obvious. It is even more visible in high-resolution data determined by the $(d,{}^2\mathrm{He})$ and $(t,{}^3\mathrm{He})$ techniques, e.g. see the data for $^{51}\mathrm{V}(d,{}^2\mathrm{He})$ in panel b of fig. 3. The data for nickel isotopes showed that the KB3 residual interaction, used in Refs. [32, 12], had some shortcomings in describing low-energy details of the GT strength

function [132]. These are better reproduced using an alternative residual interaction (GXPF1J [133]) (see panel d of Fig. 3).

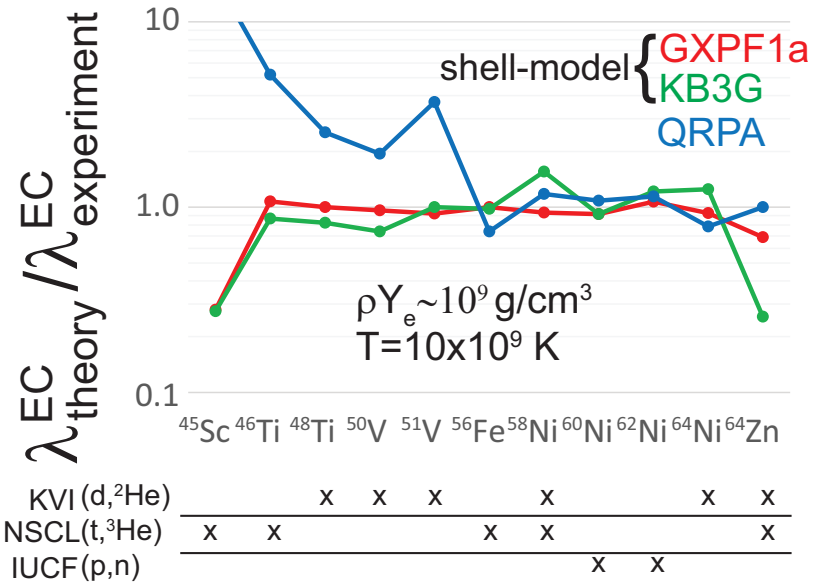

Figure 8. Comparison of electron capture rates for pf shell nuclei calculated from GT_+ distributions derived experimentally and from shell model calculations with two different residual interactions and within the QRPA approach. The astrophysical conditions represent a situation at which pf shell nuclei dominate the core composition. The rates presented are originally from [118] and used existing data from $(d, {}^2\mathrm{He})$, $(t, {}^3\mathrm{He})$, and (p, n) experiments, as discussed in Section 2. For the purpose of this review, they are supplemented with later results from the $(t, {}^3\mathrm{He})$ reactions on ^{45}Sc [111], ^{46}Ti [80], and ^{56}Fe [112].

Fig. 8 compares electron capture rates calculated for all pf shell nuclei, for which experimental GT_+ distributions have been measured, with the predictions from the shell model on the basis of two residual interactions (KB3G [134] and GXFP1a [135]). The chosen astrophysical conditions correspond to the presupernova stage of the collapse at which the pf shell nuclei dominate the abundance distribution. The GXPF1a rates giving a nearly perfect reproduction, except for ^{45}Sc. The KB3G rates are slightly worse than those based on the GXPF1a interaction, but still very good, except for ^{45}Sc and ^{64}Zn. On the other hand, the rates based on the QRPA calculations, with their restricted account of correlations, can deviate from the data and shell model rates by up to a factor of 10 for light pf nuclei, although for the heavier pf shell nuclei the rates based on the QRPA calculations do well at this stellar density.

The rates presented in Fig. 8 have been calculated solely from the ground state GT distribution. This assumes that the GT distributions of excited mother states is the same as for the ground state, shifted only by the respective excitation energy. This assumption often is called Brink-Axel hypothesis [136, 137] It cannot be strictly valid as it does not allow for deexcitations. As we will see below it is also not appropriate

for nuclei at shell closures. Ref. [138] discusses the validation of this hypothesis. A modification of the Brink-Axel hypothesis for high temperatures is proposed in [139]. A novel method to calculate electron capture rates for excited nuclear states based on the Projected Shell Model has been proposed in [140].

Ref. [12] calculated stellar beta decay and electron capture rates for more than 100 pf shell nuclei in the mass range $A = 45$–64. These calculations approximated the state-by-state formalism discussed above by considering the low-energy states and their GT distributions explicitly. These contributions were supplemented by the considerations of 'back-resonances'. These are GT transitions calculated for the inverse reaction and then inverted by detailed balance [3, 15]. The calculated energies and GT transition strengths had been replaced by experimental data whenever available. A detailed table of the weak interaction rates for the individual nuclei and for a fine grid of astrophysical conditions at which pf shell nuclei are relevant have been published in [34]. The rate table is publicly available and is incorporated in several leading supernova codes. A procedure how to interpolate between the grid points in temperature, density and Y_e value is discussed in [34], based on the work of [16].

Fig. 9 compares the shell model and FFN electron capture rates for several nuclei. The chosen nuclei represent the most abundant even-even, odd-A and odd-odd nuclei for electron captures as been identified by simulations on the basis of the FFN rates at the respective astrophysical conditions during early collapse (presupernova phase). The shell model rates are systematically smaller than the FFN rates with quite significant consequences for the presupernova evolution, as discussed below. The reasons for these differences is mainly due to the treatment of nuclear pairing which had been empirically considered in the FFN calculations. This leads in particular to the drastic changes observed for odd-odd nuclei. The shell model rates also considered experimental data which were not available at the time when the FFN rates were derived. The differences between the FFN and shell model beta decay rates are smaller than for electron capture and do not show a systematic trend [142, 12].

3.1.2. sd shell nuclei Beta decays and electron capture on sd shell nuclei (mass numbers $A = 17$–39) can occur during silicon burning in massive stars [29]. The processes are, however, of essential importance for the fate of the O-Ne-Mg core which develops at the end of hydrostatic burning in intermediate mass stars. This was the motivation for Oda et al. [33] to derive at stellar beta decay and electron capture rates for sd shell nuclei covering the relevant astrophysical conditions (temperatures 10^8–10^9 K and densities 10^8–10^{10} g cm^{-3}). The rate evaluations used the state-by-state formalism defined above. The spectra of the nuclei and the respective Gamow-Teller strength distributions for ground states and excited states were determined by diagonalization in the sd shell using the Brown-Wildenthal USD residual interaction which had been proven before to give a quite reliable account of nuclear properties for sd shell nuclei. Like for the nuclei in the pf shell the Gamow-Teller strength distributions were renormalized by a constant factor. The rates have been made available in table form for a grid of

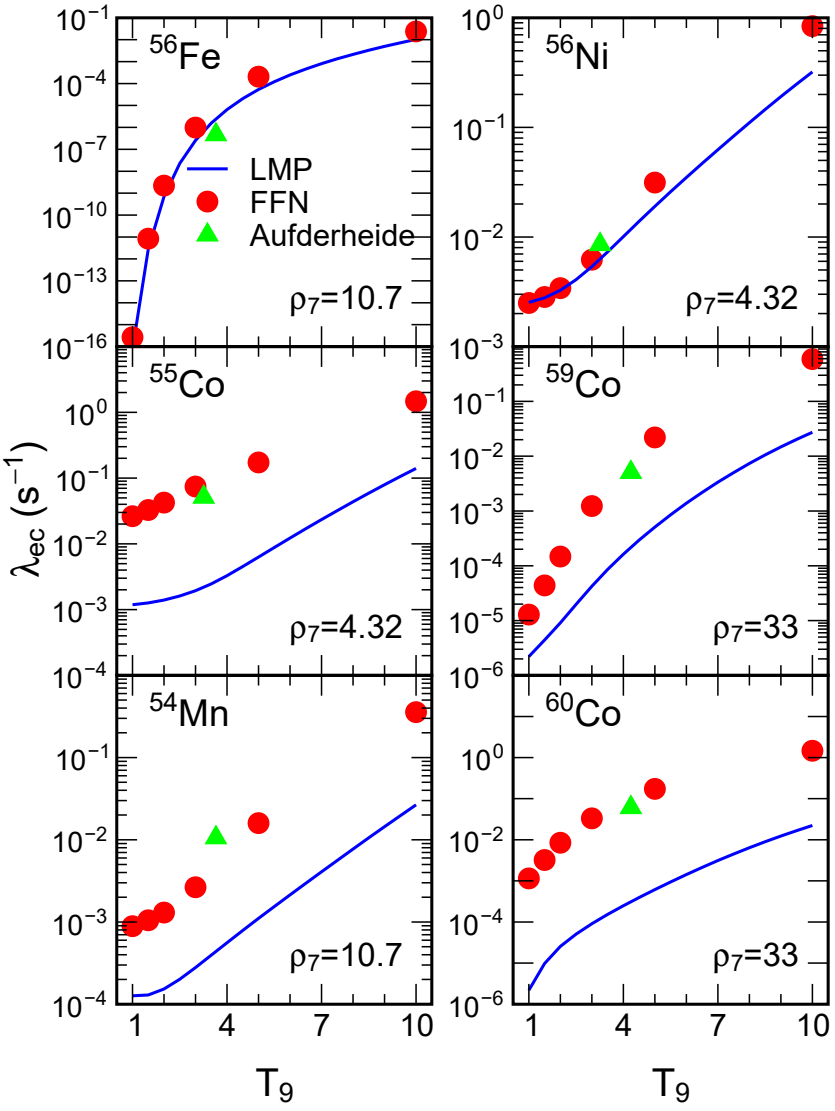

Figure 9. Comparison of the FFN and shell model rates for selected nuclei as function of temperature (in 10^9 K) and at densities (in 10^7 g cm^{-3}) at which the nuclei are relevant to the capture process in simulations which used the FFN rates. The triangles refer to shell model estimates derived on the basis of rather strong truncations [141].

temperature-density-Y_e points.

More recently, an updated rate table has been published by Suzuki which is based on the USDB residual interaction (a modified version of the USD interaction) and additional experimental information [50]. These modern shell model rates differ not too much from those of Ref. [33]. However, they are given on a finer mesh of temperature and density. This finer grid is particularly required for the study of the core evolution of stars in the mass regime 8–10 $M_\odot$. Of particular importance are the URCA pairs (^{23}Ne-^{23}Na, ^{25}Na-^{25}Mg and potentially ^{27}Mg-^{27}Al) which have Q values against electron captures which are reached during core contraction at densities around 10^9 g cm^{-3}. As the environment also has a finite temperature of order 10^8–10^9 K, which smears the electron chemical

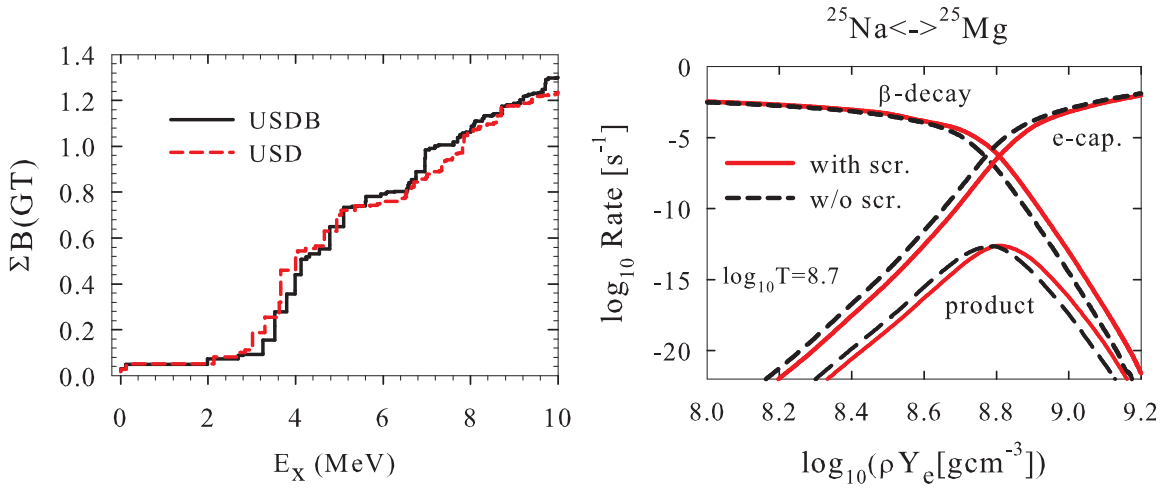

Figure 10. (left) Cumulative GT strength for ^{25}Mg calculated in *sd* shell model studies with two different interactions. The ground state strength is known experimentally. (right) Beta decay and electron capture rates for the URCA pair ^{25}Na and ^{25}Mg as function of density and a specific temperature. The curve labelled 'product' is given by the sum of the two rates and identifies the density at which the URCA pair operates most efficiently. The rates are given with and without screening corrections. (from [50])

potential and implies the presence of thermally excited states, it is possible that both electron captures and beta decays occur between the pairs of nuclei. The neutrinos produced in both processes carry energy away making the URCA pairs an efficient cooling mechanism. The operation of URCA pairs is restricted to a relatively narrow density range requiring the knowledge of weak interaction rates on a rather fine density-temperature grids. Such rates have been provided in [143, 50]. Fig. 10 compares the GT$_+$ strength for the ^{25}Mg ground state as calculated with the USD [33] and USDB [50] interactions. The transition to the ^{25}Na ground state is known experimentally. We note the rather close agreement between the two calculations. 10 shows the beta decay and electron capture rates calculated on the basis of the *sd* shell model. With increasing density, the electron chemical potential grows which reduces the beta decay rates due to Pauli final state blocking and increases the electron capture rates. At the URCA density $\log(\rho Y_e) = 8.81$ both rates match. The product of beta decay and electron capture rates indicates the density range at which the URCA pair operates. Screening effects induced by the astrophysical environment shift the URCA density to slightly larger values (see below).

While the URCA pairs cool the core, electron capture on the two abundant nuclei ^{24}Mg ($Q = 6.03$ MeV) and ^{20}Ne ($Q = 7.54$ MeV) heat it. (The third abundant nucleus ^{16}O has such a high Q-value that electron capture does not occur at the densities achieved during the evolution of the ONeMg core). Electron captures on these nuclei set in once the core density is large enough for the electron chemical potential to overcome the respective Q value. (Due to its lower Q value this occurs first on ^{24}Mg.) At these

densities the electron captures on the daughter nuclei ^{24}Na and ^{20}F, respectively, occurs then instantaneously with noticeably larger capture rates, as the odd-odd daughter nuclei have significantly smaller Q-values against electron capture due to pairing effects. As $\mu_e > Q$, the capture often leads to excited states in the final nuclei ^{24}Ne and ^{20}O which de-excite via gamma emission heating the environment.

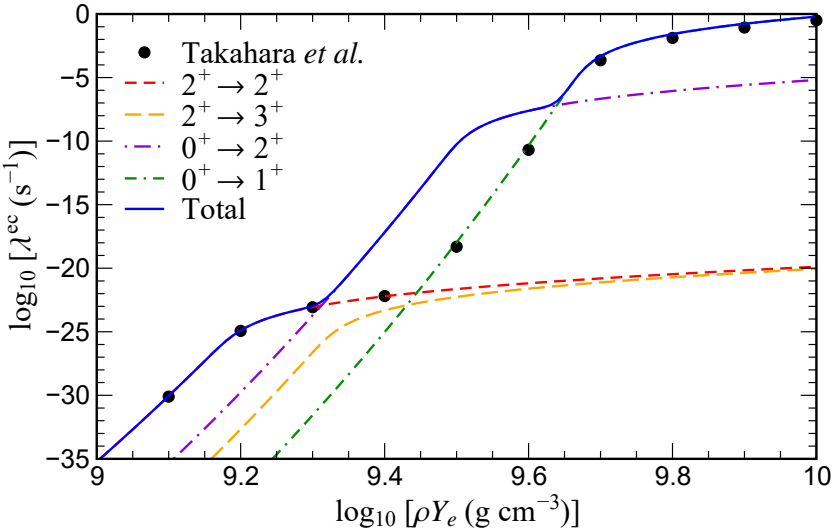

Figure 11. Electron capture rate for ^{20}Ne as function of density and for a specific temperature. The rate labelled 'Takahara et al' was evaluated from GT distributions calculated within the shell model [47]. The rate is broken down into the individual state-by-state contributions where the energies and transition strengths are all taken from experiment. The label '$0^+ \rightarrow 2^+$' identifies the contribution from the second forbidden ground-state-to-ground-state transition whose strength has been measured by Kirsebom *et al.*. [52]. This transition dominates the capture rate at the densities most relevant for the core evolution of intermediate-mass stars. (from [52]).

The electron capture rates for ^{20}Ne and ^{24}Mg and their daughters have been determined on the basis of shell model calculations by Takahara et al. [47] and Oda et al. [33]. These rates have been the default values until recently in studies of the core evolution of intermediate mass stars. The ^{24}Mg capture rate has been updated in Ref. [51] using experimental data which became available in the meantime leading to rather small modifications. This is different for the electron capture rate on ^{20}Ne which can be considered a milestone and an exception. At first, Ref. [51] showed that all relevant Gamow-Teller contributions to the rate could be derived from experiment using data from (p, n) charge-exchange measurements [144] (applying isospin symmetry) and from beta decays of ^{20}F (see Fig. 11). Furthermore, the authors noticed that, due to the relatively low temperatures of a few 10^8 K, the, at the time unknown, ^{20}Ne-^{20}F ground-state-to-ground-state might contribute to the capture rate just at the relevant densities, despite that it is highly suppressed due to angular momentum mismatch. The strength of this second forbidden transition has recently been measured in a dedicated experiment at the IGISOL facility in Jyväskylä [52, 145] and it was found large enough to increase the ^{20}Ne capture rate by several orders of magnitude as is shown in Fig. 11. We emphasize

that the electron capture rate on ^{20}Ne in the temperature-density range important for intermediate mass stars is now completely determined by experiment. This is quite an achievements and shows the great opportunities offered by modern Radioactive Ion Beam (RIB) facilities. That a second forbidden transition essentially contributes to an astrophysical electron capture rate is exceptional and due to the low temperature of the environment and the peculiar structure of ^{20}Ne. In core-collapse supernovae the temperatures are an order of magnitude higher at the same densities making allowed Gamow-Teller transitions the dominating contributor to electron capture rates.

In the astrophysical environment the weak interaction processes are modified due to screening effects. The screening corrections for electron capture have been developed in [13], the extension to beta decays is given in [51]. There are two important effects induced by the astrophysical environment. At first, screening enlarges (reduces) the energy threshold for electron captures (beta decays). Second, it reduces the electron chemical potential. Both effects together reduce the electron capture rates, while they enhance beta decay rates. Rate modifications due to screening are are relatively mild of order a factor of 2. The effects for the URCA pair ^{25}Na-^{25}Mg are shown in Fig. 10. Modifications of the electron capture rates during the collapse of a massive star are discussed in [13] and exemplified in their Fig. 10. Many tabulations of electron capture rates (e.g. Refs. [14, 3, 15, 16, 34, 33, 146, 147] do not include screening corrections. Ref. [13] presents a formalism how these rates can be approximately corrected for screening effects.

Weak-interaction rates based on diagonalization shell model exist for nuclei in the mass range $A = 17$–65, with the exception of $A = 39$–44. Studies of these nuclei require the inclusion of correlations across the $Z, N = 20$ shell closures and hence large model spaces enabling allowed Gamow-Teller and also forbidden transitions. Steps in performing such demanding calculations have been taken so that a shell model evaluation also for this mass range appears to be in reach. Weak-interaction rates for $A = 39$–44 were provided by Fuller et al in their seminal work based on the IPM, but also by Nabi and Klapdor-Kleingrothaus within the framework of the QRPA [146]. The latter reference gives electron capture rates for a wider range of nuclei.

3.2. Electron capture on nuclei with $A > 65$

Shell model studies of nuclei with mass numbers $A \geq 65$ require an accurate description of cross-shell correlations. The associated model spaces make diagonalization shell model calculations in general unfeasible. It is fortunate that by the time nuclei with $A \geq 65$ dominate the core composition the density, and accordingly the electron chemical potential, has grown sufficiently that the capture rates are mainly sensitive to the total GT strength and its centroid. For these nuclei a hybrid model [36, 39] has been proposed to evaluate the stellar capture rates. In this model the rates are calculated within an RPA approach in appropriately large model spaces using partial occupation numbers. These occupation numbers are calculated within the Shell Model Monte Carlo (SMMC)

method [40, 41] and hence consider the relevant multi-particle-multi-hole configurations required to properly describe the cross-shell correlations which are relevant for nuclei in this mass range. Moreover, the SMMC determines the nuclear properties at finite temperature as is appropriate for the astrophysical environment. The RPA approach is known to reproduce the strength and centroids of collective excitations. It does, however, usually not give a full account of the fragmentation of the strength which, as explained above, might not be needed at the astrophysical conditions at which the heavy nuclei studied by the hybrid model appear during the collapse.

The SMMC calculations of the partial occupation numbers have been performed in large model spaces (pf-sdg for nuclei with neutron numbers $N \leq 61$ and $pf_{5/2}$-sdg-$h_{11/2}$ for even heavier nuclei) using adjusted pairing+quadrupole interaction to avoid the infamous sign problem [41]. The hybrid model has been validated in [13] and applied to about 250 nuclei in the mass range $A = 66$–120 [39, 13].

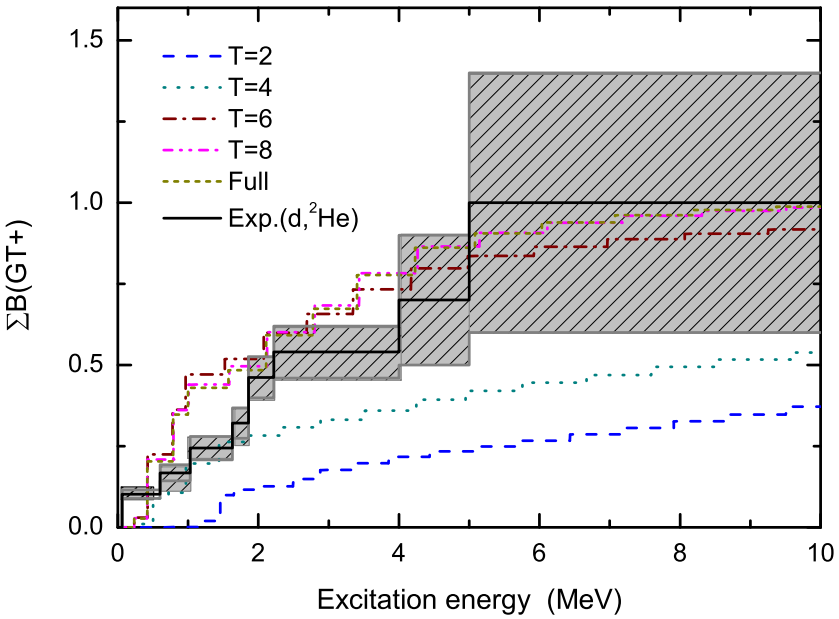

Figure 12. Comparison of experimental GT strength distribution for ^{76}Se (shown as running sum) with results obtained by shell model diagonalization using the RG residual interaction and different levels of truncations (from [148]).

In this context, a special nucleus is ^{76}Se with $Z = 34$ and $N = 42$. Thus, its GT_+ strength vanishes in the Independent Particle Model (and in the Bruenn parametrization used in supernova simulations prior to 2003 [18]). The GT strength has been experimentally determined using the $(d, {}^2\mathrm{He})$ charge-exchange technique at Groningen [38] proving that cross-shell correlations indeed unblock the GT strength (see Fig. 12). Diagonalization shell model calculations, performed in different model spaces and with different residual interactions, are able to describe the low-energy spectra of ^{76}Ge and ^{76}Se and also the GT strength (Fig. 12). These shell model calculations showed that cross-shell correlations are a relatively slowly converging process requiring the inclusion of multi-particle-multi-hole configurations. For example, the consideration

of only 2p-2h configurations does not suffix to pull enough GT strength to low energies (Fig. 12).

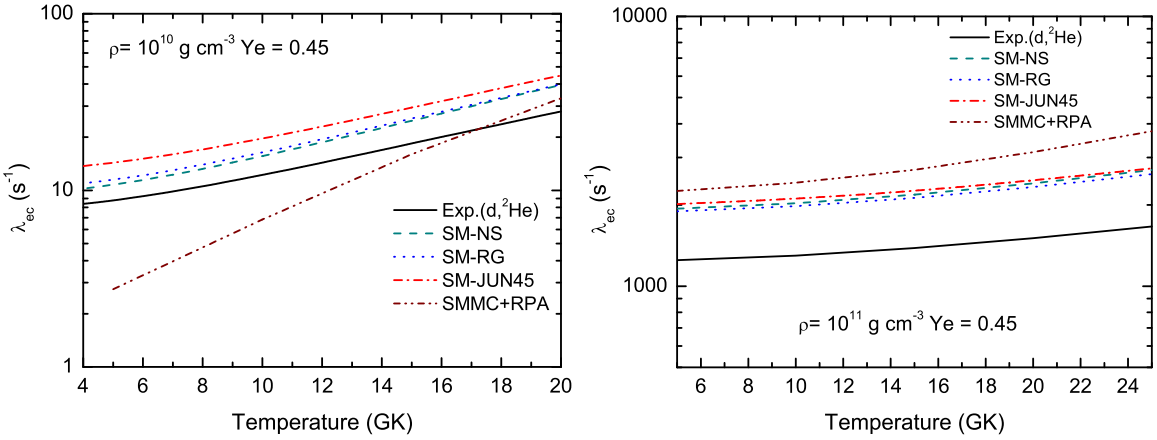

Figure 13. Electron capture rates on ^{76}Se at $\rho = 10^{10}$ g cm^{-3} (left) and $\rho = 10^{11}$ g cm^{-3} (right) as function of temperatures. The rates have been calculated from the experimental ground state data [38] and within diagonalization shell model approaches using different residual interactions. The results labelled 'SMMC+RPA' have been obtained within the hybrid model. (from [148]).

We note that ^{76}Se, being an odd-odd nucleus, is never very abundant during core collapse. Nevertheless, Fig. 13 compares the electron capture es calculated from the experimental and diagonalization shell model (for different interactions and model spaces) GT distributions with those obtained in the hybrid model for two different core densities and for various temperatures [148]. The lower density corresponds to presupernova conditions, where electron capture is dominated by pf shell nuclei. The rates calculated from the data and the shell model GT strength distributions agree quite well. The hybrid model rates agree with the other rates within a factor of 3 for the range of temperatures given, but they show a distinct different T-dependence. This is related to the fact that the hybrid model does not resolve the fragmentation of the GT strength, which is particularly important at low temperatures and densities. In fact, at the higher density, the agreement between all rates is quite satisfactory. Under these conditions the electron chemical potential is noticeable larger than the capture Q-value, making the rate less sensitive to details of the GT distribution. The hybrid model calculation considers also forbidden multipoles whose contributions increase with temperature, but are relatively small [148]. We note that the shell model and experimental rates are solely determined from the ground state GT distribution, while the hybrid model considers finite temperature effects in the calculation of the occupation numbers. These turn out to be not so relevant as the $N = 40$ gap is already strongly overcome by correlations in the ground state. This will be different for the $N = 50$ gap, discussed below.

The Thermal Quasiparticle RPA (TQRPA) model [149] is an alternative approach proposed to calculate electron capture (and neutrino-nucleus reaction) rates at finite temperatures [44, 150]. Like the SMMC, also the TQRPA is based on an equilibrium

statistical formalism and treats the many-nucleon system in a heat bath and a particle reservoir in the grand canonical ensemble. The method can be understood as a proton-neutron QRPA approach extended to finite temperatures and allows to determine temperature-dependent spectral functions which are the basis to evaluate weak-interaction rates within this model [44]. Further extensions allow to use Skyrme [151, 150] and relativistic functionals [152] to describe the thermal state and its excitation considering 2p-2h correlations.

Compared to the hybrid model, the TQRPA has the advantage to be formally consistent in treating the many-body problem. In contrast, the two parts of the hybrid model have a different complexity in dealing with the many-body states. It turns, however, to be important that the SMMC considers multi-particle-multi-hole correlations as will be discussed below.

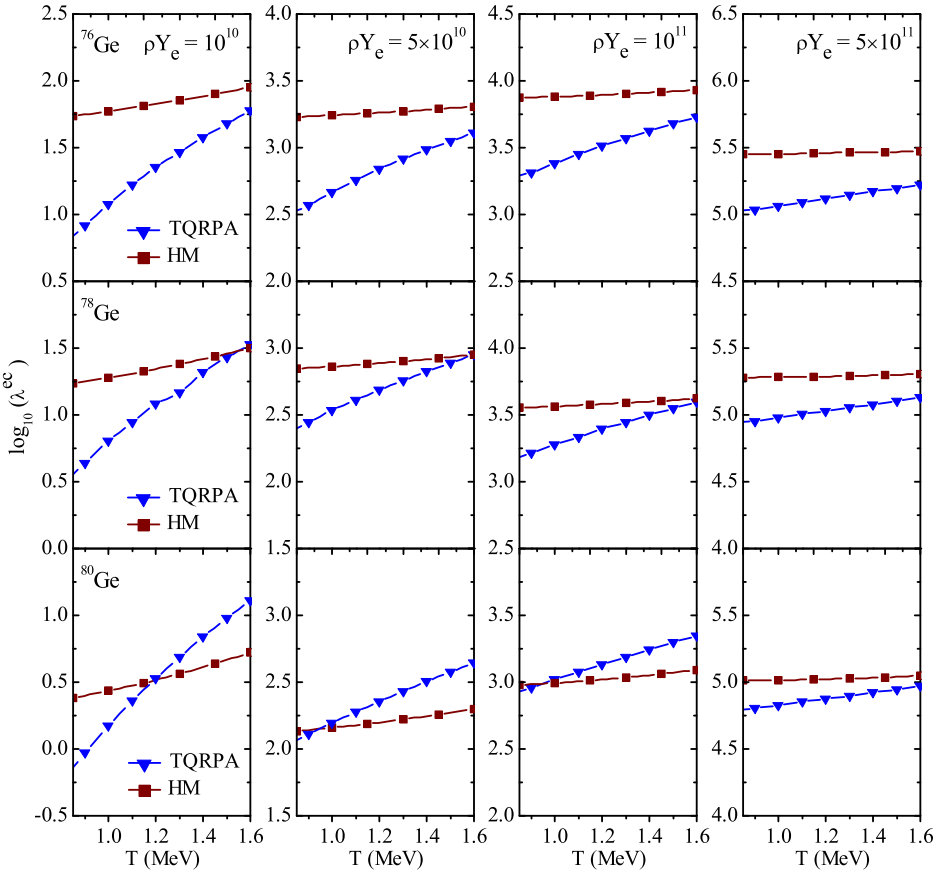

Figure 14. Comparison of electron capture rates for ^{76,78,80}Ge for different densities ρY_e and as function of temperature, calculated within the TQRPA and hybrid model (HM). (from [44]).

The TQRPA approach has been used to calculate electron capture at finite temperatures for selected Fe and Ge isotopes [44] and for nuclei at the $N = 50$ shell closure [150, 45]. The differences between the two models become illustrative in Fig. 14 which compares the electron capture rates calculated in both approaches for various

neutron-rich Ge isotopes at different densities and temperatures. In general, as the electron chemical potential grows with density and temperature, the rates increase as well where the sensitivity is larger to density than to temperature. The rates decrease with increasing neutron numbers. This has two reasons. Foremost, the Q value increases, but also the occupation of the $g_{9/2}$ neutron orbital grows decreasing the unblocking of pf shell neutron orbitals. Neutron-rich Ge isotopes appear in the core composition at temperatures ≥ 1 MeV and densities $\rho Y_e \geq 10^{11}$ g cm^{-3} and both models predict quite sizable capture rates for these conditions. There are, however, differences between the two models. In general, the hybrid model capture rates are larger than those obtained in the TQRPA, most evidently at lower densities. Furthermore, the TQRPA model shows a steeper rise of the capture rates with temperature than the hybrid model. These facts are foremost related to the increased unblocking probabilities in the hybrid model due to many-body correlations which result in larger GT strength at lower excitation energies. The differences in the rates become smaller with increasing density and temperature. This is mainly due to the growing electron chemical potential which makes the rate less sensitive to the details of the GT strength distribution. Secondly, forbidden transitions contribute increasingly with growing density and temperature. These contributions are not subject to blocking effects.

We have seen that many-body correlations overcome the $N = 40$ shell closure already in the ground state and unblock the GT contribution to the capture rate. But what happens at the magic number $N = 50$? In fact, measurements of the GT$_+$ distribution for ^{86}Kr ($Z = 36$ and $N = 50$) [109] and for ^{88}Sr ($Z = 38, N = 50$) shows only very little strength, mainly located at excitation energies between 8–10 MeV [110]. This points to a rather strong blocking of GT transitions at $N = 50$. Electron capture rates, calculated from the experimental ground state data, are indeed significantly lower than expected from systematics [110]. The results for ^{86}Kr and ^{88}Sr are surprising, given that a significant amount of GT strength (~ 0.7 units) was observed for ^{90}Zr [153] even though, based on transfer reaction experiments [154], the proton $0g_{9/2}$ occupation number for ^{88}Sr and ^{90}Zr are comparable: 0.7 and 1.0, respectively. A high-resolution experiment for ^{90}Zr will be necessary to better understand these results.

In the collapsing core, $N = 50$ nuclei (e.g. ^{82}Ge and ^{78}Ni with Y_e values of 0.39 and 0.34, respectively) are very abundant at densities in excess of about 10^{11} g cm^{-3} [4, 155] and at temperatures $T > 1$ MeV. At these high temperatures the average nuclear excitation energy is about $\langle E \rangle = 10$ MeV, which is larger than the $Z = 28$ proton gap and the $N = 50$ neutron gap. This implies that the capture at the stellar temperatures occurs on average on states with important many-body correlations across the two gaps, in this way unblocking the GT contribution to the capture rate. This is indeed born out in TQRPA calculations performed for $N = 50$ nuclei between ^{78}Ni and ^{88}Sr. The obtained capture rates are shown in Fig. 15. Satisfyingly the TQRPA calculations finds no GT strength in the ^{86}Kr and ^{88}Sr ground states at low energies, in agreement with observation. In fact the TQRPA capture rates, calculated solely from the $T = 0$ GT distributions, agree with those obtained from the experimental GT distributions for

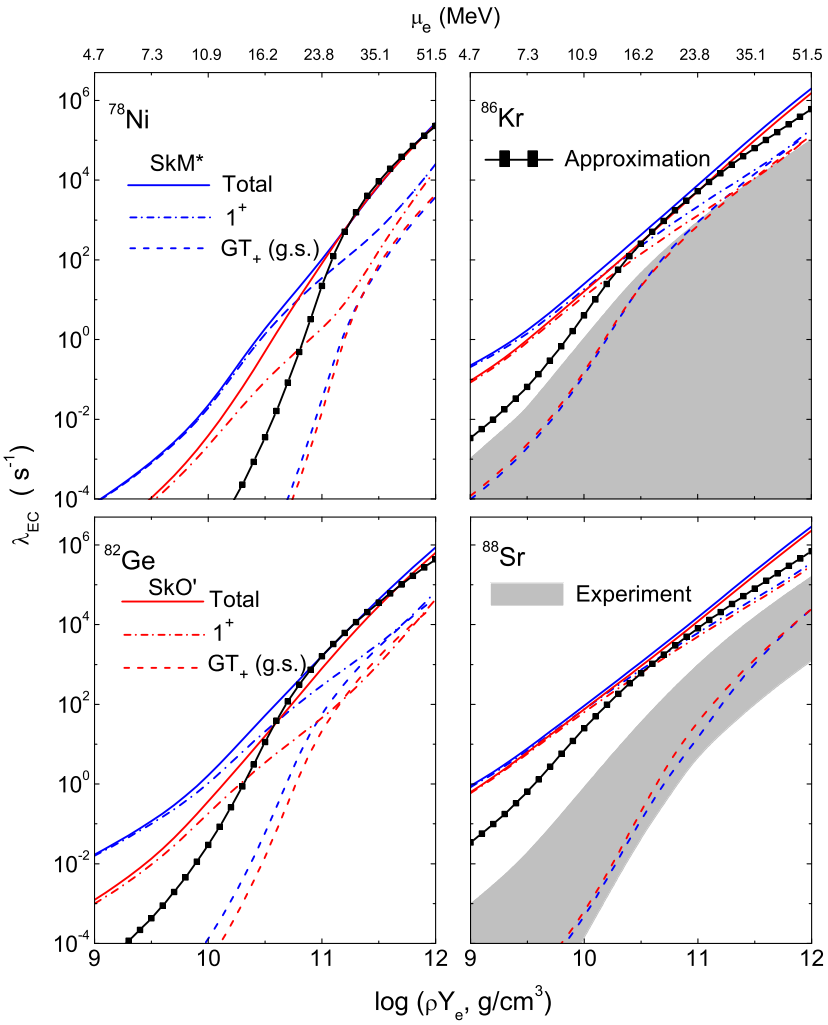

Figure 15. TQRPA electron capture rates for selected $N = 50$ nuclei calculated at $T = 0$ and at $T = 1$ MeV and as function of density. The upper axis shows the corresponding electron chemical potential. The calculations have been performed for two Skyrme interactions: SkM* (blue lines) and SkO' (red lines). The calculated total capture rates include also contributions from forbidden transitions; the GT contribution is presented individually. The shaded area is the rate obtained from the experimental ground state GT distribution (taken from [110]. The thick line labelled 'Approximation' represents the 'single state approximation' adopted from [39]. (from [45]).

both nuclei (see Fig. 15). The TQRPA calculation shows, however, a strong thermal unblocking of the GT strength as protons are moved into the $g_{9/2}$ orbital and neutrons out of the pf shell. This leads to a strong increase in the capture rate for all nuclei (see Fig. 15). Thermal unblocking of the GT strength has the largest effect at small electron chemical potentials μ_e (low densities), while its relative importance decreases with growing μ_e. With increasing density contributions from forbidden transitions become more important and dominate the rate for densities of order $\rho Y_e > 10^{11}$ g cm^{-3}, hence at the conditions where $N = 50$ nuclei are abundant in the collapse. The capture

rates also increase with increasing proton numbers, i.e. from ^{78}Ni to ^{88}Sr. This has two reasons: the growing Q value with neutron excess and the increased promotion of protons into the $g_{9/2}$ orbital.

In summary, GT measurements for nuclei which become relevant in the high density/temperature environment during supernova collapse are indispensable to constrain nuclear models and to create trust in them. However, they cannot directly been used to determine the stellar capture rate as thermal unblocking effects modify the rates under such conditions noticeably. This is in particular true at shell closures, i.e. for $N = 50$ nuclei. For these nuclei forbidden transitions might be as relevant as GT transitions and should be experimentally constrained as well.

Fig. 15 also shows the rate estimated by a parametrization put forward in Ref. [39]. This simple parametrization assumes that the capture proceeds through a single transition from an excited state in the parent nucleus at E_i to a state in the daughter nucleus at E_f with $\Delta E = E_f - E_i$ (single-state approximation). Then the capture rate can be written as [16]

$$\lambda = \frac{\ln(2)B}{K}\left(\frac{T}{m_e c^2}\right)^5 \left[F_4(\eta) + 2\chi F_3(\eta) + \chi^2 F_2(\eta)\right] \tag{4}$$

where $\chi = (Q + \Delta E)/T$, $\eta = (\mu_e - Q - \Delta E)/T$, $K = 6146$ s and B represents a typical (Gamow-Teller plus forbidden) matrix element. The quantities F_k are the relativistic Fermi integrals of order k. Q is the ground state ground state Q-value that is positive for capture in protons and neutron-rich nuclei. This approximation was used in Refs. [39, 42] to estimate the rates of the many heavy nuclei which are abundant at larger densities and for which no rates existed at that time. The two parameters (energy position and GT strength) were fitted to the rates of about 200 nuclei for which individual pf shell model and hybrid model rates were available. Fig. 16 compares the shell model rates with the single-state approximation (4) using $B = 4.6$ and $\Delta E = 2.5$ MeV. We note that the approximation does not consider nuclear structure effects (or a dependence on the average excitation energy) which result in quite a significant scatter of the shell model rates with respect to the single-state rate. For the reasons discussed above, the fluctuations get noticeably reduced with increasing density. It is worth noting that there is no systematic difference between the approximation and the shell model rates so that differences might at least partially cancel out. At the intermediate density the single-state approximation shows some tendency to overestimate the rate. In conclusion, the approximation in its simple form (4) should not be used at low densities say below a few 10^{10} g cm^{-3}. In this density regime the nuclear composition is largely dominated by nuclei for which shell model rates exist. The general trend seen in Fig. 16 is also borne out in Fig. 15 where the approximation badly fails at low densities, but gives reasonable agreement at $\rho Y_e > 10^{11}$ g cm^{-3}. Ref. [155] compares the shell model and single-state rates at slightly different astrophysical conditions.

The single-state parametrization has been adopted for heavy nuclei in supernova simulations which systematically studied the influence of nuclear ingredients (electron capture rates, Equation of State, mass models) on the collapse dynamics [155, 156] (see

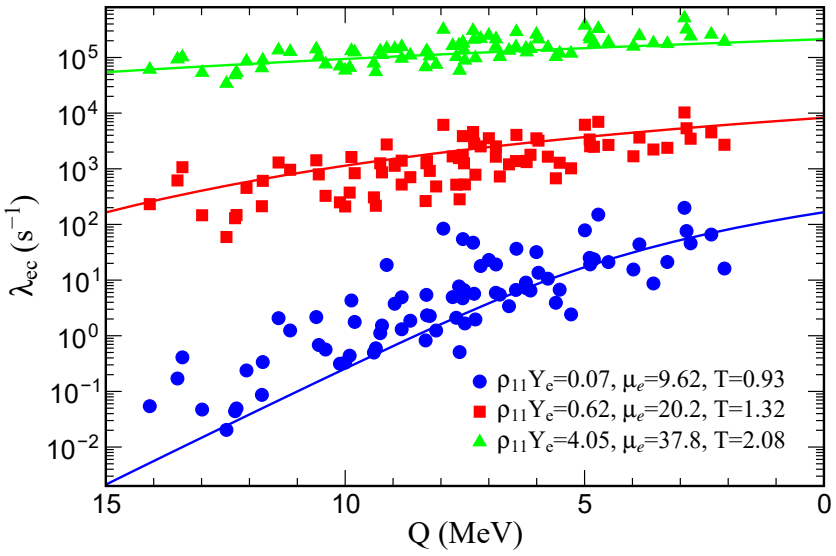

Figure 16. Electron capture rates on nuclei, for which individual shell model rates exist, as function of Q value for 3 different stellar conditions. Temperatures are measured in MeV, density in 10^{11} g cm^{-3}. The solid lines represent the rates obtained from the single-state approximation 4. (from [39]).

below), where Ref. [156] used the improved single-state parametrization of [157] (see below).

3.3. Rate Tables

Most supernova codes now use the rate table as provided by Juodagalvis *et al.* [13]. This table defines electron capture rates on a grid of the three important parameters characterizing the astrophysical conditions during collapse: temperature, density, Y_e value. The rate evaluation assumes the core composition to be given by nuclear statistical equilibrium, hence it does not provide rates for individual nuclei.

The rate table is based on the hierarchical strategy defined above. For the nuclei with $A < 65$ the shell model rates of Oda *et al.* [33] (*sd* shell) and of Langanke and Martinez-Pinedo [34] (*pf* shell) have been adopted. This guarantees a reliable and detailed reproduction of the GT strengths for the important nuclei at collapse conditions where $\mu_e \sim Q$. The rates for nuclei in the range $A = 39 - 44$ have been taken from Fuller, Fowler and Newman [3]. For the heavier nuclei the table adopts the rates from hybrid model calculations. For about 200 nuclei in the mass range $A = 65 - 110$ these were calculated by using SMMC partial occupation numbers in RPA calculations. For a few nuclei in this mass regime and for even heavier nuclei, in total about 2700 nuclei, the rates were evaluated on the basis of a parametrization of the occupation numbers, derived in accordance with the SMMC studies, and RPA response calculations. In this way the most relevant nuclear structure input, like shell gaps, are accounted for. Screening corrections due to the astrophysical environment have been incorporated into the rates.

Weak-interaction rates for *sd* shell nuclei are important for the core evolution of intermediate mass stars. Rates for individual nuclei for the relevant density and temperature regime are given in [33] and updated in [50].

Nuclei in the mass range $A = 45$–65 are essential for the early phase of core collapse supernovae and for the nucleosynthesis in thermonuclear (Type Ia) supernovae. The weak-interaction rates for these *pf* shell nuclei are individually given in [34]. The rates are not corrected for screening, which, however can be accounted for using the formalism developed in [13].

We note that at specific astrophysical conditions (e.g. during silicon burning), at which the *sd* and *pf* shell nuclei are relevant, the temperature is in general not high enough to establish an NSE composition. Hence the knowledge of individual rates is essential.

To make it easier to incorporate complete sets of electron-capture rates in astrophysical simulations, a library of rates was created [155, 158, 159] based on the rate tables for specific mass regions described above and on the single-state approximation for nuclei where rates based on microscopic calculations are not available. This library is incorporated in the weak-rate library NuLib [160].

4. Electron captures in astrophysical applications

4.1. Core-collapse supernovae

Simulations of the evolution of massive stars distinguish two distinct phases motivated by their specific needs and requirements. 1) During hydrostatic burning energy released by nuclear reactions in the star's interior are essential to balance gravity. The densities are low enough that neutrinos, produced in weak interactions, can leave the star unhindered transporting energy away. This loss has to be considered in the energy balance, but a detailed treatment of neutrino transport is not required. However, the simulations have to incorporate a detailed network of nuclear reactions to follow the nuclear energy production and the change in composition. This stellar evolution period lasts to the so-called presupernova phase when the core density has reached values of about 10^{10} g cm^{-3} and the inner part of the iron core collapses with velocities in excess of 1000 km s^{-1} [161, 29].

The final models obtained by the stellar evolution codes become the input for the supernova codes in which the gravitational collapse of the iron core and the explosion are simulated. The astrophysical conditions relevant during these simulation lead to two important changes compared to stellar evolution. The temperatures are sufficiently high ($T >$ a few GK) so that the nuclear composition can be well approximated by an NSE distribution, without the need to follow a complicated network of nuclear reactions. On the other hand, the involved densities require a detailed bookkeeping of neutrinos. This is achieved by Boltzmann transport. An additional complication arises from the fact that the assumption of spherical symmetry, which

holds approximately during hydrostatic stellar evolution, is not valid during the core collapse and explosion. This requires multidimensional treatments which is extremely challenging and computationally demanding. Reviews about the recent impressive progress in supernova modelling can be found in [162, 163, 164, 165]. These codes consider electron capture via the rates provided by [13].

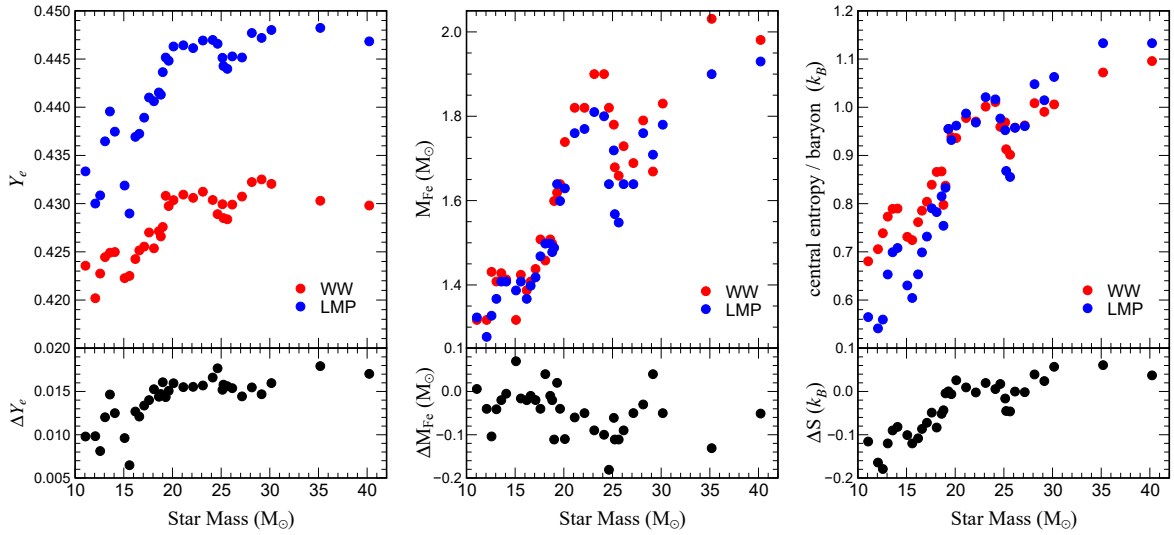

Figure 17. Comparison of the center values of Y_e (left), the iron core sizes (middle) and the central entropy (right) for $11-40M_\odot$ stars between the models using the FFN rates (WW models [161]) and models which used the shell model weak interaction rates (LMP [35]). The lower panels show the changes in the 3 quantities between the WW and LMP models.

Heger *et al.* have investigated which effect the diagonalization shell model rates have on the presupernova evolution for stars in the mass range $M = 13$–40 $M_\odot$ [29, 35]. To this end they repeated calculations of Weaver and Woosley [161], keeping the stellar physics as much as possible, but replacing the weak interaction rates for pf shell nuclei by those of Ref. [34] (LMP rates). Fig. 17 summarizes which consequences the shell model rates have on three quantities which are relevant for the following collapse. The central Y_e value is larger by $\Delta Y_e = 0.01$–0.015 at the onset of collapse. This has two reasons. First, the shell model rates are noticeably smaller than the FFN rates (Fig. 9), hence reducing leptonization. Second, during silicon burning β decays can compete with electron captures. Although this does not occur by specific URCA pairs, but rather by an ensemble of nuclei, the effect is the same: the star is additional cooled, while the Y_e is kept constant. The study confirmed that β decays become increasingly Pauli blocked with growing density and can be safely neglected during collapse. Fig. 17 also indicates that the iron core masses are generally smaller with the LMP rates. However, this is not a continuous effect and shows variations among the models with different stellar masses. Finally, the LMP rates lead to presupernova models with lower core entropy for stars with $M < 20$ $M_\odot$. For the more massive stars, the effect is not unique; stars with $M = 30$–40 $M_\odot$ show an increased core entropy. We mention that lower (larger) core

entropy implies less (more) free protons in the nuclear composition, which, however, is overwhelmingly dominated by nuclei.

The continuous electron capture drives the NSE composition of the core more neutron-rich and towards heavier nuclei. At densities in access of a few 10^{10} g cm^{-3} the composition is dominated by nuclei with $Z < 40$ and $N > 40$ for which, for a long time, it was assumed that electron captures vanish (e.g. [18]) due to Pauli blocking of the GT strength. As a consequence the capture process at the later of the collapse continued solely on free protons, which are, however, less abundant than heavy nuclei by orders of magnitude. As we have discussed above, the GT strength at the $N = 40$ shell gap is unblocked by multi-nucleon correlations. Furthermore, the blocking at the $N = 50$ shell closure, which results in a strong reduction in the experimental ground state GT strength, is overcome at the finite-temperature core conditions by thermal excitations.

Arguable the most important result reported in Refs. [39, 42] is the fact that electron capture proceeds on nuclei rather than on free protons during the entire collapse, in contrast to previous belief (e.g. [1]. These findings are based on supernova simulations performed independently by the Garching and Oak Ridge groups which both adopted the hybrid model capture rates for more than 100 nuclei in the mass range $A = 65$–110, supplemented by the shell model rates for pf shell nuclei. For the heavy nuclei, the capture rates were estimated by the single-state approximation. The capture rate on free protons was taken from [18].

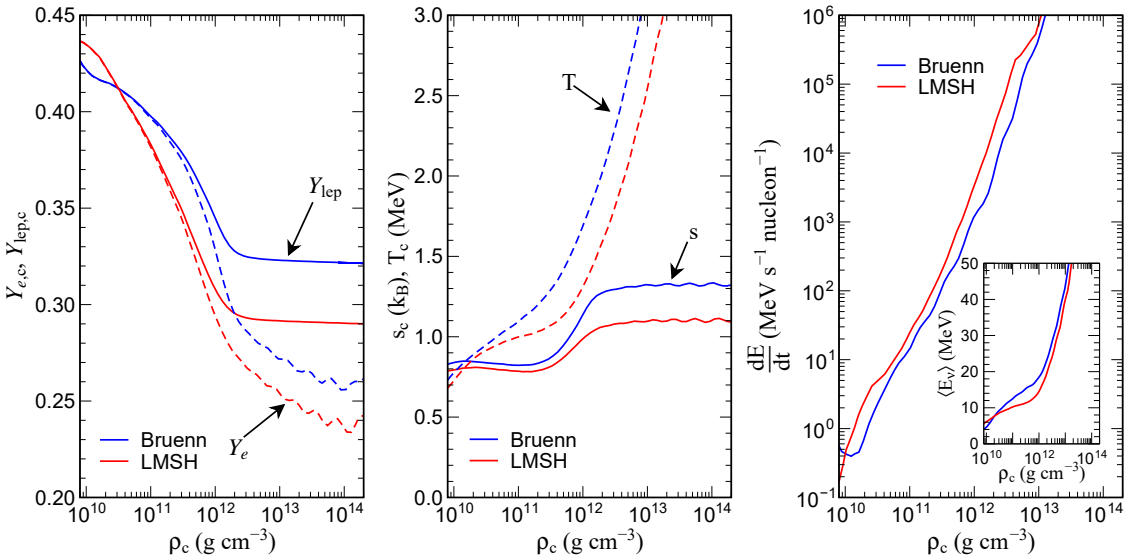

Figure 18. Comparison of a supernova simulation for a 15 $M_\odot$ star using the shell model weak interaction rates from Ref. [28] (labelled LMSH) and the Bruenn parametrization which neglects capture on nuclei for $N > 40$ [18] (labelled Bruenn). The figure shows the central core values for Y_e and Y_lep (electrons plus neutrinos) (left), the entropy and temperature (middle) and the neutrino emission rate (right) as function of core density. The insert in the right figure shows the average energy of the emitted neutrinos (courtesy of Hans-Thomas Janka).

Fig. 18 compares some important quantities obtained in the simulations of refs. [39, 42] with previous studies which neglected electron captures on heavy nuclei. Obviously the capture on nuclei is an additional source of deleptonization, adding to the capture on free protons. This results in significantly lower values for Y_e at neutrino trapping at densities around 10^{12} g cm^{-3}. At higher densities the total lepton fraction $Y_{\rm lep}$ becomes constant, while the electron fraction Y_e still decreases. This is related to neutrino tapping and the formation of the homologous core [1]. In this regime, continuous electron captures reduce the electron abundance, but the neutrinos generated by this process interact with matter mainly by coherent scattering on nuclei with a rate large enough that their diffusion time scale is longer than the core collapse time scale. Neutrinos are trapped and add to the total lepton fraction in the core. But before trapping, the neutrinos can still leave the star and are an additional cooling mechanism leading to smaller core entropies than obtained in previous calculations. Lower entropies reduce the abundance of free protons in the NSE composition, which increases the importance of capture on nuclei due to their increased abundances. Neutrinos produced by capture on nuclei have smaller average energies due to the higher Q-value than neutrinos produced by capture on free protons. Hence the luminosity of electron neutrinos is increased due to more captures, but their average energies are shifted to lower values. We stress that the rate for capture on individual nuclei is noticeably smaller than the capture rate on free protons. The dominance of capture on nuclei results for the overwhelmingly higher abundance of nuclei compared to free protons and are a result of the low entropy, i.e. of the capture process.

The fact that electron capture on nuclei proceeds until neutrino trapping is reached reflects itself also in the core dynamics and profiles. In the simulations with the improved rates, as shown in Fig. 19 the shock forms with significantly less mass included (smaller 'homologous core' size) and a smaller velocity difference across the shock. Despite this mass reduction, the radius from which the shock is launched is actually slightly pushed outwards due to changes in the density profile. Despite these significant alterations also one-dimensional supernova models employing the new electron capture rates fail to explode. No noticeable differences in the simulations are observed if the rate set of Juodagalvis *et al.* [13] is used which replaces the rates for nuclei, for which in [42] the single-state approximation was used, by rates estimated in the spirit of the hybrid model. Multidimensional supernova simulations describe electron capture now by the rates of Ref. [13]. However, no dedicated investigation of the role of electron capture (i.e. in comparison to the case where capture on heavy nuclei is neglected) has been performed.

In a recent supernova simulation [166] electron capture on nuclei has been identified as the dominating weak-interaction process and the main source of electron neutrinos during collapse. However, it was shown that pair-deexcitation of thermally excited nuclear states is an important source of the other neutrino types (electron anti-neutrinos, muon and tau neutrinos and their antiparticles).

The contribution of a particular nucleus to the reduction of Y_e during collapse,

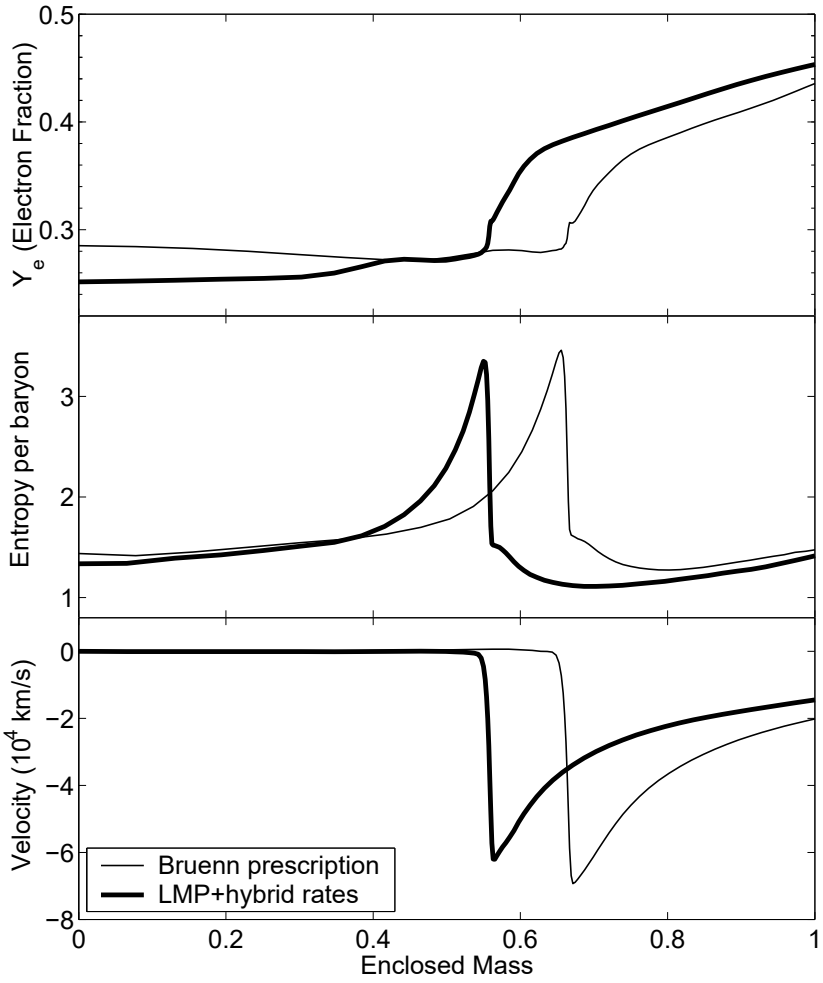

Figure 19. Comparison of Y_e (upper), entropy (middle) and velocity profiles (lower panel) at bounce obtained in supernova simulations with the shell model rates for nuclei in the mass range $A = 45$–110 ([34, 39], thick line) and the Bruenn rate parametrization ([18], thin line). (from [42]).

depends on the product of its abundance and of its capture rate. Both quantities are time-dependent and have to be integrated over the duration of the collapse. This study has been performed by Sullivan *et al.* [155] using rates calculated based on microscopic nuclear models where available. For the heavy nuclei, for which such rates are not individually available, they adopted the single-state approximation of Eq. (4).

Fig. 20 shows in the upper panel which nuclear ranges contribute to the change of Y_e with time, $\dot{Y}_e$. The top axis shows the time until bounce. The corresponding densities are 1.41×10^{11}, 4.06×10^{11}, 1.42×10^{12} g cm^{-3} at $t - t_b = -20, -10, -5$ ms, respectively. We note that $\dot{Y}_e$ grows with time during collapse and reaches its maximum after trapping has already set in. The increase reflects the fact that the electron chemical potential grows faster than other scales, in particular the average nuclear Q value of the composition,resulting in strong increases of the capture rates. The change in the capture rate is mainly driven by nuclei in the mass range $A = 65$-105. Rates calculated within

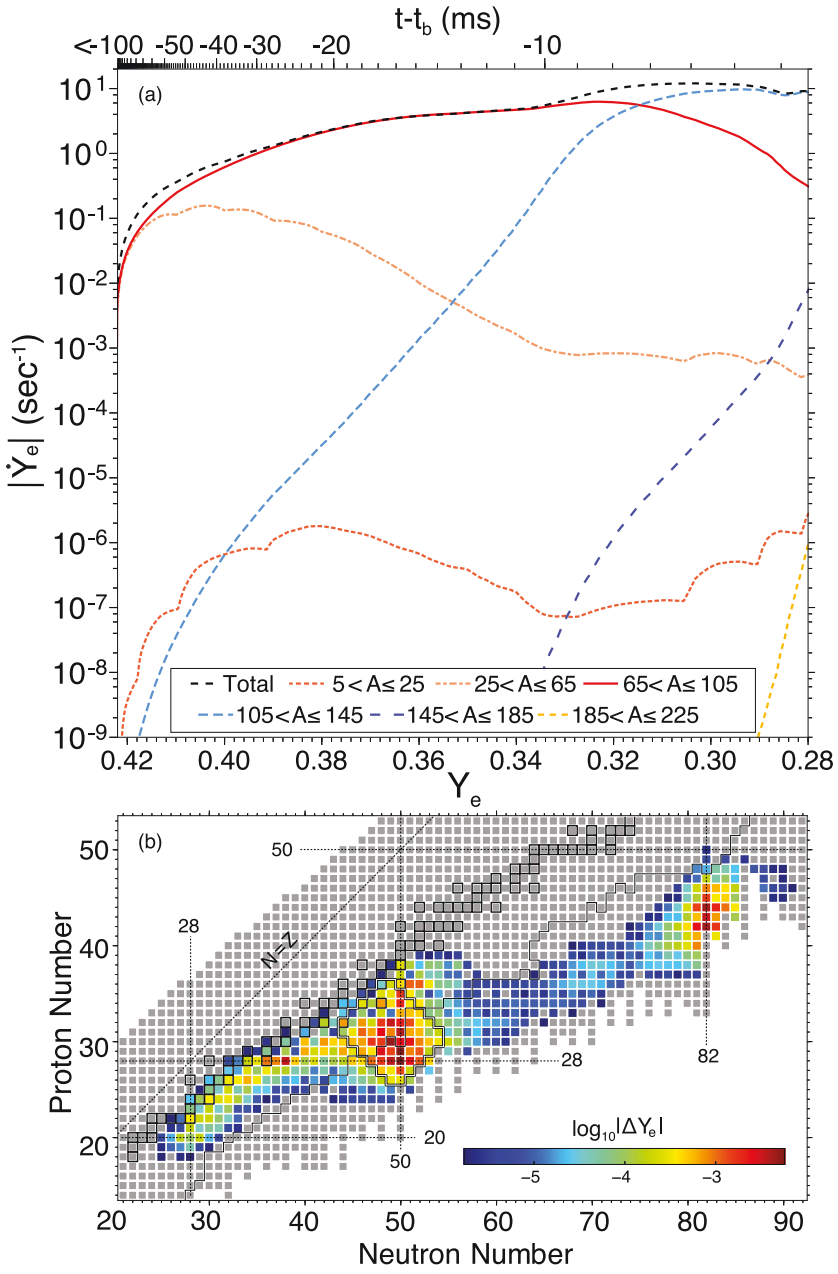

Figure 20. upper panel (a): The contribution of nuclear electron capture to the change of Y_e as function of Y_e which continuously reduces with time. As reference the upper axis vindicates the time until bounce. lower panel (b) The top 500 nuclei which contribute strongest to electron capture. (from [155]).

the hybrid model exist for about 200 nuclei in this range, which, however, does not cover all nuclei which contribute. The pf shell nuclei, for which accurate diagonalization shell model rates exist, dominate in the early collapse. Here capture rates are, however, smaller due to the smaller electron chemical potentials involved. Nuclei heavier than $A = 105$ contribute or dominate just before and during trapping.

The lower panel of Fig. 20 identifies how individual nuclei contribute to $\dot{Y}_e$, determined by integrating the respective contributions during collapse until trapping occurs. Due to this study, the relevant nuclei are those around the $N = 50$ shell closure centred in this range from ^{78}Ni to ^{82}Ge.

Sullivan *et al.* [155] also investigated which effect a systematic modification of the electron capture rates has on the supernova dynamics. When scaling the capture rates for all nuclei by factors between 0.1 and 10, they observed significant modifications. A systematic reduction of the rates throttles the effects which captures on nuclei have during collapse, as outlined above, driving the results back towards those where capture on nuclei were neglected. A systematic rate reduction by a factor 10 indeed increases the enclosed mass at bounce by about 16%, which is a similar effect as reported in Ref. [42]. Sullivan *et al.* [158] and Pascal *et al.* [156] argue that the single-state approximation might overestimate the rates for nuclei close to the $N = 50$ shell gap. A similar conclusion was drawn from the measurements of Gamow-Teller distributions for the ground states of the $N = 50$ nuclei ^{86}Kr [109] and ^{88}Sr [110]. As discussed above, the single-state approximation in fact does not consider nuclear structure effects which should be quite relevant in particular at shell closures. We note that structure effects are considered in the shell model rates used in Ref. [13] to set up a rate table for electron capture under collapse conditions, assuming, however, NSE for the nuclear composition. It has been shown that the use of alternative and improved Equations of State has rather small effects on the supernova dynamics [155, 156]. The dependence of the core composition on different equation of states and its indirect impact on stellar electron capture rates has been investigated in Refs. [167, 168]. An improved version of the single-state approximation is presented in [157]. The impact of a reduction of the $N = 50$ shell gap has been explored on ref. [169]. We also mention again that the TQRPA calculations and the hybrid model indicate that the blocking of the GT strength around $N = 50$ is largely overcome at stellar conditions due to thermal unblocking. Furthermore, both models predict sizable contributions from forbidden transitions at the astrophysical conditions at which $N = 50$ nuclei are abundant during the collapse.

4.2. Nucleosynthesis in thermonuclear supernovae

Thermonuclear, or Type Ia, supernovae are a class of supernovae which are distinct from the core-collapse version by their explosion mechanism and also due to their spectral composition (Type Ia spectra do no exhibit hydrogen lines, in contrast to spectra of core-collapse or Type II supernovae). In the currently favored model Type Ia supernovae correspond to the explosion of a White Dwarf in a binary star system triggered by mass

accretion from its companion star when this enters the Red Giant phase, White Dwarfs are a compact object produced as the final fate of intermediate mass stars. They are mainly composed of $N = Z$ nuclei, i.e. ^{12}C, ^{16}O, ^{20}Ne. The accretion adds to the White Dwarf mass bringing it towards the Chandrasekhar limit and increases the density in its interior to the point where carbon burning can be ignited. As the burning occurs in a highly degenerate environment, the energy set free cannot lead to expansion, but rather heats the surrounding. This results in a self-reinforcing acceleration of the burning until degeneracy can be lifted and the entire White Dwarfs is disrupted. The explosion mechanism - complete disruption of a White Dwarf in a thermonuclear runaway - leads to similarity among Type Ia events. For example, the observed peak magnitude and width of the lightcurves obey a simple scaling law (Philipps relation [170]) which makes Type Ia supernovae to standard candles for cosmological distances. This fact has been exploited to deduce the current acceleration of our Universe.

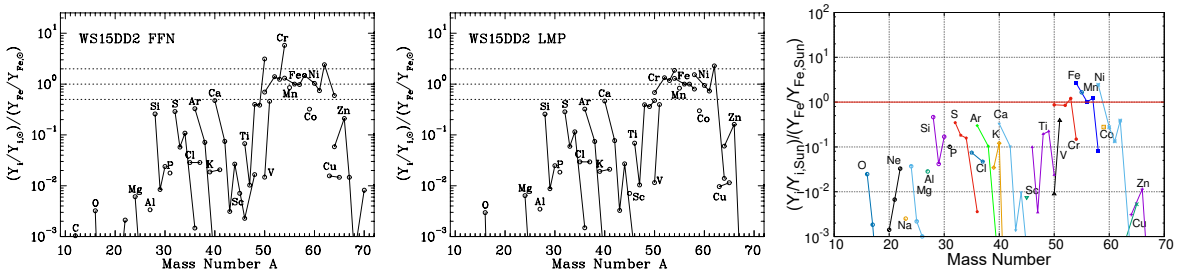

Figure 21. Influence of electron capture rates on type Ia nucleosynthesis. The two left panels show yields calculated for the WS15 progenitor model of Ref. [171] calculated with the FFN (left) and LMP (middle) electron capture rates (courtesy of F. Brachwitz, from [28]). The right panel shows the yields calculated for the W7 progenitor model of Ref. [171] replacing the LMP rates with improved shell model rates for selected nuclei in the Ni-Fe region (from [172]). All yields are relative to the solar abundances. The ordinate is normalized to ^{56}Fe).

After the burning flame has moved through the matter, the inner material behind the front, with a mass of about 1 $M_\odot$, has reached temperatures sufficiently high to drive the nuclear composition into nuclear statistical equilibrium. As the White Dwarf was composed of $N = Z$ nuclei, mainly ^{56}Ni is produced. Deviations towards nuclei with neutron excess occur due to electron captures in the hot and dense matter behind the front. The impact of these captures depend, besides the astrophysical conditions of density (about 10^9 g cm^{-3} and temperature ($T \sim 10^9$ K), on the speed of the flame (i.e. the time for electron captures before the star is disrupted) and obviously on the rates themselves. As discussed above, the diagonalization shell model (LMP) rates are systematically lower than the FFN rates for pf shell nuclei, in particular for the nuclei in the Ni-Fe mass range which are of importance for captures behind the type Ia burning front. Brachwitz *et al.* have performed nucleosynthesis studies in a one-dimensional supernova simulation based on the well known W15 progenitor model of Ref. [171] which starts from a 1.38 $M_\odot$ C-O White Dwarf [10, 173]. The faster FFN

rates lead to a stronger deleptonization in the innermost 0.1 $M_\odot$ core mass, reaching values down to $Y_e = 0.44$ in the center, while the slower LMP rates produce $Y_e = 0.45$ as the minimum value. As a consequence, the FFN rates predict an appreciable amount of neutron-rich nuclei like ^{50}Ti or ^{52}Cr, which are strongly overproduced compared to the solar abundances (left panel of Fig. 21). This overproduction constituted a serious problem [9] as roughly half of the ^{56}Fe content of the solar abundances are synthesized in type Ia supernovae and hence all nuclides, produced in type Ia, should not have overproduction factors larger than 2 as otherwise their relative abundances are in conflict with observation. As is shown in the middle panel of Fig. 21, the overproduction is removed when the slower LMP shell model rates are used. Suzuki has recently confirmed this finding in a study which replaced the LMP shell model rates for selected nuclei in the Ni-Fe mass range by those obtained with the GXPF1 residual interaction which gives better agreement with the measured GT strength in Ni isotopes [172]. Suzuki used a different progenitor model than Ref. [173] (the W7 model of [171]). But also his study shows that the overproduction of neutron-rich nuclei is removed if modern diagonalization shell model capture rates are used rather than the FFN rates (right panel in Fig. 21). Satisfyingly Suzuki only observes a small difference of 4% in the calculated abundances based on his shell model rates and on the LMP rates. Detailed studies of the sensitivity of nucleosynthesis in type Ia supernova can be found in refs [48, 49].

Electron captures and beta-decays, operating via URCA pairs (see section 3.1.2), are also important during the accretion and simmering phases of the evolution of CO WDs before the type Ia supernova explosion as they determine the neutron excess and the density at which the thermal runaway occurs [174]. Particularly important during these phases is the $^{13}\mathrm{N}(e^-, \nu_e)^{13}\mathrm{C}$ rate whose value is determined by beta-decay and charge-exchange data [175].

4.3. Accreting neutron stars and mergers

An old isolated neutron star can be described in beta equilibrium. However, such an equilibrium is broken in the crust if the star accretes mass from the interstellar medium (ISM) or from a binary star. For an old neutron star traversing the ISM, a mass of order 10^{-16} $M_\odot$ per year will be accreted as a layer on the neutron star surface. The temperature of the layer is low and is usually approximated as $T = 0$ [176]. In a binary system the mass flow can be higher leading to repeating burning of a surface layer with characteristic emission of X-rays with typical durations up to ~ 100 s (X-ray burster [177, 178]). Due to the re-occurrence of the break-outs, with typical periods of order a year, the ashes of previous events are pushed to higher densities and temperatures of order a few 10^8 K can be reached. These binary systems can also exhibit rare day-long X-ray bursts (so-called superbursts). Here carbon flashes, triggered by the fusion of two ^{12}C nuclei, heat the neutron star envelope so that hydrogen and helium burning becomes stable, suppressing the usual shorter x-ray bursts. These can only occur after

the envelope has sufficiently cooled [179]. Electron captures play interesting roles in both accretion scenarios.

The ISM matter which an old isolated neutron star accretes is mainly hydrogen. At sufficiently high densities hydrogen can start a sequence of nuclear reactions. However, in contrast to stellar hydrostatic burning this is not initiated by temperature, but by density fluctuations triggering so-called pycnonuclear reactions [180, 181]. The nuclear reaction sequence includes hydrogen and helium burning, producing nuclides up to ^{28}Si. Particular challenging is the evaluation of the pycnonuclear triple-alpha reaction rate as neither the ^{8}Be intermediate state nor the Hole state in ^{12}C can be thermally reached [182, 183, 184]. The fresh material produced by pycnonuclear reactions rests on original neutron star crust material, i.e ^{56}Fe or ^{62}Ni.

Electron captures can occur once the density reaches a value at which the electron chemical potential can overcome the nuclear Q value. For ^{16}O, which is the main product produced by pycnonuclear helium reactions, this happens at $\rho \sim 3 \times 10^{10}$ g cm^{-3}. As beta decay of the daughter nucleus ^{16}N is prohibited due to complete filling of the electron phase space at $T = 0$, the daughter nucleus immediately undergoes a second electron capture to ^{16}C as the required density is less than for ^{16}O. At the density required for the double electron capture on ^{16}O the underlying material of ^{56}Fe and ^{62}Ni has already undergone double electron captures to ^{56}Cr, followed to ^{56}Ti, and ^{62}Fe, respectively (see below). As shown in Ref. [176] this leads to several unstable situations where a denser layer (i.e. ^{16}C) rests on less denser layers (i.e. ^{56}Ti or ^{62}Fe), resulting in an overturn of the unstable interfaces. This scenario had been proposed as a possible explanation for gamma-ray bursts before these were identified as extra-galactical events with luminosities larger than observed for supernovae.

Double electron captures are expected also to occur in the crust of an accreting neutron star in a binary system. When accretion pushes the original surface layer, made mainly of ^{56}Fe, to higher densities, electron captures will transform ^{56}Fe to ^{56}Cr once $\rho > 1.5 \times 10^{9}$ g cm^{-3}. Haensel and Zdunik have studied the consequences for the accreted neutron star crust, build on a single-nucleus (^{56}Fe) approach [7] (see also [185, 186]. Upon pushing the matter to even higher densities, further double electron captures proceed (^{56}Cr $\rightarrow$ ^{56}Ti at $\rho = 1.1 \times 10^{10}$ g cm^{-3}, ^{56}Ti $\rightarrow$ ^{56}Ca at $\rho = 8 \times 10^{10}$ g cm^{-3}, ^{56}Ca $\rightarrow$ ^{56}Ar at $\rho = 2.5 \times 10^{11}$ g cm^{-3}), before the density is reached at which neutrons are emitted from the nucleus ($\rho = 4.1 \times 10^{11}$ g cm^{-3}, neutron drip). Thus, the double electron capture of ^{56}Ar is accompanied by the emission of free neutrons, ^{56}Ar $\rightarrow$ ^{52}S $+ 4n$. The successive electron captures lowers the charge of the nuclei so that pycnonuclear fusion reactions, induced by zero-point motion fluctuations in the Coulomb lattice become possible. The double electron captures, but in particular pycnonuclear fusion reactions are considerable heat source, as is discussed in [7, 187].

The crust composition, containing other nuclei than ^{56}Fe, complicates the situation. This is also true for the ashes of X-ray burst events which, due to repeating outbursts, are also successively pushed to higher densities and run through a similar sequence, to the one described above, of double electron captures, neutron deliberation and

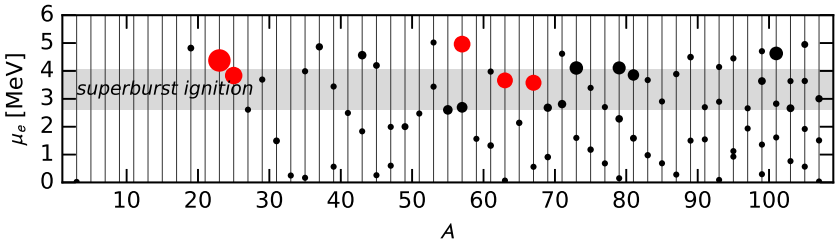

Figure 22. Depth at which URCA pairs of mass number A operate in neutron stars. The size of the data points corresponds to the neutrino luminosity of the pair, setting its mass fraction to $X = 1$. (The top 5 are colored in red.) The grey band indicates constraints for superburst ignition assuming an ignition at a column depth between $0.5–3 \times 10^{12}$ g cm^{-2}. (from [188]).

pycnonuclear fusion reactions [189]. As pointed out by Schatz *et al.* [8] the ashes of former burst events have finite temperatures (a few 10^8 K) which, although small compared to typical electron capture Q values, open up a small energy window at which beta decays of electron capture daughters can occur. For such an URCA process to occur the electron capture process has to satisfy two conditions: it must be mediated by an allowed transition to a state at excitation energies $E_x < T$ and the beta-decaying nucleus must no have a strong electron capture branch. On general grounds even-even nuclei, which are the most abundant nuclei in the crust, do not form URCA pairs but rather perform double electron captures [188]. On the other hand, nearly all odd-A nuclei can form URCA pairs. The authors of Ref. [188] have identified about 85 URCA pairs. Fig. 22 shows the neutrino luminosities of these pairs (setting the mass fraction of the nucleus on which an electron is captured to $X = 1$) and at which depth in the neutron star they operate. As pointed out in [8] cooling by URCA pairs in the crust reduces the heat transport from the crust into the region of the x-ray burst or superburst ashes which reside at less dense regions (this region is often called the ocean). This lowers the steady-state temperature in the ocean. This puts constrains on the ignition of the $^{12}\mathrm{C} + {}^{12}\mathrm{C}$ fusion reaction to start the next burst cycle. This ignition has now to occur at higher densities [188]. URCA pairs can also directly operate in the ocean. However, due to the lower densities nuclei are less neutron-rich with smaller Q values for electron captures than those in the crust. As the neutrino luminosity scales with Q^5, This strongly reduces the effectiveness of URCA pairs in the ocean [188].

Due to the simultaneous observation of the gravitational wave and the electromagnetic signal from GW170817, the merger of two neutron stars in a binary system has been identified as one of the astrophysical sites, see e.g. [190], where the r-process [191, 192, 193, 194] operates. Particularly important to determine nucleosynthesis in mergers is the Y_e value of the ejected material that is determined by weak processes. The initial Y_e profile of the neutron stars can be determined from beta-equilibrium. However, as the neutron stars approach each other and finally merge the temperature increases and neutrino emission becomes very important. An accurate prediction of the neutrino luminosities requires a description of high density neutrino-

matter interactions [195] and its implementation in neutrino radiation transport as is currently done in core-collapse supernova [196]. The absorption of both ν_e and $\bar{\nu}_e$ together with electron and positron captures leads to substantial changes on the Y_e of the ejected material particularly in the polar regions [197, 198, 199, 200]. These processes occur when the material is hot and constitutes mainly of neutrons and protons.

Another important source of material is the so-called secular ejecta originating from the accretion disk that surrounds the central remnant produced by the merger. If this is a long-lived neutron star, the neutrino luminosities are large enough to affect the neutron-to-proton ratio of the ejected material [201]. If the central object is a black-hole, the neutron-to-proton ratio is determined by a dynamical beta-equilibrium [202] between electron, positron captures and beta-decays operating in the accretion disk [203, 204, 205] on hot material that mainly is made of neutrons and protons. Due to the current understanding, electron capture on nuclei does not play an important role for r-process nucleosynthesis in neutron-star merger events.

4.4. Fate of intermediate-mass stars

The final fate of stars depend on their masses at birth. Stars with masses less than about 8 $M_\odot$ advance through hydrogen and helium burning. As they suffer significant mass losses by stellar winds their masses at the end of helium burning is not sufficient to ignite further burning stages. They end their lives as White Dwarfs, which are compact objects with a mass limit of 1.44 $M_\odot$ (Chandrasekhar mass), stabilized by electron degeneracy pressure. Stars with masses in excess of about 11 $M_\odot$ develop a core at the end of each burning phase which exceeds the Chandrasekhar mass. As a consequence they can ignite the full cycle of hydrostatic burning and end their lives as core-collapse supernovae, leaving either neutron stars or black holes as remnants. The fate of intermediate-mass stars (8–11 $M_\odot$) balances on a knife edge between collapsing into a neutron star or ending in a thermonuclear runaway which disrupts most of the core [206]. Simulations of such stars are quite sensitive to astrophysical uncertainties like convective mixing or mass loss rates [206]. On the other hand the major nuclear uncertainty, related to electron capture on ^{20}Ne, has recently been removed as this rate, as we have described above, is now known experimentally at the relevant astrophysical conditions. We briefly summarize the consequences which this nuclear milestone has for the fate of intermediate mass stars.

Intermediate mass stars go through hydrostatic hydrogen, helium and core carbon burning, but are not massive enough to ignite further advanced burning stages. In the center of the star a core develops which mainly consists of ^{16}O and ^{20}Ne, with smaller amounts of ^{23}Na and ^{24,25}Mg. Due to its position on the Hertzsprung-Russell diagram stars with such an ONe core are referred to as Super Asymptotic Giant Branch (AGB) stars. It is important to note that cores of Super-AGB stars are more dense than their counterparts after helium burning in more massive stars. As nuclear burning has ceased in the ONe core its gravitational collapse is counteracted by the electron

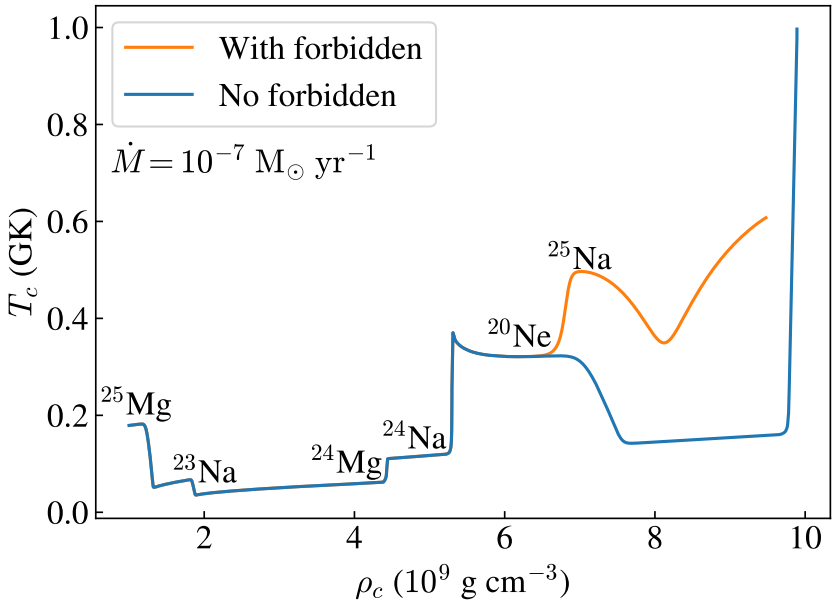

Figure 23. Temperature-density evolution of the ONeMg core of an intermediate mass star. The labels indicate at which densities the URCA pairs and the electron captures on ^{24}Mg and ^{20}Ne operate. The red (blue) lines show the evolution with (without) inclusion of the forbidden ground-state-to-ground-state contribution to the ^{20}Ne electron capture rate.The calculation assumes that the ONe core accretes a mass of 10^{-7} M$_\odot$ per year from ongoing hydrostatic burning. (from [52]).

degeneracy pressure. However, the densities achieved in the core result in electron chemical potentials large enough to initiate electron capture reactions, which reduce the pressure against collapse. Here two distinct processes play the essential role for the development of the core. This is shown in Fig. 23 which displays the final temperature-density evolution of the core center. First, several URCA pairs (^{25}Mg-^{25}Na, ^{23}Na-^{23}Ne, ^{25}Na-^{25}Ne) operate at various phases of this final evolution. These pairs are efficient cooling mechanism. Second, electron captures also occur on the abundant α-nuclei ^{24}Mg and ^{20}Ne once the electron chemical potentials overcome the capture Q values (the Q value of ^{16}O is too high for electron captures at these densities). But for these $N = Z$ nuclei, the electron capture daughters (^{24}Na and ^{20}F) also capture electron which due to their smaller Q values than in the first captures occur significantly faster than competing β-decays. Furthermore the second capture proceeds often to excited states in their daughters which then decay by γ emission to the ground states and heat the environment (see Fig. 23). Due to its lower initial Q-value the double electron capture on ^{24}Mg proceeds at lower densities than the one on ^{20}Ne. Recognizing the low temperature at the onset of electron capture on ^{20}Ne (about 300 keV), basically due to the efficient URCA cooling [207], the authors of Ref. [51] pointed out that the transition from the ^{20}Ne 0^+ ground state to the ^{20}F 2^+ ground state, although second forbidden, could dominate the rate at core conditions as all other transitions were exponentially suppressed by either the tail of the electron distribution or a Boltzmann factor due to

thermal exc

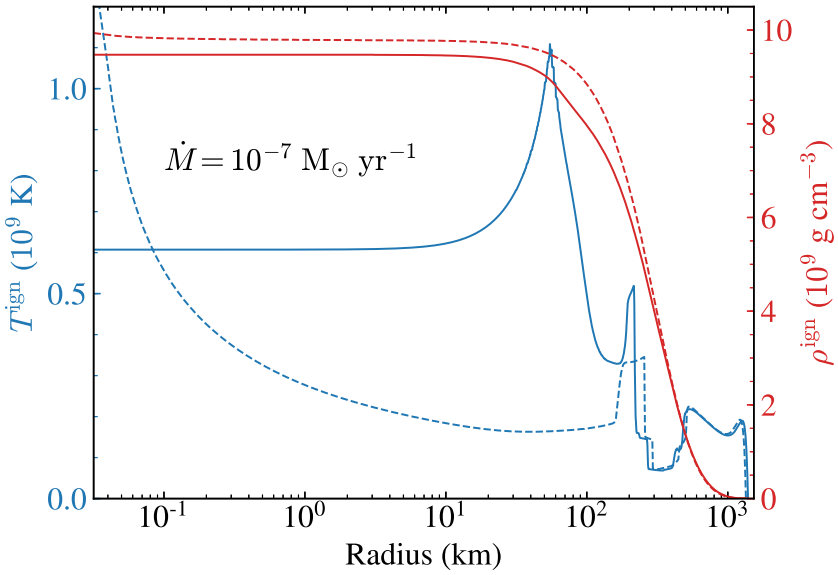

Figure 24. Temperature (blue) and density (red) profiles of an ONe core at ignition of oxygen fusion, calculated with (solid lines) and without (dashed lines) consideration of the forbidden ground-state-to-ground-state transition in the ^{20}Ne electron capture rate. The calculations were performed using the spherical MESA code [208] and assuming that the ONe core accretes a mass of $10^{-7} M_\odot$ per year from ongoing hydrostatic burning. (from [52]).

The inclusion of the 'forbidden' ground-state-to-ground-state transition in the electron capture rate on ^{20}Ne shifts the onset of this capture to lower densities before the last epoch of URCA cooling by the ^{25}Na-^{25}Ne pair (see Fig. 23). This shift in density has, however, important impact on the fate of the star ending either as gravitational collapse or thermonuclear explosion. This fate is determined by the competition between electron capture and nuclear energy generation by oxygen fusion [206]. If the ignition of oxygen (requiring temperatures in excess of 10^9 K) occurs at low enough densities, the fusion generates sufficient energy to reverse the collapse and to disrupt the star in a thermonuclear explosion. At higher densities, the deleptonization behind the burning front is so rapid that the loss of pressure cannot be recovered by nuclear burning. In this case the core continues to collapse, ending as a neutron star. The increase of the ^{20}Ne electron capture rate due to the contribution of the forbidden transition seems to shift the fate towards thermonuclear explosions [52]. This is demonstrated in Fig. 24 which is based on a spherical simulation of the core evolution. In the calculation, performed without the inclusion of the forbidden contribution to the rate, oxygen is ignited in the center, while in the case using the experimental ^{20}Ne capture rate with inclusion of the forbidden transition, the star develops an isothermal core with temperatures below the ignition value. In this inner core double electron capture on ^{20}Ne continues generating heating which leads to an off-center ignition of oxygen burning (at a radius of 58 km for the case shown in Fig. 24). We also note that, without the forbidden contribution, the

core reaches a higher density at ignition.

To determine the fate of the star requires to study the propagation of the burning front, which needs a 3D hydrodynamical treatment to resolve the relevant length scales. Such studies have been reported in [52] and all simulations, matched to the parameters of the spherical MESA results ended in thermonuclear explosions producing an ONeFe White Dwarf remnant. This has significant implications for the total nucleosynthesis yields of intermediate mass stars as thermonuclear explosions eject about 0.01 $M_\odot$ more mass than gravitational collapse and intermediate mass stars are much more abundant than heavier stars. A first exploration shows that the ejecta of thermonuclear explosions are particularly rich in certain neutron-rich Ca, Ti, Cr isotopes and in trans-iron elements Zn, Se and Kr [52]. This might have interesting implications for the understanding of the early chemical evolution of our galaxy [209].

4.5. Helium flashes in accreting Helium White Dwarfs

Subluminous B stars are core-helium burning stars with thin hydrogen envelopes and masses of about 0.5 $M_\odot$ [210]. Often these stars exist in tight binaries with White Dwarfs [211]. When the White Dwarf accretes matter from the unburned outer layers of its companion star, also some amount of ^{14}N is present depending on the initial metallicity of the donor star. Electron capture on ^{14}N is then a decisive factor for the fate of the accreted material.

Due to its low Q value of 0.667 MeV, electrons are captured on ^{14}N once the density of the accreted matter on the WD surface exceeds a threshold value of about 1.156×10^6 g cm^{-3} [212]. As the respective temperatures are rather low (T less than a few 10^8 K), the capture solely proceeds by the allowed transition between the ^{14}N and ^{14}C ground states. The respective transition matrix element is known from the ^{14}C beta decay. Coulomb corrections due to environment effects are relatively minor, but are considered in recent astrophysical applications [212].

For the temperatures involved and for densities larger than about 10^6 g cm^{-3}, the electron capture rate is larger than the competing β decay and, in the helium-rich environment, the electron capture is followed by an α capture on ^{14}C [213]. The energy generation by this so-called NCO reaction ($^{14}\mathrm{N}(e^-,\nu_e)^{14}\mathrm{C}(\alpha,\gamma)^{18}\mathrm{O}$) [214] — despite some uncertainties in the α-capture rate on ^{14}C [215] — is larger than by the triple-alpha reaction in the relevant temperature-density range. Thus, it is the NCO reaction which triggers a rather steep rise of the temperature in the environment so that as a second step also the triple-alpha reaction will be ignited. This finally leads to a thermonuclear instability which is observed as helium flashes.

The evolution of these flashes depend crucially on the accretion mass flow [213]. If the mass flow is large (10^{-8} $M_\odot$ yr^{-1}), the energy released from the gravitational contraction leads to heating of the environment enabling the ^{14}C nucleus to capture an α particle fast. The electron capture process controls the NCO reaction sequence and no significant amount of ^{14}C is being built up. For smaller mass flows (10^{-9} $M_\odot$ yr^{-1})

the energy released by contraction can be radiated away, keeping the temperature in the core low. Hence, when the core density exceeds the value for electron capture the temperature is too low to ignite α captures on ^{14}C. This occurs at conditions with higher densities and after ^{14}N has been completely converted to ^{14}C. Simulations also show that for smaller accretion rates, the core becomes convectively unstable. The time scale on which the flashes develop depend also on the accretion rate and are significantly shorter for smaller rates (a few 10^7 yr for 10^{-9} $M_\odot$ yr^{-1})

5. Summary

In his authoritative review on core-collapse supernovae, Hans Bethe stated in 1990 [1]: "The theory of electron capture has gone a full circle and a half." He was referring to the fact that in early models, capture was assumed to occur on free protons. This was put into question by BBAL [2] who noted that the concentration of free protons during collapse is very low and that the capture takes place on nuclei with mass numbers A = 60–80, changing a proton in the $f_{7/2}$ shell to a neutron in the $f_{5/2}$ orbital by allowed Gamow-Teller transition. Following Bethe, the third semi-circle is due to Fuller's observation that the neutron $f_{5/2}$ orbitals are occupied at neutron number $N = 38$ [17], blocking Gamow-Teller transitions within the pf shell. Hence at the time when Bethe wrote his famous article, electron capture in supernovae was assumed to occur on free protons and capture on nuclei was switched off for nuclei with $N > 38$ [18].

As we have summarized in this manuscript, the experimental and theoretical work of the last two decades implies that this picture is too simple. Experimental techniques to measure Gamow-Teller strength distributions based on charge-exchange reactions with progressively better energy resolutions — advancing from the pioneering (n, p) reactions to much more refined $(d, ^2\mathrm{He})$ and $(t, ^3\mathrm{He})$ reactions — give clear evidence that nuclear correlations play a decisive role in the total strength, and even more, for the fragmentation of the GT distribution, thus invalidating the Independent Particle Model on which the early electron capture work, which was discussed and reviewed by Bethe in 1990 [1], were based. In parallel, many-body models became available which were capable to account for the relevant nuclear correlations and which describe the experimental GT data quite well. Importantly, these models, and also experimental data, imply that the GT strength is not blocked at the shell gap between the pf and $g_{9/2}$ orbitals caused by strong nuclear cross-shell correlations. As a major consequence, electron capture takes place on nuclei during the entire collapse. With this result, the theory of electron capture has gone now two complete circles.

The evaluation of stellar electron capture for core-collapse supernovae rests on the fact that, with progressing core density, the electron chemical potential grows significantly faster than the average Q value which dominate the core composition. As a consequence, detailed description of the nuclear strength functions (i.e. Gamow-Teller) are only needed for nuclei in the Fe-Ni mass range (A = 45–65), which are most abundant during the early collapse phase, while for the neutron-rich, heavy nuclei,

which dominate later in the collapse at higher densities, a more overall reproduction of the strength functions (now, however, including forbidden transitions) suffice. This is a quite fortunate situation.

For those nuclei, for which the calculation of stellar capture rates requires detailed descriptions of the allowed strength functions (pf- and sd-shell nuclei, where the latter occur in burning stages prior to collapse), diagonalization shell model calculations can be performed which in general reproduce the measured GT strength functions quite well. In fact, if the capture rates are calculated solely from the ground state distributions, the rates obtained from data and from shell model agree within better than a factor of 2 at the relevant astrophysical conditions. The theoretical capture rates (i.e. [34, 13]) consider from excited states also from shell model calculations, accounting for the fact that each nuclear state has its own individual strength distribution. There are no indications that the shell model results for excited states might be less reliable than for the ground states. However, there is concern that the procedure applied in [34] might slightly underestimate the partition function at higher temperatures [139].

The fact that cross-shell correlations unblock Gamow-Teller transitions even in the ground states of nuclei with proton numbers $Z < 40$) and neutron numbers $N > 40$ has been experimentally proven by experimental data for Gamow-Teller strength distributions and also from spectroscopic information obtained from transfer reactions. Thus, the assumption that GT transitions are Pauli blocked for nuclei with $N > 38$ has been disproven by experiment. Modern many-body models like the diagonalization shell model (for selected nuclei) and the Shell Model Monte Carlo approach can reproduce such cross-shell correlations. The latter approach has been adopted to determine partial occupation numbers in large model spaces including the shell gaps at $N = 40$ and 50. The capture rates were then calculated within a 'hybrid model' from these occupation numbers within the framework of the Random Phase Approximation, exploiting the fact that these heavier nuclei become abundant during the collapse at sufficiently high densities requiring only the overall, but not the detailed reproduction of the GT strength functions. Contributions from forbidden transitions were included, which become progressively important with increasing density. The hybrid model indicates that the gaps at $N = 40$ and 50 lead to some reduction of the capture rates, but the rares are clearly large enough so that captures on nuclei dominate the one on free protons during the entire collapse. This is clearly borne out in modern supernova simulations, thus closing the second circle as referred to by Hans Bethe.

The unblocking of the GT strength at the neutron numbers $N = 40$ and 50 has also been confirmed by calculations performed within the Thermal Quasiparticle RPA approach, which consistently considers correlations up to the 2p-2h level. As cross-shell correlations require in general correlations higher than 2p-2h, GT strength, in particular at low excitation energies, can be missed. This translates into the observation that at modest temperatures and densities capture rates obtained within the Thermal QRPA are somewhat smaller than in the hybrid model. At higher temperatures and densities the two models give very similar results, including the neutron-rich nuclei with $N = 50$,

which significantly contribute to the capture process at these astrophysical conditions. Both theoretical approaches imply that at the respective temperatures of order $T = 1$ MeV, configurations from higher shells, which are strongly reduced in the ground state, are present in the thermally excited nuclear states and significantly unblock the GT strength. This observation is quite important as the ground state GT distribution for such nuclei has been experimentally observed to have nearly vanishing strength and the electron capture rate would nearly be blocked if calculated from the ground state distribution. While the unblocking appears to be quite solid on theoretical ground, experimental verification is desirable.

Although core-collapse supernovae are arguably the most important astrophysical application, electron captures play also a role in other astrophysical environments. In thermonuclear supernovae the rate of electron captures on nuclei determine the production yield of neutron-rich nuclei. As the relevant nuclei are those in the Fe-Ni mass range, the experimental and theoretical (by diagonalization shell model calculations) progress have constrained the relevant capture rates significantly up to a degree that improved description of details of the GT strength distribution changed the nucleosynthesis yields by only a few percent. The description of capture rates for *sd*-shell nuclei, again based on shell model calculations and data, has reached a similar degree of accuracy which appears to be sufficient for the simulation of this process for the core evolution of intermediate mass stars. However, attention has been drawn recently to the fact that in the low-temperature-low-density environment of such stellar cores only a few transitions dominate the capture rates and that in exceptional situations also a forbidden transition can noticeably contribute to the rate. Such a situation happens for the capture on ^{20}Ne where the second forbidden transition from the ^{20}Ne ground-state to the ^{20}F ground state enhances the capture rate just at the most crucial conditions for the core evolution. The transition strength has now been measured so that the entire electron capture rate on ^{20}Ne is now experimentally determined in the relevant temperature-density regime.

Double electron captures, initiated on abundant even-even nuclei, are relevant for the crust evolution of accreting neutron stars. The process is triggered once the electron chemical potential (i.e. the core density) is high enough for electrons to overcome the Q value between the even-even mother nucleus and the odd-odd daughter. As the Q value of the second capture step on the odd-odd nucleus is smaller due to nuclear pairing, this energy gain can be transferred into crust heating. For simulations of the crust evolution, generally one is not so much interested in the capture rate (which is often fasted than competing time scales), but in the portion of the energy gain which is translated into heat. As this can involve quite exotic neutron-rich nuclei a detailed determination of this energy portion is a formidable nuclear structure challenge and current models are likely too uncertain.

Despite the progress which has been achieved in recent years in the determination of stellar electron capture rates, further improvements are certainly desirable and, in specific cases, needed. Additional precision measurements of Gamow-Teller strength

distributions for *sd*- and *pf*-shell nuclei will lead to further improvements and to refinements of the shell model calculations, however, it is not expected that these improvements will have significant impact on supernova dynamics or nucleosynthesis. It is, however, desirable that the gap of nuclei (with mass numbers $A = 38$–45), for which no shell model electron capture rates exist, should be filled. Such calculations are challenging as they require an accurate description of cross-shell correlations. They would certainly benefit from some detailed experimental GT distribution measurements. A particularly interesting and important case is ^{40}Ar, which serves as material for neutrino detectors like ICARUS [216, 217, 218], which holds potential for the detection of supernova neutrinos. Detailed GT$_-$ data from (p, n) [219] and $(^3\mathrm{He}, t)$ charge-exchange data [220] and M1 data from (γ, γ') photon scattering reactions [221] can serve as experimental constraints for the determination of charged-current (ν_e, e^-) and neutral-current (ν, ν') cross sections on ^{40}Ar. However, GT$_+$ data, which are relevant for electron capture and charged-current $(\bar{\nu}_e, e^+)$ cross sections do not exist yet. In principle, forbidden transitions, not considered in the shell model electron capture rates for *sd* and *pf*-shell nuclei, can contribute to the rates. But such contributions will only be relevant in core-collapse supernovae at higher temperatures than those at which these nuclei dominate the core composition. The case of ^{20}Ne, for which a second forbidden transition dominates the capture rate at the relevant conditions during the core evolution of intermediate mass stars, shows, however, that such exceptional cases can occur in cases of rather low temperatures where only a few transitions contribute to the capture rate. No other case has yet been identified, however, caution is asked for.

The shell gaps at neutron numbers $N = 40$ and 50 do not block electron capture on nuclei in current supernova models. In both cases, this is based on modern many-body models which at $N = 40$ overcome the gap by nucleon correlations, while for $N = 50$ thermal excitations are the main unblocking mechanism (plus contributions from other multipoles than Gamow-Teller). For $N = 40$, the finding is supported by experimental data, although yet quite limited. It would be desirable if the data pool could be enlarged. It is particularly tempting that recent developments open up the measurements of GT distributions for unstable neutron-rich nuclei, based on charge-exchange reactions performed in inverse kinematics. Such additional data would certainly be welcome to further constrain models. At $N = 50$, theoretical models imply that cross-shell correlations induced by thermal excitation render ground state GT distributions not applicable for the calculation of capture rates at the finite temperatures which exist in the astrophysical environment when these heavier and very neutron-rich nuclei dominate the capture process. Although the two models which have been applied to $N = 50$ nuclei agree rather well in their rate predictions, improvements of the models are conceivable. On one hand, the finite-temperature QRPA model should be extended to non-spherical nuclei and, in the midterm, also to include higher correlations like in second QRPA approach. On the other hand, the Shell Model Monte Carlo approach is uniquely suited to study nuclear properties at the finite temperatures of relevance. It might be interesting to calculate the GT strength function at those temperatures

directly within the SMMC approach. This presupposes the handling of a numerically ill-defined inverse Laplace transformation. First steps in this direction have been taken in Ref. [222].

Of course, it is always conceivable that observations or astrophysical simulations of supernovae or other astrophysical objects point to the need of particular electron capture rates which then require specific experimental and theoretical attention.

In summary, the description of stellar electron capture has come a long and winding way. The experimental and theoretical progress of recent years has probably firmly established that electron capture proceeds on nuclei during core-collapse supernovae. The circle, as attributed to by Hans Bethe, might have come to an end.

Acknowledgements

The authors gratefully acknowledge support and assistance by their colleagues Sam M. Austin, B. A. Brown, E. Caurier, S. Couch, D. J. Dean, J. Engel, T. Fischer, Y. Fujita, A. Heger, H.-T. Janka, A. Juodagalvis, R. W. Hix, E. Kolbe, O. Kirsebom, A. Mezzacappa, F. Nowacki, E. O'Connor, A. Poves, J. Sampaio, H. Schatz, A. Spyrou, T. Suzuki, F.-K. Thielemann, S. E. Woosley, Y. Zhi, and A. P. Zuker. G.M.P. acknowledges the support of the Deutsche Forschungsgemeinschaft (DFG, German Research Foundation) – Project-ID 279384907 – SFB 1245 "Nuclei: From Fundamental Interactions to Structure and Stars" and the "ChETEC" COST Action (CA16117), funded by COST (European Cooperation in Science and Technology). R.Z. gratefully acknowledges support by the US National Science Foundation under Grants PHY-1913554 (Windows on the Universe: Nuclear Astrophysics at the NSCL), PHY-1430152 (JINA Center for the Evolution of the Elements), and PHY-1927130 (AccelNet-WOU: International Research Network for Nuclear Astrophysics [IReNA])

References

[1] Bethe H A 1990 *Rev. Mod. Phys.* **62** 801–866
[2] Bethe H, Brown G, Applegate J and Lattimer J 1979 *Nucl. Phys. A* **324** 487–533
[3] Fuller G M, Fowler W A and Newman M J 1982 *Astrophys. J. Suppl.* **48** 279
[4] Janka H T, Langanke K, Marek A, Martínez-Pinedo G and Müller B 2007 *Phys. Rep.* **442** 38–74
[5] Doherty C L, Gil-Pons P, Siess L and Lattanzio J C 2017 *Publ. Astron. Soc. Austr.* **34** e056
[6] Nomoto K and Leung S C 2017 *Electron Capture Supernovae from Super Asymptotic Giant Branch Stars* (Cham: Springer International Publishing)
[7] Haensel P and Zdunik J L 1990 *Astron. & Astrophys.* **227** 431
[8] Schatz H, Gupta S, Möller P, Beard M, Brown E F, Deibel A T, Gasques L R, Hix W R, Keek L, Lau R, Steiner A W and Wiescher M 2014 *Nature* **505** 62–5
[9] Iwamoto K, Brachwitz F, Nomoto K, Kishimoto N, Umeda H, Hix W R and Thielemann F 1999 *Astrophys. J. Suppl.* **125** 439–462
[10] Brachwitz F, Dean D J, Hix W R, Iwamoto K, Langanke K, Martínez-Pinedo G, Nomoto K, Strayer M R, Thielemann F and Umeda H 2000 *Astrophys. J.* **536** 934–947
[11] Cooperstein J and Wambach J 1984 *Nucl. Phys. A* **420** 591–620
[12] Langanke K and Martínez-Pinedo G 2000 *Nucl. Phys. A* **673** 481–508

[13] Juodagalvis A, Langanke K, Hix W, Martínez-Pinedo G and Sampaio J 2010 *Nucl. Phys. A* **848** 454–478
[14] Fuller G M, Fowler W A and Newman M J 1980 *Astrophys. J. Suppl.* **42** 447–473
[15] Fuller G M, Fowler W A and Newman M J 1982 *Astrophys. J.* **252** 715
[16] Fuller G M, Fowler W A and Newman M J 1985 *Astrophys. J.* **293** 1
[17] Fuller G M 1982 *Astrophys. J.* **252** 741–764
[18] Bruenn S W 1985 *Astrophys. J. Suppl.* **58** 771–841
[19] Gaarde C, Rapaport J, Taddeucci T N, Goodman C D, Foster C C, Bainum D E, Goulding C A, Greenfield M B, Horen D J and Sugarbaker E 1981 *Nucl. Phys. A* **369** 258
[20] Osterfeld F 1992 *Rev. Mod. Phys.* **64** 491–557
[21] Vetterli M C, Haeusser O, Abegg R, Alford W P, Celler A, Frekers D, Helmer R, Henderson R, Hicks K H, Jackson K P, Jeppesen R G, Miller C A, Raywood K and Yen S 1990 *Phys. Rev. C* **40** 559–569
[22] Vetterli M C, Jackson K P, Celler A, Engel J, Frekers D, Häusser O, Helmer R, Henderson R, Hicks K H, Jeppesen R G, Larson B, Pointon B, Trudel A and Yen S 1992 *Phys. Rev. C* **45** 997–1004
[23] Helmer R L, Punyasena M A, Abegg R, Alford W P, Celler A, El-Kateb S, Engel J, Frekers D, Henderson R S, Jackson K P, Long S, Miller C A, Olsen W C, Spicer B M, Trudel A and Vetterli M C 1997 *Phys. Rev. C* **55**
[24] Frekers D 2006 *Prog. Part. Nucl. Phys.* **57** 217–225
[25] Martínez-Pinedo G, Liebendörfer M and Frekers D 2006 *Nucl. Phys. A* **777** 395–423
[26] Frekers D and Alanssari M 2018 *Eur. Phys. J. A* **54** 177
[27] Zegers R G T, Akimune H, Austin S M, Bazin D, Berg A M d, Berg G P A, Brown B A, Brown J, Cole A L, Daito I, Fujita Y, Fujiwara M, Galès S, Harakeh M N, Hashimoto H, Hayami R, Hitt G W, Howard M E, Itoh M, Jänecke J, Kawabata T, Kawase K, Kinoshita M, Nakamura T, Nakanishi K, Nakayama S, Okumura S, Richter W A, Roberts D A, Sherrill B M, Shimbara Y, Steiner M, Uchida M, Ueno H, Yamagata T and Yosoi M 2006 *Phys. Rev. C* **74** 024309
[28] Langanke K and Martínez-Pinedo G 2003 *Rev. Mod. Phys.* **75** 819–862
[29] Heger A, Woosley S E, Martínez-Pinedo G and Langanke K 2001 *Astrophys. J.* **560** 307–325
[30] Caurier E, Martínez-Pinedo G, Nowacki F, Poves A and Zuker A P 2005 *Rev. Mod. Phys.* **77** 427–488
[31] Brown B A and Wildenthal B H 1988 *Annu. Rev. Nucl. Part. Sci.* **38** 29–66
[32] Caurier E, Langanke K, Martínez-Pinedo G and Nowacki F 1999 *Nucl. Phys. A* **653** 439–452
[33] Oda T, Hino M, Muto K, Takahara M and Sato K 1994 *At. Data Nucl. Data Tables* **56** 231–403
[34] Langanke K and Martínez-Pinedo G 2001 *At. Data Nucl. Data Tables* **79** 1–46
[35] Heger A, Langanke K, Martínez-Pinedo G and Woosley S E 2001 *Phys. Rev. Lett.* **86** 1678–1681
[36] Langanke K, Kolbe E and Dean D J 2001 *Phys. Rev. C* **63** 032801
[37] Zhi Q, Caurier E, Cuenca-García J J, Langanke K, Martínez-Pinedo G and Sieja K 2013 *Phys. Rev. C* **87** 025803
[38] Grewe E W, Bäumer C, Dohmann H, Frekers D, Harakeh M N, Hollstein S, Johansson H, Popescu L, Rakers S, Savran D, Simon H, Thies J H, van den Berg A M, Wörtche H J and Zilges A 2008 *Phys. Rev. C* **78** 044301
[39] Langanke K, Martínez-Pinedo G, Sampaio J M, Dean D J, Hix W R, Messer O E B, Mezzacappa A, Liebendörfer M, Janka H T and Rampp M 2003 *Phys. Rev. Lett.* **90** 241102
[40] Johnson C W, Koonin S E, Lang G H and Ormand W E 1992 *Phys. Rev. Lett.* **69** 3157–3160
[41] Koonin S E, Dean D J and Langanke K 1997 *Phys. Rep.* **278** 1–77
[42] Hix W R, Messer O E B, Mezzacappa A, Liebendörfer M, Sampaio J, Langanke K, Dean D J and Martínez-Pinedo G 2003 *Phys. Rev. Lett.* **91** 201102
[43] Hix W R and Thielemann F K 1996 *Astrophys. J.* **460** 869–894
[44] Dzhioev A A, Vdovin A I, Ponomarev V Y, Wambach J, Langanke K and Martínez-Pinedo G 2010 *Phys. Rev. C* **81** 015804

[45] Dzhioev A A, Langanke K, Martínez-Pinedo G, Vdovin A I and Stoyanov C 2020 *Phys. Rev. C* **101** 025805
[46] Nomoto K 1987 *Astrophys. J.* **322** 206–214
[47] Takahara M, Hino M, Oda T, Muto K, Wolters A, Glaudemans P and Sato K 1989 *Nucl. Phys. A* **504** 167–192
[48] Parikh A, José J, Seitenzahl I R and Röpke F K 2013 *Astron. & Astrophys.* **557** A3
[49] Bravo E 2019 *Astron. & Astrophys.* **624** A139
[50] Suzuki T, Toki H and Nomoto K 2016 *Astrophys. J.* **817** 163
[51] Martínez-Pinedo G, Lam Y H, Langanke K, Zegers R G T and Sullivan C 2014 *Phys. Rev. C* **89** 045806
[52] Kirsebom O S, Jones S, Strömberg D F, Martínez-Pinedo G, Langanke K, Röpke F K, Brown B A, Eronen T, Fynbo H O U, Hukkanen M, Idini A, Jokinen A, Kankainen A, Kostensalo J, Moore I, Möller H, Ohlmann S T, Penttilä H, Riisager K, Rinta-Antila S, Srivastava P C, Suhonen J, Trzaska W H and Äystö J 2019 *Phys. Rev. Lett.* **123** 262701
[53] Bahcall J N 1962 *Phys. Rev.* **128** 1297–1301
[54] Bahcall J N and Moeller C P 1969 *Astrophys. J.* **155** 511
[55] Johnson C W, Kolbe E, Koonin S E and Langanke K 1992 *Astrophys. J.* **392** 320–327
[56] Adelberger E G, Austin S M, Bahcall J N, Balantekin A B, Bogaert G, Brown L S, Buchmann L, Cecil F E, Champagne A E, de Braeckeleer L, Duba C A, Elliott S R, Freedman S J, Gai M, Goldring G, Gould C R, Gruzinov A, Haxton W C, Heeger K M, Henley E, Johnson C W, Kamionkowski M, Kavanagh R W, Koonin S E, Kubodera K, Langanke K, Motobayashi T, Pandharipande V, Parker P, Robertson R G, Rolfs C, Sawyer R F, Shaviv N, Shoppa T D, Snover K A, Swanson E, Tribble R E, Turck-Chièze S and Wilkerson J F 1998 *Rev. Mod. Phys.* **70** 1265–1291
[57] Adelberger E G, García A, Robertson R G H, Snover K A, Balantekin A B, Heeger K, Ramsey-Musolf M J, Bemmerer D, Junghans A, Bertulani C A, Chen J W, Costantini H, Prati P, Couder M, Uberseder E, Wiescher M, Cyburt R, Davids B, Freedman S J, Gai M, Gazit D, Gialanella L, Imbriani G, Greife U, Hass M, Haxton W C, Itahashi T, Kubodera K, Langanke K, Leitner D, Leitner M, Vetter P, Winslow L, Marcucci L E, Motobayashi T, Mukhamedzhanov A, Tribble R E, Nollett K M, Nunes F M, Park T S, Parker P D, Schiavilla R, Simpson E C, Spitaleri C, Strieder F, Trautvetter H P, Suemmerer K and Typel S 2011 *Rev. Mod. Phys.* **83** 195–246
[58] Simonucci S, Taioli S, Palmerini S and Busso M 2013 *Astrophys. J.* **764** 118
[59] Clayton D D 1968 *Principles of stellar evolution and nucleosynthesis* (New York: McGraw-Hill, 1968)
[60] Takahashi K and Yokoi K 1983 *Nucl. Phys. A* **404** 578–598
[61] Takahashi K and Yokoi K 1987 *At. Data Nucl. Data Tables* **36** 375–409
[62] Yokoi K, Takahashi K and Arnould M 1985 *Astron. & Astrophys.* **145** 339–346
[63] Kappeler F, Beer H and Wisshak K 1989 *Rep. Prog. Phys.* **52** 945–1013
[64] Käppeler F, Gallino R, Bisterzo S and Aoki W 2011 *Rev. Mod. Phys.* **83** 157–194
[65] Harakeh M N and van der Woude A 2001 *Giant Resonances: Fundamental High-Frequency Modes of Nuclear Excitations* (New York: Oxford University Press)
[66] Ichimura M, Sakai H and Wakasa T 2006 *Prog. Part. Nucl. Phys.* **56** 446–531
[67] Fujita Y, Rubio B and Gelletly W 2011 *Prog. Part. Nucl. Phys.* **66** 549 – 606
[68] Taddeucci T, Goulding C, Carey T, Byrd R, Goodman C, Gaarde C, Larsen J, Horen D, Rapaport J and Sugarbaker E 1987 *Nucl. Phys. A* **469** 125 – 172
[69] Fujita Y, Rubio B and Gelletly W 2011 *Prog. Part. Nucl. Phys.* **66** 549 – 606
[70] Ikeda K, Fujii S and Fujita J 1963 *Phys. Lett. B* **3** 271 – 272
[71] Gaarde C *et al.* 1981 *Nucl. Phys.* **A369** 258
[72] Gaarde C 1985 *Proc. Niels Bohr Centennial Conference on Nuclear Structure, Copenhagen* ed Broglia R A, Hagemann G B and Herskind B (North-Holland, Amsterdam) p 449c

[73] Langanke K and Kolbe E 2001 *At. Data. Nucl. Data Tables* **79** 293–315
[74] Balasi K, Langanke K and Martínez-Pinedo G 2015 *Prog. Part. Nucl. Phys.* **85** 33–81
[75] Love W G and Franey M A 1981 *Phys. Rev. C* **24** 1073–1094
[76] Sasano M, Sakai H, Yako K, Wakasa T, Asaji S, Fujita K, Fujita Y, Greenfield M B, Hagihara Y, Hatanaka K, Kawabata T, Kuboki H, Maeda Y, Okamura H, Saito T, Sakemi Y, Sekiguchi K, Shimizu Y, Takahashi Y, Tameshige Y and Tamii A 2009 *Phys. Rev. C* **79** 024602
[77] Zegers R G T, Adachi T, Akimune H, Austin S M, van den Berg A M, Brown B A, Fujita Y, Fujiwara M, Galès S, Guess C J, Harakeh M N, Hashimoto H, Hatanaka K, Hayami R, Hitt G W, Howard M E, Itoh M, Kawabata T, Kawase K, Kinoshita M, Matsubara M, Nakanishi K, Nakayama S, Okumura S, Ohta T, Sakemi Y, Shimbara Y, Shimizu Y, Scholl C, Simenel C, Tameshige Y, Tamii A, Uchida M, Yamagata T and Yosoi M 2007 *Phys. Rev. Lett.* **99** 202501
[78] Perdikakis G, Zegers R G T, Austin S M, Bazin D, Caesar C, Deaven J M, Gade A, Galaviz D, Grinyer G F, Guess C J, Herlitzius C, Hitt G W, Howard M E, Meharchand R, Noji S, Sakai H, Shimbara Y, Smith E E and Tur C 2011 *Phys. Rev. C* **83** 054614
[79] Moinester M, Trudel A, Raywood K, Yen S, Spicer B, Abegg R, Alford W, Auerbach N, Celler A, Frekers D, Husser O, Helmer R, Henderson R, Hicks K, Jackson K, Jeppesen R, King N, Long S, Miller C, Vetterli M, Watson J and Yavin A 1989 *Phys. Lett. B* **230** 41 – 45
[80] Noji S, Zegers R G T, Austin S M, Baugher T, Bazin D, Brown B A, Campbell C M, Cole A L, Doster H J, Gade A, Guess C J, Gupta S, Hitt G W, Langer C, Lipschutz S, Lunderberg E, Meharchand R, Meisel Z, Perdikakis G, Pereira J, Recchia F, Schatz H, Scott M, Stroberg S R, Sullivan C, Valdez L, Walz C, Weisshaar D, Williams S J and Wimmer K 2014 *Phys. Rev. Lett.* **112** 252501
[81] Miki K, Sakai H, Uesaka T, Baba H, Bai C L, Berg G P A, Fukuda N, Kameda D, Kawabata T, Kawase S, Kubo T, Michimasa S, Miya H, Noji S, Ohnishi T, Ota S, Saito A, Sasamoto Y, Sagawa H, Sasano M, Shimoura S, Takeda H, Tokieda H, Yako K, Yanagisawa Y and Zegers R G T 2012 *Phys. Rev. Lett.* **108** 262503
[82] Auerbach N 1998 *Comments Nucl. Part. Phys.* **22** 223
[83] Auerbach N, Osterfeld F and Udagawa T 1989 *Phys. Lett. B* **219** 184 – 188
[84] Hitt G, Austin S M, Bazin D, Cole A, Dietrich J, Gade A, Howard M, Reitzner S, Sherrill B, Simenel C, Smith E, Stetson J, Stolz A and Zegers R 2006 *Nuclear Instruments and Methods in Physics Research Section A: Accelerators, Spectrometers, Detectors and Associated Equipment* **566** 264 – 269
[85] Helmer R 1987 *Can. J. Phys.* **65** 588
[86] Yen S 1987 *Can. J. Phys.* **65** 595
[87] Alford W P, Helmer R L, Abegg R, Celler A, Frekers D, Green P, Haeusser O, Henderson K, Hicks K, Jackson K P, Jeppesen R, Miller C A, Trudel A, Vetterli M, Yen S, Pourang H, Watson J, Brown B A and Engel J 1990 *Nucl. Phys. A* **514** 49–65
[88] Alford W P, Celler A, Brown B A, Abegg R, Ferguson K, Helmer R, Jackson K P, Long S, Raywood K and Yen S 1991 *Nucl. Phys. A* **531** 97–111
[89] Alford W P, Brown B A, Burzynski S, Celler A, Frekers D, Helmer R, Henderson R, Jackson K P, Lee K, Rahav A, Trudel A and Vetterli M C 1993 *Phys. Rev. C* **48** 2818
[90] Vetterli M C, Häusser O, Alford W P, Frekers D, Helmer R, Henderson R, Hicks K, Jackson K P, Jeppesen R G, Miller C A, Moinester M A, Raywood K and Yen S 1987 *Phys. Rev. Lett.* **59** 439
[91] Vetterli M C, Häusser O, Abegg R, Alford W P, Celler A, Frekers D, Helmer R, Henderson R, Hicks K H, Jackson K P, Jeppesen R G, Miller C A, Raywood K and Yen S 1989 *Phys. Rev. C* **40** 559
[92] El-Kateb S, Jackson K P, Alford W P, Abegg R, Azuma R E, Brown B A, Celler A, Frekers D, Haeusser O, Helmer R, Henderson R S, Hicks K H, Jeppesen R, King J D, Raywood K, Shute G G, Spicer B M, Trudel A, Vetterli M and Yen S 1994 *Phys. Rev. C* **49** 3128–3136
[93] Williams A L, Alford W P, Brash E, Brown B A, Burzynski S, Fortune H T, Haeusser O, Helmer

R, Henderson R, Hui P P, Jackson K P, Larson B, McKinzie M G, Smith D A, Trudel A and Vetterli M 1995 *Phys. Rev. C* **51** 1144–1153

[94] Ohnuma H, Hatanaka K, Hayakawa S I, Hosaka M, Ichihara T, Ishida S, Kato S, Niizeki T, Ohura M, Okamura H, Orihara H, Sakai H, Shimizu H, Tajima Y, Toyokawa H, Yoshida H Y and Yosoi M 1993 *Phys. Rev. C* **47** 648–651

[95] Xu H M, Ajupova G K, Betker A C, Gagliardi C A, Kokenge B, Lui Y W and Zaruba A F 1995 *Phys. Rev. C* **52** R1161–R1165

[96] Rakers S, Ellinghaus F, Bassini R, Bäumer C, [van den Berg] A, Frekers D, Frenne] D D, Hagemann M, Hannen V, Harakeh M, Hartig M, Henderson R, Heyse J, [de Huu] M, Jacobs E, Mielke M, Schippers J, Schmidt R, [van der Werf] S and Wörtche H 2002 *Nuclear Instruments and Methods in Physics Research Section A: Accelerators, Spectrometers, Detectors and Associated Equipment* **481** 253 – 261

[97] Bäumer C, van den Berg A M, Davids B, Frekers D, Frenne D D, Grewe E W, Haefner P, Harakeh M N, Hofmann F, Hunyadi M, Jacobs E, Junk B C, Korff A, Langanke K, Martínez-Pinedo G, Negret A, von Neumann-Cosel P, Popescu L, Rakers S, Richter A and Wörtche H J 2003 *Phys. Rev. C* **68** 031303(R)

[98] Sasano M, Perdikakis G, Zegers R G T, Austin S M, Bazin D, Brown B A, Caesar C, Cole A L, Deaven J M, Ferrante N, Guess C J, Hitt G W, Meharchand R, Montes F, Palardy J, Prinke A, Riley L A, Sakai H, Scott M, Stolz A, Valdez L and Yako K 2011 *Phys. Rev. Lett.* **107** 202501

[99] Rakers S, Bäumer C, van den Berg A M, Davids B, Frekers D, De Frenne D, Fujita Y, Grewe E W, Haefner P, Harakeh M N, Hunyadi M, Jacobs E, Johansson H, Junk B C, Korff A, Negret A, Popescu L, Simon H and Wörtche H J 2004 *Phys. Rev. C* **70**(5) 054302

[100] Bäumer C, van den Berg A M, Davids B, Frekers D, Frenne D D, Grewe E W, Haefner P, Harakeh M N, Hofmann F, Hollstein S, Hunyadi M, de Huu M A, Jacobs E, Junk B C, Korff A, Langanke K, Martínez-Pinedo G, Negret A, von Neumann-Cosel P, Popescu L, Rakers S, Richter A and Wörtche H J 2005 *Phys. Rev. C* **71** 024603

[101] Hagemann M, van de Berg A M, Frenne D D, Hannen V M, Harakeh M N, Heyse J, de Huu M A, Jacobs E, Langanke K, Martínez-Pinedo G and Wörtche H J 2004 *Phys. Lett. B* **579** 251

[102] Hagemann M, Bäumer C, van den Berg A M, Frenne D D, Frekers D, Hannen V M, Harakeh M N, Heyse J, de Huu E Jacobs M A, Langanke K, Martínez-Pinedo G, Negret A, Popescu L, Rakers S, Schmidt R and Wörtche H J 2005 *Phys. Rev. C* **71** 014606

[103] Popescu L, Bäumer C, van den Berg A M, Frekers D, Frenne D D, Fujita Y, Grewe E W, Haefner P, Harakeh M N, Hunyadi M, de Huu M A, Jacobs E, Johansson H, Korff A, Negret A, von Neumann-Cosel P, Rakers S, Richter A, Ryezayeva N, Shevchenko A, Simon H and Wörtche H J 2007 *Phys. Rev. C* **75** 054312

[104] Grewe E W, Bäumer C, Dohmann H, Frekers D, Harakeh M N, Hollstein S, Johansson H, Langanke K, Martínez-Pinedo G, Nowacki F, Petermann I, Popescu L, Rakers S, Savran D, Sieja K, Simon H, Thies J H, Berg A M v d, Wörtche H J and Zilges A 2008 *Phys. Rev. C* **77** 064303

[105] Guillot J, Galès S, Beaumel D, Fortier S, Rich E, Giai N V, Colò G, Berg A M v d, Brandenburg S, Davids B, Harakeh M N, Hunyadi M, Huu M d, Werf S Y v d, Wörtche H J, Bäumer C, Frekers D, Grewe E W, Haefner P, Junk B C and Fujiwara M 2006 *Phys. Rev. C* **73** 014616

[106] Bazin D, Caggiano J A, Sherrill B M, Yurkon J and Zeller A 2003 *Nucl. Inst. Meth.* **B204** 629

[107] Fujita H, Fujita Y, Berg G P A, Bacher A D, Foster C C, Hara K, Hatanaka K, Kawabata T, Noro T, Sakaguchi H, Shimbara Y, Shinada T, Stephenson E J, Ueno H and Yosoi M 2002 *Nucl. Instr. Meth. Phys. Res. A* **484** 17 – 26

[108] Gao B, Zegers R G T, Zamora J C, Bazin D, Brown B A, Bender P, Crawford H L, Engel J, Falduto A, Gade A, Gastis P, Ginter T, Guess C J, Lipschutz S, Macchiavelli A O, Miki K, Ney E M, Longfellow B, Noji S, Pereira J, Schmitt J, Sullivan C, Titus R and Weisshaar D 2020 *Phys. Rev. C* **101** 014308

[109] Titus R, Ney E M, Zegers R G T, Bazin D, Belarge J, Bender P C, Brown B A, Campbell

C M, Elman B, Engel J, Gade A, Gao B, Kwan E, Lipschutz S, Longfellow B, Lunderberg E, Mijatović T, Noji S, Pereira J, Schmitt J, Sullivan C, Weisshaar D and Zamora J C 2019 *Phys. Rev. C* **100** 045805

[110] Zamora J C, Zegers R G T, Austin S M, Bazin D, Brown B A, Bender P C, Crawford H L, Engel J, Falduto A, Gade A, Gastis P, Gao B, Ginter T, Guess C J, Lipschutz S, Longfellow B, Macchiavelli A O, Miki K, Ney E, Noji S, Pereira J, Schmitt J, Sullivan C, Titus R and Weisshaar D 2019 *Phys. Rev. C* **100** 032801

[111] Noji S, Zegers R G T, Austin S M, Baugher T, Bazin D, Brown B A, Campbell C M, Cole A L, Doster H J, Gade A, Guess C J, Gupta S, Hitt G W, Langer C, Lipschutz S, Lunderberg E, Meharchand R, Meisel Z, Perdikakis G, Pereira J, Recchia F, Schatz H, Scott M, Stroberg S R, Sullivan C, Valdez L, Walz C, Weisshaar D, Williams S J and Wimmer K 2015 *Phys. Rev. C* **92** 024312

[112] Scott M, Shimbara Y, Austin S M, Bazin D, Brown B A, Deaven J M, Fujita Y, Guess C J, Gupta S, Hitt G W, Koeppe D, Meharchand R, Nagashima M, Perdikakis G, Prinke A, Sasano M, Sullivan C, Valdez L and Zegers R G T 2014 *Phys. Rev. C* **90** 025801

[113] Hitt G W, Zegers R G T, Austin S M, Bazin D, Gade A, Galaviz D, Guess C J, Horoi M, Howard M E, Rae W D M, Shimbara Y, Smith E E and Tur C 2009 *Phys. Rev. C* **80** 014313

[114] Cole A L, Akimune H, Austin S M, Bazin D, Berg A M v d, Berg G P A, Brown J, Daito I, Fujita Y, Fujiwara M, Gupta S, Hara K, Harakeh M N, Jänecke J, Kawabata T, Nakamura T, Roberts D A, Sherrill B M, Steiner M, Ueno H and Zegers R G T 2006 *Phys. Rev. C* **74** 034333

[115] Paschalis S, Lee I, Macchiavelli A, Campbell C, Cromaz M, Gros S, Pavan J, Qian J, Clark R, Crawford H, Doering D, Fallon P, Lionberger C, Loew T, Petri M, Stezelberger T, Zimmermann S, Radford D, Lagergren K, Weisshaar D, Winkler R, Glasmacher T, Anderson J and Beausang C 2013 *Nucl. Instr. Meth. Phys. Res. A* **709** 44 – 55

[116] Bohr A and Mottelson B R 1969 *Nuclear Structure, vol. I* (New York: Benjamin)

[117] Anantaraman N, Austin S M, Brown B A, Crawley G M, Galonsky A, Zegers R G T, Anderson B D, Baldwin A R, Flanders B S, Madey R, Watson J W and Foster C C 2008 *Phys. Rev. C* **78** 065803

[118] Cole A L, Anderson T S, Zegers R G T, Austin S M, Brown B A, Valdez L, Gupta S, Hitt G W and Fawwaz O 2012 *Phys. Rev. C* **86** 015809

[119] Sasano M, Perdikakis G, Zegers R G T, Austin S M, Bazin D, Brown B A, Caesar C, Cole A L, Deaven J M, Ferrante N, Guess C J, Hitt G W, Honma M, Meharchand R, Montes F, Palardy J, Prinke A, Riley L A, Sakai H, Scott M, Stolz A, Suzuki T, Valdez L and Yako K 2012 *Phys. Rev. C* **86** 034324

[120] Perdikakis G, Sasano M, Austin S M, Bazin D, Caesar C, Cannon S, Deaven J, Doster H, Guess C, Hitt G, Marks J, Meharchand R, Nguyen D, Peterman D, Prinke A, Scott M, Shimbara Y, Thorne K, Valdez L and Zegers R 2012 *Nuclear Instruments and Methods in Physics Research Section A: Accelerators, Spectrometers, Detectors and Associated Equipment* **686** 117 – 124

[121] Yasuda J, Sasano M, Zegers R G T, Baba H, Bazin D, Chao W, Dozono M, Fukuda N, Inabe N, Isobe T, Jhang G, Kameda D, Kaneko M, Kisamori K, Kobayashi M, Kobayashi N, Kobayashi T, Koyama S, Kondo Y, Krasznahorkay A J, Kubo T, Kubota Y, Kurata-Nishimura M, Lee C S, Lee J W, Matsuda Y, Milman E, Michimasa S, Motobayashi T, Muecher D, Murakami T, Nakamura T, Nakatsuka N, Ota S, Otsu H, Panin V, Powell W, Reichert S, Sakaguchi S, Sakai H, Sako M, Sato H, Shimizu Y, Shikata M, Shimoura S, Stuhl L, Sumikama T, Suzuki H, Tangwancharoen S, Takaki M, Takeda H, Tako T, Togano Y, Tokieda H, Tsubota J, Uesaka T, Wakasa T, Yako K, Yoneda K and Zenihiro J 2018 *Phys. Rev. Lett.* **121** 132501

[122] Zegers R G T, Meharchand R, Shimbara Y, Austin S M, Bazin D, Brown B A, Diget C A, Gade A, Guess C J, Hausmann M, Hitt G W, Howard M E, King M, Miller D, Noji S, Signoracci A, Starosta K, Tur C, Vaman C, Voss P, Weisshaar D and Yurkon J 2010 *Phys. Rev. Lett.* **104** 212504

[123] Meharchand R, Zegers R G T, Brown B A, Austin S M, Baugher T, Bazin D, Deaven J, Gade A, Grinyer G F, Guess C J, Howard M E, Iwasaki H, McDaniel S, Meierbachtol K, Perdikakis G, Pereira J, Prinke A M, Ratkiewicz A, Signoracci A, Stroberg S, Valdez L, Voss P, Walsh K A, Weisshaar D and Winkler R 2012 *Phys. Rev. Lett.* **108** 122501
[124] Ayyad Y, Abgrall N, Ahn T, Álvarez-Pol H, Bazin D, Beceiro-Novo S, Carpenter L, Cooper R, Cortesi M, Macchiavelli A, Mittig W, Olaizola B, Randhawa J, Santamaria C, Watwood N, Zamora J and Zegers R 2020 *Nuclear Instruments and Methods in Physics Research Section A: Accelerators, Spectrometers, Detectors and Associated Equipment* **954** 161341 symposium on Radiation Measurements and Applications XVII
[125] Dzhioev A A, Vdovin A I, Wambach J and Ponomarev V Y 2014 *Phys. Rev. C* **89** 035805
[126] Dzhioev A A, Vdovin A I and Wambach J 2015 *Phys. Rev. C* **92** 045804
[127] Langanke K, Dean D J, Radha P B, Alhassid Y and Koonin S E 1995 *Phys. Rev. C* **52** 718–725
[128] Martínez-Pinedo G, Poves A, Caurier E and Zuker A P 1996 *Phys. Rev. C* **53** R2602–R2605
[129] Caurier E, Poves A and Zuker A P 1995 *Phys. Rev. Lett.* **74** 1517–1520
[130] Wakasa T, Sakai H, Okamura H, Otsu H, Fujita S, Ishida S, Sakamoto N, Uesaka T, Satou Y, Greenfield M B and Hatanaka K 1997 *Phys. Rev. C* **55** 2909–2922
[131] Gysbers P, Hagen G, Holt J D, Jansen G R, Morris T D, Navrátil P, Papenbrock T, Quaglioni S, Schwenk A, Stroberg S R and Wendt K A 2019 *Nature Physics* **15** 428–431
[132] Suzuki T, Honma M, Mao H, Otsuka T and Kajino T 2011 *Phys. Rev. C* **83** 044619
[133] Honma M, Otsuka T, Mizusaki T, Hjorth-Jensen M and Brown B A 2005 *J. Phys.: Conf. Ser.* **20** 002
[134] Poves A, Sánchez-Solano J, Caurier E and Nowacki F 2001 *Nucl. Phys. A* **694** 157–198
[135] Honma M, Otsuka T, Brown B A and Mizusaki T 2002 *Phys. Rev. C* **65** 061301
[136] Brink D M 1955 Ph.D. thesis Oxford University
[137] Axel P 1968 Simple nuclear excitations distributed among closely spaced levels *Proceedings on International Symposium on Nuclear Structure* (Dubna: IAEA Vienna) p 299
[138] Langanke K and Martínez-Pinedo G 1999 *Phys. Lett. B* **453** 187–193
[139] Misch G W, Fuller G M and Brown B A 2014 *Phys. Rev. C* **90** 065808
[140] Tan L, Liu Y X, Wang L J, Li Z and Sun Y 2020 *Phys. Lett. B* **805** 135432
[141] Aufderheide M B, Fushiki I, Woosley S E and Hartmann D H 1994 *Astrophys. J. Suppl.* **91** 389–417
[142] Martínez-Pinedo G, Langanke K and Dean D J 2000 *Astrophys. J. Suppl.* **126** 493–499
[143] Toki H, Suzuki T, Nomoto K, Jones S and Hirschi R 2013 *Phys. Rev. C* **88** 015806
[144] Anderson B D, Tamimi N, Baldwin A R, Elaasar M, Madey R, Manley D M, Mostajabodda'vati M, Watson J W, Zhang W M and Foster C C 1991 *Phys. Rev. C* **43** 50–58
[145] Kirsebom O S, Hukkanen M, Kankainen A, Trzaska W H, Strömberg D F, Martínez-Pinedo G, Andersen K, Bodewits E, Brown B A, Canete L, Cederkäll J, Enqvist T, Eronen T, Fynbo H O U, Geldhof S, de Groote R, Jenkins D G, Jokinen A, Joshi P, Khanam A, Kostensalo J, Kuusiniemi P, Langanke K, Moore I, Munch M, Nesterenko D A, Ovejas J D, Penttilä H, Pohjalainen I, Reponen M, Rinta-Antila S, Riisager K, de Roubin A, Schotanus P, Srivastava P C, Suhonen J, Swartz J A, Tengblad O, Vilen M, Vínals S and Äystö J 2019 *Phys. Rev. C* **100** 065805
[146] Nabi J U and Klapdor-Kleingrothaus H V 1999 *Eur. Phys. J. A* **5** 337–339
[147] Pruet J and Fuller G M 2003 *Astrophys. J. Suppl.* **149** 189–203
[148] Zhi Q, Langanke K, Martínez-Pinedo G, Nowacki F and Sieja K 2011 *Nucl. Phys. A* **859** 172–184
[149] Takahasi Y and Umezawa H 1975 *Collect. Phenom.* **2** 55–80
[150] Dzhioev A A, Vdovin A I and Stoyanov C 2019 *Phys. Rev. C* **100** 025801
[151] Paar N, Colò G, Khan E and Vretenar D 2009 *Phys. Rev. C* **80** 055801
[152] Niu Y F, Paar N, Vretenar D and Meng J 2011 *Phys. Rev. C* **83** 045807
[153] Yako K *et al.* 2005 *Phys. Lett. B* **615** 193 – 199
[154] Pfeiffer A *et al.* 1986 *Nucl. Phys. A* **455** 381 – 398

[155] Sullivan C, O'Connor E, Zegers R G T, Grubb T and Austin S M 2016 *Astrophys. J.* **816** 44
[156] Pascal A, Giraud S, Fantina A F, Gulminelli F, Novak J, Oertel M and Raduta A R 2020 *Phys. Rev. C* **101**(1) 015803
[157] Raduta A R, Gulminelli F and Oertel M 2017 *Phys. Rev. C* **95** 025805
[158] Titus R, Sullivan C, Zegers R G T, Brown B A and Gao B 2018 *J. Phys. G: Nucl. Part. Phys.* **45** 014004
[159] Weak Rate Library https://groups.nscl.msu.edu/charge_exchange/weakrates.html
[160] O'Connor E 2015 *Astrophys. J. Supp.* **219** 24
[161] Woosley S E and Weaver T A 1995 *Astrophys. J. Suppl.* **101** 181
[162] Kotake K, Sumiyoshi K, Yamada S, Takiwaki T, Kuroda T, Suwa Y and Nagakura H 2012 *Prog. Theor. Exp. Phys.* **2012** 01A301
[163] Burrows A 2013 *Rev. Mod. Phys.* **85** 245–261
[164] Janka H T, Melson T and Summa A 2016 *Annu. Rev. Nucl. Part. Sci.* **66** 341–375
[165] Müller B 2020 *Living Rev. Comput. Astrophys.* **6** 3
[166] Fischer T, Langanke K and Martínez-Pinedo G 2013 *Phys. Rev. C* **88** 065804
[167] Furusawa S 2018 *Phys. Rev. C* **98** 065802
[168] Nagakura H, Furusawa S, Togashi H, Richers S, Sumiyoshi K and Yamada S 2019 *Astrophys. J. Suppl.* **240** 38
[169] Raduta A R, Gulminelli F and Oertel M 2016 *Phys. Rev. C* **93**(2) 025803
[170] Phillips M M 1993 *Astrophys. J. Lett.* **413** L105
[171] Nomoto K, Thielemann F K and Yokoi K 1984 *Astrophys. J.* **286** 644–658
[172] Suzuki T 2017 *Memorie della Societa Astronomica Italiana* **88** 282
[173] Brachwitz F 2001 *Neutron-rich nucleosyntheis in Chandrasekhar mass models of type Ia supernovae* Ph.D. thesis Universität Basel
[174] Piersanti L, Bravo E, Cristallo S, Domínguez I, Straniero O, Tornambé A and Martínez-Pinedo G 2017 *Astrophys. J. Lett.* **836** L9
[175] Zegers R G T, Brown E F, Akimune H, Austin S M, Berg A M v d, Brown B A, Chamulak D A, Fujita Y, Fujiwara M, Galès S, Harakeh M N, Hashimoto H, Hayami R, Hitt G W, Itoh M, Kawabata T, Kawase K, Kinoshita M, Nakanishi K, Nakayama S, Okumura S, Shimbara Y, Uchida M, Ueno H, Yamagata T and Yosoi M 2008 *Phys. Rev. C* **77** 024307
[176] Blaes O, Blandford R, Madau P and Koonin S 1990 *Astrophys. J.* **363** 612
[177] Woosley S E, Heger A, Cumming A, Hoffman R D, Pruet J, Rauscher T, Fisker J L, Schatz H, Brown B A and Wiescher M 2004 *Astrophys. J. Suppl.* **151** 75–102
[178] Galloway D K, Muno M P, Hartman J M, Psaltis D and Chakrabarty D 2008 *Astrophys. J. Suppl.* **179** 360–422
[179] Keek L, Heger A and in't Zand J J M 2012 *Astrophys. J.* **752** 150
[180] Cameron A G W 1959 *Astrophys. J.* **130** 916
[181] Gasques L R, Afanasjev A V, Beard M, Chamon L C, Ring P and Wiescher M 2005 *Nucl. Phys. A* **758** 134–137
[182] Fushiki I and Lamb D Q 1987 *Astrophys. J. Lett.* **323** L55
[183] Schramm S, Langanke K and Koonin S E 1992 *Astrophys. J.* **397** 579
[184] Müller H M and Langanke K 1994 *Phys. Rev. C* **49** 524–532
[185] Sato K 1979 *Prog. Theor. Phys.* **62** 957
[186] Bisnovatyi-Kogan G S and Chechetkin V M 1979 *Soviet Phys. Uspekhi* **22** 89
[187] Yakovlev D G, Haensel P, Baym G and Pethick C 2013 *Physics Uspekhi* **56** 289–295
[188] Deibel A, Meisel Z, Schatz H, Brown E F and Cumming A 2016 *Astrophys. J.* **831** 13
[189] Schatz H, Aprahamian A, Görres J, Wiescher M, Rauscher T, Rembges J F, Thielemann F K, Pfeiffer B, Möller P, Kratz K L, Herndl H, Brown B A and Rebel H 1998 *Phys. Rep.* **294** 167–263
[190] Kasen D, Metzger B, Barnes J, Quataert E and Ramirez-Ruiz E 2017 *Nature* **551** 80–84
[191] Burbidge E M, Burbidge G R, Fowler W A and Hoyle F 1957 *Rev. Mod. Phys.* **29** 547–650

[192] Cameron A G W 1957 Stellar evolution, nuclear astrophysics, and nucleogenesis Report CRL-41 Chalk River
[193] Cowan J J, Thielemann F K and Truran J W 1991 *Phys. Rep.* **208** 267–394
[194] Cowan J J, Sneden C, Lawler J E, Aprahamian A, Wiescher M, Langanke K, Martínez-Pinedo G and Thielemann F K 2019 *Rev. Mod. Phys.* in press (*Preprint* 1901.01410)
[195] Burrows A, Reddy S and Thompson T A 2006 *Nucl. Phys. A* **777** 356–394
[196] Janka H T 2017 *Neutrino Emission from Supernovae* (Cham: Springer International Publishing)
[197] Wanajo S, Sekiguchi Y, Nishimura N, Kiuchi K, Kyutoku K and Shibata M 2014 *Astrophys. J.* **789** L39
[198] Goriely S, Bauswein A, Just O, Pllumbi E and Janka H T 2015 *Mon. Not. Roy. Astron. Soc.* **452** 3894–3904
[199] Martin D, Perego A, Kastaun W and Arcones A 2018 *Class. Quantum Gravity* **35** 034001
[200] Radice D, Perego A, Hotokezaka K, Fromm S A, Bernuzzi S and Roberts L F 2018 *Astrophys. J.* **869** 130
[201] Shibata M and Hotokezaka K 2019 *Annu. Rev. Nucl. Part. Sci.* **69** 41–64
[202] Arcones A, Martínez-Pinedo G, Roberts L F and Woosley S E 2010 *Astron. & Astrophys.* **522** A25
[203] Beloborodov A M 2003 *Astrophys. J.* **588** 931–944
[204] Siegel D M and Metzger B D 2018 *Astrophys. J.* **858** 52
[205] Fujibayashi S, Shibata M, Wanajo S, Kiuchi K, Kyutoku K and Sekiguchi Y 2020 *Phys. Rev. D* **101** 083029
[206] Jones S, Röpke F K, Pakmor R, Seitenzahl I R, Ohlmann S T and Edelmann P V F 2016 *Astron. & Astrophys.* **593** A72
[207] Schwab J, Bildsten L and Quataert E 2017 *Mon. Not. Roy. Astron. Soc.* **472** 3390–3406
[208] Paxton B, Schwab J, Bauer E B, Bildsten L, Blinnikov S, Duffell P, Farmer R, Goldberg J A, Marchant P, Sorokina E, Thoul A, Townsend R H D and Timmes F X 2018 *Astrophys. J. Suppl.* **234** 34
[209] Jones S, Röpke F K, Fryer C, Ruiter A J, Seitenzahl I R, Nittler L R, Ohlmann S T, Reifarth R, Pignatari M and Belczynski K 2019 *Astron. & Astrophys.* **622** A74
[210] Heber U 2009 *Annu. Rev. Astron. Astrophys.* **47** 211–251
[211] Geier S, Østensen R H, Nemeth P, Gentile Fusillo N P, Gänsicke B T, Telting J H, Green E M and Schaffenroth J 2017 *Astron. & Astrophys.* **600** A50
[212] Bauer E B, Schwab J and Bildsten L 2017 *Astrophys. J.* **845** 97
[213] Hashimoto M A, Nomoto K I, Arai K and Kaminisi K 1986 *Astrophys. J.* **307** 687–693
[214] Kaminisi K, Arai K and Yoshinaga K 1975 *Prog. Theor. Phys.* **53** 1855–1856
[215] Iliadis C, Longland R, Champagne A E, Coc A and Fitzgerald R 2010 *Nucl. Phys. A* **841** 31–250
[216] Bueno A, Gil-Botella I and Rubbia A 2003 *arXiv e-prints* (*Preprint* hep-ph/0307222)
[217] Gil-Botella I and Rubbia A 2003 *J. Cosmology Astropart. Phys.* **2003** 009
[218] Scholberg K 2012 *Annu. Rev. Nucl. Part. Sci.* **62** 81–103
[219] Bhattacharya M, Goodman C D and García A 2009 *Phys. Rev. C* **80** 055501
[220] Karakoç M, Zegers R G T, Brown B A, Fujita Y, Adachi T, Boztosun I, Fujita H, Csatlós M, Deaven J M, Guess C J, Gulyás J, Hatanaka K, Hirota K, Ishikawa D, Krasznahorkay A, Matsubara H, Meharchand R, Molina F, Okamura H, Ong H J, Perdikakis G, Scholl C, Shimbara Y, Susoy G, Suzuki T, Tamii A, Thies J H and Zenihiro J 2014 *Phys. Rev. C* **89** 064313
[221] Li T C, Pietralla N, Tonchev A P, Ahmed M W, Ahn T, Angell C, Blackston M A, Costin A, Keeter K J, Li J, Lisetskiy A, Mikhailov S, Parpottas Y, Perdue B A, Rainovski G, Tornow W, Weller H R and Wu Y K 2006 *Phys. Rev. C* **73** 054306
[222] Radha P B, Dean D J, Koonin S E, Kuo T T S, Langanke K, Poves A, Retamosa J and Vogel P 1996 *Phys. Rev. Lett.* **76** 2642